Design, Modelling, and Characterisation of Millimetre-Wave Antennas for 5G Wireless Applications

by

Syeda Fizzah Jilani

A thesis submitted in partial fulfilment of the requirements for the degree of Doctor of Philosophy

School of Electronic Engineering and Computer Science
Queen Mary University of London
United Kingdom

June 2018

Declaration

I, Syeda Fizzah Jilani, confirm that the research included within this thesis is my own work or that where it has been carried out in collaboration with, or supported by others, that this is duly acknowledged below and my contribution indicated. Previously published material is also acknowledged.

I attest that I have exercised reasonable care to ensure that the work is original, and does not to the best of my knowledge break any UK law, infringe any third partys copyright or other Intellectual Property Right, or contain any confidential material. I accept that the College has the right to use plagiarism detection software to check the electronic version of the thesis. I confirm that this thesis has not been previously submitted for the award of a degree by this or any other university. The copyright of this thesis rests with the author and no quotation from it or information derived from it may be published without the prior written consent of the author.

Signature: Syeda Fizzah Jilani 

Date: 12th June 2018

TO MY FAMILY

Abstract

Future 5G systems and beyond are expected to implement compact and versatile antennas in highly densified millimetre-wave (MMW) wireless networks. This research emphasises on the realisation of 5G antennas provided with wide bandwidth, high gain, adaptable performance, preferably conformal implementation, and feasible bulk fabrication. K_a–band (26.5–40 GHz) is selected based on recent 5G standardisation, and novel antenna geometries are developed in this work on both rigid and flexible substrates by implementing advanced techniques of frequency reconfiguration, multiple-input-multiple-output (MIMO) assembly, as well as wideband and multiband antennas and arrays.

Novel MMW wideband antennas are presented for 5G and spatial diversity at the antenna front-ends is substantially improved by deploying wideband antennas in a MIMO topology for simultaneous multiple-channel communication. However, wideband operation is often associated with efficiency degradation, which demands a more versatile approach that allows the adaptable antenna to select the operating frequency. In this research, high performance reconfigurable antennas are designed for frequency selection over K_a–band. Also, an efficient and conformal antenna front-end solution is developed, which integrates both frequency reconfiguration and MIMO technology.

Gain of the antenna is critically important for 5G systems to mitigate high propagation losses. Antenna design with both high gain and bandwidth is challenging as wideband antennas are traditionally gain-limited, while antenna arrays deliver high gain over a narrow bandwidth. An Enhanced Franklin array model is proposed in this thesis, which aggregates multiband response with high gain performance. Furthermore, novel flexible monopole antenna and array configurations are realised to attain high gain profile over the complete K_a–band. These proposed 5G antennas are anticipated as potential contribution in the progress towards the realisation of future wireless networks.

Acknowledgments

First and foremost, I wish to express my deepest gratitude for my supervisor, Dr Akram Alomainy for giving me the opportunity to perform this research work under his supervision. Thank you for the tremendous academic support, guidance and motivation you gave to me to develop and embellish my research capabilities. My profound appreciation goes to Dr Qammer H. Abassi from University of Glasgow for his technical support, valuable suggestions and fruitful comments to improve my work. I am also hugely grateful to Dr Tian H. Loh for providing me with an opportunity to perform experimental testing in National Physical Laboratory (NPL). My sincere appreciation to Dr Khalid Rajab and Dr Maged Elkashlan for their valuable suggestions and assessments during my PhD. I am also grateful to Mrs Melissa Yao for her efforts in keeping the track record of my stages in PhD. I would also like to acknowledge Mrs Geetha Bommireddy and Mr Kok Ho Huen for their always welcoming attitude and excellent cooperation. I would like to express my huge appreciation to Dr Max Munoz for sharing his expertise to equip me with a hands-on experience on electronic instruments and measurement chambers.

I would like to extend thanks to my colleagues, who generously contributed to this work especially Mr Ardavan Rahimian for teaching me skills of academic writing, Mr Shaker Alkaraki for helping me with NSI near-field scanning, Dr Andre Sarker Andy for the help with profilometer measurements and quasi-optic bench, Mr Ahmed Aziz for the valuable suggestions, Dr Deepak Nagarkoti and Dr Peter Alizedeh for sharing their skills of antenna measurements with me. I am thankful to the Queen Mary University of London for the EECS Fees Waiver Award and National University of Sciences and Technology for providing me with the financial support for the entire duration of PhD, without this help my research would not have been possible. Also, special thanks to my family for being a great source of encouragement, love and inspiration for me.

Publications

Journal papers

1. **S. F. Jilani**, Q. H. Abbasi, and A. Alomainy, "Millimeter-wave liquid crystal polymer based antenna array for conformal 5G applications," *IEEE Antennas and Wireless Propagation letters.* (accepted)

   - The work contributes to Chapter 6

2. **S. F. Jilani**, A. Rahimian, Y. Alfadhl, and A. Alomainy, "Flexible and low-profile inkjet-printed frequency-reconfigurable millimeter-wave MIMO antenna for 5G applications," *Flexible and Printed Electronics-IOPscience*, vol. 3, no. 3, pp. 1–8, 2018. doi.org/10.1088/2058-8585/aad392

   - The work contributes to Chapter 4

3. **S. F. Jilani**,Q. H. Abbasi, Z. U. Khan, T.-H. Loh, and A. Alomainy, "A K_a–band Antenna based on an enhanced Franklin model for 5G cellular networks," *Microwave and Optical Technology Letters.* pp. 1562–1566, 2018, `https://doi.org/10.1002/mop.31194`

   - The work contributes to Chapter 5

4. **S. F. Jilani** and A. Alomainy, "Millimetre-wave T-shaped MIMO antenna with defected ground structures for 5G cellular networks," *IET Microwaves, Antennas*

Propagation, pp. 1–6, 2018, DOI: 10.1049/iet-map.2017.0467.

- The work contributes to Chapter 3

5. **S. F. Jilani** and A. Alomainy, "A multiband millimetre-wave two-dimensional array based on enhanced Franklin antenna for 5G wireless systems," *IEEE Antennas and Wireless Propagation Letters*, vol. 16, pp. 2983–2986, 2017.

   - The work contributes to Chapter 5

Conference papers

1. **S. F. Jilani**, A. K. Aziz, Q. H. Abbasi, and A. Alomainy, "Ka-band flexible Koch fractal antenna with defected ground structure for 5G wearable and conformal applications, " *IEEE 29th Annual Int. Symp. on Personal, Indoor, and Mobile Radio Commun. (PIMRC) - Workshop WS-11 on WIreless Body COMunications in Medicine (WIBCOMM)*, 09–12 Sep. 2018.

2. **S. F. Jilani**, Q. H. Abbasi, and A. Alomainy, "Inkjet-printed millimetre-wave PET-based flexible antenna for 5G wireless applications, " *2018 IEEE MTT-S International Microwave Workshop Series on 5G Hardware and System Technologies.*, 30–31 Aug. 2018.

3. **S. F. Jilani** and A. Alomainy, "An inkjet-printed MMW frequency-reconfigurable antenna on a flexible PET substrate for 5G wireless systems," *Loughborough Antennas Propagation Conference (LAPC)*, 2017. (**Finalist–Student Paper Competition**)

4. **S. F. Jilani** and A. Alomainy, "Millimeter-wave conformal antenna array for 5G wireless applications," *IEEE Int. Symp. Antennas Propag. Society (APSURSI)*, 2017, pp. 1439–1440. (**Finalist–Student Paper Competition**)

5. **S. F. Jilani** and A. Alomainy, "Millimetre-wave T-shaped antenna with defected

ground structures for 5G wireless networks," *Loughborough Antennas Propagation Conf. (LAPC)*, 2016, pp. 1–3. (**3rd Best Student Paper Award**)

6. **S. F. Jilani**, B. Greinke, Y. Hao, and A. Alomainy, "Flexible millimetre-wave frequency reconfigurable antenna for wearable applications in 5G networks," *URSI Int. Symp. Electromagnetic Theory (EMTS)*, 2016, pp. 846–848.

7. **S. F. Jilani** and A. Alomainy, "Planar millimeter-wave antenna on low-cost flexible PET substrate for 5G applications," *10th European Conference on Antennas and Propagation (EuCAP)*, 2016, pp. 1–3.

8. **S. F. Jilani**, S. M. Abbas, K. P. Esselle, and A. Alomainy, "Millimeter-wave frequency reconfigurable T-shaped antenna for 5G networks," *IEEE 11th Int. Conf. Wireless Mobile Computing, Networking Communications (WiMob)*, 2015, pp. 100–102.

Book Chapters

1. **S. F. Jilani**, Q. H. Abbasi, and A. Alomainy, "Millimetre Wave Flexible Wearable Antenna Design and Challenges," *Low Electromagnetic Emission Wireless Network Technologies: 5G and Beyond*, The IET. (Chapter's abstract accepted)

2. **S. F. Jilani**, Q. H. Abbasi, and A. Alomainy, "Millimetre Wave Antenna Designs for 5G Applications," *5G Reference*, Wiley. (Chapter's abstract accepted)

Contribution in Other Related Projects

1. A. Rahimian, **S. F. Jilani**, Q. H. Abbasi, A. Alomainy, and Y. Alfadhl, "A millimetre-wave two-dimensional 64-element array for large-scale 5G antenna subsystems," *Microwave and Optical Technology Letters*. (Submitted)

2. Z. U. Khan, **S. F. Jilani**, A. Belenguer, T. H Loh, and A. Alomainy, "Empty

substrate integrated waveguide-fed MMW aperture-coupled patch antenna for 5G" *12th European Conference on Antennas and Propagation*, 2018, pp. 1–3.

3. A. K. Aziz, **S. F. Jilani**, A. Alomainy, K. Z. Rajab, "High sensitivity inkjet-printed terahertz metallic hole array sensor," *12th European Conference on Antennas and Propagation*, 2018, pp. 1–4.

4. A. da C. Andrade, I. P. Fonseca, **S. F. Jilani** and A. Alomainy, "Reconfigurable textile-based ultra-wideband antenna for wearable applications," *10th European Conference on Antennas and Propagation, EuCAP*, 2016, pp. 1–4.

Table of Contents

List of Figures

List of Tables

List of Abbreviations

1D	One-Dimensional
2D	Two-Dimensional
3D	Three-Dimensional
3G	Third Generation
4G	Fourth-Generation
4G LTE	Fourth-Generation Long Term Evolution
5G	Fifth-Generation
AR	Axial Ratio
AT&T	American Telephone & Telegraph
BS	Base Stations
CoA	Collinear array
CP	Circular Polarisation
CPW	Coplanar Waveguide
DC	Direct current
DD	Dense Dielectric
DGS	Defected Ground Structures
DMP	Dimatix Materials Printer
DTC	Digitally Tuneable Capacitor
DVB-H	Digital Video Broadcasting-Handheld
EBG	Electronic Bandgap

EIRP	Effective Isotropic Radiated Power
FCC	Federal Communications Commission
FET	Field Effect Transistor
HMIC	Heterolithic Microwave Integrated Circuit
ICT	Information and Communication Technology
IEEE	Institute of Electrical and Electronics Engineers
LCP	Liquid Crystal Polymer
LOS	Line of Sight
LP	Linear Polarisation
LPKF	Leiterplatten Kopier Frsen
LWA	Leaky-wave Antenna
MIMO	Multiple Input Multiple Output
ME	Magneto-electric
MEMS	Micro-ElectroMechanical Systems
MMIC	Monolithic Microwave Integrated Circuit
MMW	Millimetre-wave
NLOS	Non-line-of-sight
NPL	National Physical Laboratory
Ofcom	Office of Communication
PCB	Printed Circuit Boards
PIN	Positive-Intrinsic-Negative
PIFA	Planar Inverted-F Antenna
PET	Polyethylene Terephthalate
PU	Polyurethane
PHY	Physical
QMUL	Queen Mary University of London
RF	Radio Frequency

RSC	Radio Spectrum Committee
Rx	Receiver
SAR	Specific Absorption Rate
SIW	Substrate Integrated Waveguide
Tx	Transmitter
UV	Ultraviolet
WiMAX	Worldwide Interoperability for Microwave Access
WLAN	Wireless Local Area Network

Chapter 1

Introduction

1.1 Introduction

Wireless communications has successfully accomplished numerous milestones of development in the past few years. Massive advancements in the information and communications technology (ICT), and an ever-growing number of wireless users and applications are responsible of erratic increase in the demand of high data rates and channel capacity. It is believed that the next generation of cellular communications will bring unprecedented challenges [1]. Cellular communication today is extensively deployed in sub-6 GHz band and especially frequencies below 3 GHz spectrum are severely affected by congestion. While choosing a frequency range for upcoming fifth-generation (5G) networks, millimetre-wave (MMW) frequencies are highly capable of offering compactness, miniaturised size and wider available bandwidth. However, the major reason of reluctance in realising MMW channel experience is propagation effects including higher atmospheric absorptions, poor diffraction and scattering issues. At higher frequencies, the atmosphere becomes more absorbing which results in high attenuation of signal power at the receiver (Rx) end. The signal attenuation depends mainly on the operating frequency, propagation distance and weather conditions such as fog, rain, etc. It is antic-

ipated that 5G architecture should comprise of short-range cells of sizes less than 200 m so that atmospheric attenuations will not be obvious except in the most severe circumstances [2, 3]. In dense cell deployment, a large number of users are located indoors, and a traditional outdoor coverage from a base station (BS) would be more challenging in 5G systems due to high penetration losses at higher frequencies through windows and house walls. Realisation of short-range cellular communication with the deployment of indoor BS units and multiple access points in the outdoor environment is essential which will increase the overall cost of the infrastructure.

The challenges of high frequency spectrum have encouraged antenna designers to come up with versatile antennas to ensure an efficient signal transmission and reception. The role of antenna in 5G architecture is extremely important and there is a need of adaptable antennas capable to perform well in the changing conditions [4]. Frequency selection is one of the key requirements which uses a cognitive approach and enables the antenna to select its frequency of operation. Frequency reconfiguration is vastly utilised in current cellular systems and mobile antennas are versatile enough to select from up to ten different frequency bands [5]. Another approach to increase the channel capacity is by using multiple-input-multiple-output (MIMO) antenna arrays. MIMO systems are capable of supporting multiple channels simultaneously, where each antenna element performs individually. At frequencies below 3 GHz, the size of antenna is large and limits the integration of large number of antennas in massive MIMO assembly for cellular applications. At high frequencies, smaller antenna size has facilitated the implementation of MIMO antenna systems distributed in both azimuth and elevation plane, to enable an adaptive control on multichannel transmission [6, 7]. Additionally, smaller dimensions of MMW antennas also allow the realisation of large-scale antenna arrays to provide high gain to overcome attenuations. The number of MMW antennas that can be easily integrated in a BS are typically in the range from 256 to 1024 [7].

Conventional geometries of patch antennas offer limited gain and bandwidth performance. High gain profiles could be achieve by using antenna arrays but it is difficult

to deal with the bandwidth improvement for antenna arrays. Reasonable efforts are in progress for the development of multiband antenna arrays, which provide the advantages of high gain as well as simultaneous access to a wide frequency range [8]. As 5G systems demand massive channel capacity to run multiple applications for a large number of users, and require high gain to deal with transmission losses, the approaches of utilising MMW-based reconfigurable antennas, MIMO arrays, and multiband and wideband arrays are particularly important to implement. This research has paid huge consideration to the above-mentioned approaches while suggesting 5G antenna solutions.

Efficiency, reliability and system's cost are envisioned as important considerations for future wireless devices. In addition, the conformity and flexibility are also desired features as the demand of wearable electronics is exponentially increasing [9]. Flexible substrates offer the advantages of lighter weight, thinner structures, and conformity to be a part of wearables, body-centric and medical applications [9, 10]. Though MMW antennas are well suited for devices with small form factor, yet precise fabrication is essential for the smaller device size. 5G is intended for smaller and highly dense cell deployments particularly in urban environments, which has raised a need of efficient and cost-effective bulk-fabrication techniques to facilitate mass production. While designing antenna systems, the choice of substrate becomes more critical at MMWs mainly due to dielectric losses. One of the promising solutions is the utilisation of low-loss flexible substrates such as paper, polymers, polyimides and polyester films.

1.2 Research Motivation and Objectives

Design of 5G architecture has gathered huge attention in the research and development sectors as it is anticipated to determine the future of wireless technology. 5G is aiming to meet the prospective demands of high data rates, faster connectivity and much more versatility than the current wireless networks. This can be achieved by increasing the system capacity by deploying wider available bandwidth, antennas with fast adap-

tive mechanisms and efficient channel modelling techniques. MMW spectrum is less exploited in past as compared to microwave and RF spectrum especially for cellular communication purposes. This results in little exploration and understanding about the possible benefits and challenges of MMW propagation particularly in densely populated indoor and outdoor environments. Frequency bands in the range of 24.25–86 GHz are highly focused for the 5G implementation, provided that the propagation limitations at such frequencies are carefully handled. Substantial developments in the architecture of existing wireless systems are desperately required in order to implement 5G technology. The real inspiration of this study is to participate in this massive development of wireless technology, which will start a new era of communication. The challenges that have motivated this research and emphasised on the requirement of proposing efficient, compact and cost-effective antenna designs for 5G applications can be summarised as follows:

- The antenna requirements for 5G systems are still not clearly defined. Based on the current wireless networks, it is anticipated that antennas provided with control of selecting the frequency of operation and reconfiguring the operating states to adjust with the environmental changes will be highly promising for 5G.

- Most of the reconfigurable antennas for cellular networks are demonstrated for frequencies below 6 GHz. There is a need of extensive exploitation of MMW spectrum and presenting novel designs of reconfigurable antennas. This research progress will eventually deliver the desired performance of the MMW cellular antennas.

- Most of the reported antennas with adaptability are bulky and very complex. This research is mainly focused on the design of lightweight antennas printed on thin films of flexible substrate. The intention is to develop planar antenna geometries with relatively lesser design complexity and better efficiency.

- Another objective of 5G is to enhance the flexibility of cellular devices. Smart and wearable gadgets are gaining huge attention at the user end in modern wireless systems. Development of flexible components not only contributes to implementation

of wearable devices, but also adds an ease to be mounted on the irregular surfaces. Therefore, this research considers not just rigid substrates but also look into the usability of flexible films in developing MMW antennas.

- After the success of MIMO antennas in 4G systems, it is projected that 5G will be exclusively based on MIMO systems. Notable work has been performed in suggesting the characteristics of MIMO antennas for future networks, but needs more efforts to achieve the desired level of maturity to be incorporated efficiently in cellular devices. It is highly desirable to contribute in the development of MMW MIMO antenna systems and also integrate MIMO technology with flexible electronics.

- Research in antenna design for 5G systems is centred primarily on deployment of antenna arrays to handle attenuations and path loss issues. Traditional arrays usually exhibit single band operation and it is difficult to achieve multiband or wideband response from antenna arrays. Applicability of multiband arrays at MMWs cellular networks will provide benefits of high gain over a large bandwidth.

- The antenna size is greatly reduced at high frequencies which leads to compact wireless devices. This also requires a high accuracy in fabrication as small variation in the dimensions could affect the performance. There is a need for precise and accurate fabrication methods to attain desired outcomes. Moreover, the number of devices will also increase for dense deployment of short-range cells which will raise the system's cost. It is important to comprehend the need of efficient and cost-effective ways of mass production. Processes like inkjet printing, photolithography and laser etching are found promising in this regard.

1.3 Key Contributions

Antenna design methodology comprises of a series of steps including simulation and modelling, parametric analysis, fabrication, and experimental evaluation for the validation

of results. In this research, the key objectives are to inspect the potential of various antenna design techniques in the implementation of high-frequency 5G antennas. The distinctive features and major contributions made in this work can be summarised as;

- 5G antennas are anticipated to offer high operating bandwidth and this work is mainly focused on the design of wideband and multiband antennas which cover the targeted bands of 28- and 38-GHz and 26 GHz suggested by 5G standards. This research has proposed novel designs of wideband antennas based on the defected ground structures (DGS) technique and presented an Enhanced Franklin array model which can be used for generating additional resonances for high bandwidth.

- Most of the antennas proposed in this work are planar structures, in which the simplicity of design has been maintained by avoiding multilayer structures. Compactness has been preserved by avoiding parasitic structures, and flexibility and conformity has been introduced to add another degree of freedom that does not require a planar surface for the antenna placement.

- Frequency reconfigurable antennas have been successful deployed in current cellular hand-sets and are capable of tuning on up to ten distinct frequency bands. This technology is also desirable for MMW 5G antennas and several designs have already been reported. This research also contributes in the development of frequency reconfiguration on the proposed bands for 5G wireless networks.

- MIMO antennas have gained huge success in 4G networks and considered as a promising technology for 5G systems. MIMO configurations of the proposed wideband and frequency reconfigurable antennas are presented in this work. This shows the potential of designed antennas in 5G MIMO assembly and contributes in the state-of-the-art development towards 5G architecture.

- Increasing demand of wearable electronics has encouraged the design of flexible and conformal antennas. A considerable amount of work in this research is on developing wideband, frequency reconfigurable antennas and MIMO antennas on flexible

substrates. For instance, a DGS based wideband antenna reported in Chapter 3, reconfigurable antennas and reconfigurable MIMO antennas developed in Chapter 4, a wideband franklin array antenna in Chapter 5, and a high gain LCP-based wideband antenna and its array topology in Chapter 6, are all flexible 5G antennas.

1.4 Outline of the Thesis

This section provides an overview of the thesis organisation in terms of the contents of chapters and the progress made so far in this research. **Chapter 1** delivers the introduction of 5G and a glimpse of suitability of MMW spectrum for future wireless networks. It further highlights the desirable research objectives, possible challenges may involve, motivation behind this work and key contributions. The upcoming thesis chapters are summarised here as follows:

Chapter 2 provides a comprehensive literature review on 5G networks, prospects of future wireless communication on MMW spectrum, and possible challenges in the realisation of MMW based wireless architecture. The advanced antenna configurations at MMW spectrum such as reconfigurable antennas, MIMO antennas, and multiband arrays are also discussed for potential integration in 5G networks. Additionally, precise fabrication considerations for MMW antenna and state-of-the-art manufacturing techniques are addressed in this chapter.

Chapter 3 demonstrates the design and implementation of K_a–band 5G antennas with high bandwidth profile and relatively lesser fabrication complexity. The antennas are designed on both rigid and flexible substrates by employing DGS to enhance the bandwidth. The DGS antenna is also deployed into 4-element MIMO assembly to validate the scope of antenna design for 5G multichannel transmission scenarios.

Chapter 4 is structured to deliver novel designs of MMW frequency reconfigurable antennas by implementing resistors and PIN diodes. The reconfiguration mechanism

at the antenna end is demonstrated to provide the ability of making an selection, and adjusting its state automatically for the desired frequency band. The work based on proposing novel geometries of reconfigurable antennas designed on both rigid and flexible substrates is presented in detail. Flexible films of polyethylene terephthalate (PET) and liquid crystal polymers (LCP) are used as substrate in the antenna design to develop conformal antennas, which can be integrated in both planar and non-planar surfaces.

Chapter 5 discussed about the wideband and multiband antenna arrays and their suitability for 5G systems. Enhanced Franklin array model is developed to generate multiband behaviour and novel geometries of 1D and 2D antenna arrays are presented by deploying this model. Additionally, the concept is implemented on flexible PET material to develop a wideband beam-steering leaky-wave antenna for 5G wearable devices.

Chapter 6 proposed an efficient K_a-band flexible antenna design with distinctive feature of high bandwidth and gain to be employed for 5G applications. The design is further incorporated in a two-element array assembly, which shows promising high-gain results in the complete operating range. Moreover, an highly time-efficient way of heat sintering is also presented on the inkjet printed prototypes.

Chapter 7 summarises the outcomes achieved in this work and future prospective of the research are presented in this chapter.

Chapter 2

Literature Review on 5G Antenna Front-End Solutions

2.1 Introduction

Communication technology has endured an outstanding progress to keep pace with the rapidly increasing demand of wireless devices and applications during the last two decades. 5G signifies the next level of mobile telecommunications standards and expects to bring an innovative advancement in wireless technology and its applications in the future. It is anticipated that 5G will lead to an ultra-fast, ultra-flexible, low latency and unified network comprising of interconnect between different network types to bring communication diversity, and one estimate states that 5G cloud will be able to connect 50 billion nodes by 2020 [11]. Many of the applications have already been accomplished on a small scale with the deployment of 4G standards. In 4G LTE, several heterogeneous systems and networks are interconnected to provide an ultra-fast, efficient and high-speed communication for the users. More network capacity, efficient use of spectrum, low latency, more reliability, high security, and faster connectivity are important considerations to achieve a real wireless world until 2020.

Current wireless cellular spectrum comprises of a bandwidth from 300 MHz to 3 GHz [12]. The selection of the frequency band for cellular networks is mainly determined by its penetration ability towards the obstacles, low atmospheric attenuations, weather fading, and antenna size compatible to fit in a mobile handset. In order to expand the capacity of frequency spectrum and to get the best out of the available bandwidth resources, several smart algorithms are in practice employing compression techniques with high degree of complexity to maximise the throughput. In addition, other adaptive techniques including MIMO antennas, reconfigurable antennas and phased arrays are suggested for short-range coverage cells to establish faster communication links among wireless devices. The current cellular spectrum has theoretically reached its maximum system utilisation due to a massive number of applications and has left with no sufficient space to allow further upgradation beyond 4G LTE [11, 13].

The road map is to diversify the communication system by using higher frequencies, which will lead to a denser but smaller cell size, and huge bandwidth capable of simultaneous functioning of numerous services. While deciding about the technological aspects of 5G, it is necessary to consider installation expense of the new infrastructure as well as the energy efficiency [13]. In addition, selection of a feasible high-frequency band, atmospheric effects on signal strength and appropriate antenna designs with suitable features of transmission and reception have been investigated in the literature [12, 13]. The final challenge is to analyse a vast variety of proposed solutions, and eventually developing a novel system, which fulfils future demands and ensures the best user experience. Notable contribution in defining 5G standards and desirable outcomes is from Federal Communications Commission (FCC) USA and Office of Communication (Ofcom) UK. FCC has recommended 28 GHz, 38 GHz and 72 GHz while Ofcom mainly focuses on 26.5 GHz band for 5G networks. However, it has been unanimously agreed on all forums to use MMW spectrum above 24 GHz for 5G networks [14, 15].

This chapter starts with providing a comprehensive overview of the potential of MMWs for 5G, possible challenges and favourable choices of unused frequency bands

at MMW spectrum. The performance of antenna is of extreme importance in wireless systems. MMW antennas may include several critical aspects in terms of design, realisation and validation, based on the requirements of a novel architecture of short-range picocells [6]. The further discussion is on patch antennas, which have gained huge success in wireless systems due to the ease of design and integration in planar geometries. The chapter also emphasises on the need of several efficient antenna topologies such as, MIMO configurations, frequency reconfiguration, as well as wideband and multiband antenna arrays as potential candidates of 5G applications. Shorter wavelengths at MMW spectrum lead to smaller antenna dimensions, which demand a high degree of fabrication accuracy. Many novel techniques of antenna fabrication have been introduced to deliver a fast, precise and low-cost fabrication, and some of these are discussed in later stages of this chapter. The evolution of 5G will bring much more versatility and flexibility in terms of wearable gadgets and costumes; hence, it is important to look for the scope of an antenna design on flexible materials and its performance attributes. Putting these ideas together, this chapter provides a literature review of 5G requirements and prospective antenna configurations to ensure efficient communication.

2.2 Millimetre-wave Spectrum for 5G Networks

Unused bands of MMWs are attractive to deal with bandwidth scarcity issues in the upcoming wireless networks [16]. The frequencies of 28 GHz or above where the spectrum is less crowded, have a potential to accommodate future 5G systems, where high capacity and fast speed are the key objectives to achieve [17, 18]. MMW spectrum offers various advantages such as; shorter wavelengths to allow compact antenna form factor, available bandwidth to improve channel width, wideband spread-spectrum capability for reduced multipath and clutter, and availability of certain high-attenuation bands for highly secure short-distance communication [18–19]. In past, reluctance towards adopting MMW spectrum for wireless networks was mainly due to its poor penetration power

in urban areas responsible for low network coverage, especially in bad weather conditions. There are several critical limitations necessary to be resolved at MMW spectrum, for instance, atmospheric attenuations and rain fades become more obvious at high frequencies. MMW communication is badly affected by severe weather conditions and the attenuations rise rapidly with the distance to the target. Moreover, MMW antennas are much smaller and more power is required for transmission and reception as compared to currently deployed cellular antennas. While moving towards short-range communication, dense installation of a much larger number of antennas will be required which will eventually increase the hardware cost as compact structures require precise manufacturing strategies. In addition to this, the short wavelength of MMWs leads to devices which are sensitive to edge diffraction in comparison with microwave range devices [18]. Moreover, commercially available MMW switching and circuit devices are expensive and many of these technologies proposed for MMWs are still immature and require more upgradation efforts to be well established in the industry.

Efficient manufacturing processes are essential for MMW circuitries to make the overall system cost-effective. The issue of low coverage range could be solved by reducing the cell area up to an optimum distance, where signal attenuations are not so obvious. Line-of-sight (LOS) link should be established where required to overcome path loss and to attain high speed at much cheaper rates. Though, the suggested low-power transmission will not be suitable for long-distance propagation, but this aspect can be useful for highly secure communication that will decrease the chance of co-channel interference. Studies have demonstrated that implementation of MMW antennas in a short-range cell minimises weather effects along with the advantage of frequency reuse. Developing a wireless network by integrating the benefits of MMWs and handling the limitations of the spectrum is a massive task. In order to address these challenges, efforts have been set forth to deal with these shortcomings, while designing a wireless architecture based on MMW frequencies. Several network architecture models have been suggesting MMWs as future of 5G networks [20]. In the meeting held on July 2016, FCC voted to approve a new

set of rules to facilitate 5G progress in the US. According to the FCC, the objectives of setting these new rules are to simplify the innovative process without any further delays. This standardisation of 5G bands has recommended release of approximately 11 GHz of spectrum for flexible, mobile and fixed-use wireless broadband. The overall approved bandwidth constitutes 3.85 GHz for licensed spectrum comprising of 28 GHz, 37 GHz and 39 GHz bands and an additional 7 GHz in the range of 64–71 GHz for unlicensed spectrum [14]. US companies like Verizon and AT&T have already publicised their 5G testing plans, and many others are on the way to follow the trend in future.

Another major contributor is the Ofcom, the regulatory authority for communication network in UK, which has recently published two major reports about 5G progress. The report presented in 2017 has covered an update about progress of 5G in UK and provided an overview of the process that anticipates the selection of 26 GHz as the pioneer MMW based spectrum for 5G in Europe [15]. The Radio Spectrum Committee (RSC) agreed on the roadmap to develop corresponding technical conditions at 3.25 GHz of spectrum between 24.25–27.5 GHz, which support 5G architecture in Europe. Ofcom also emphasised on facilitating access to all or part of 26 GHz band for 5G services as soon as practicable. In the second report, Ofcom published the goals for spectrum access and desired features of 5G systems. The report presents the vision of future mobile networks to be more flexible and adaptive as well as expected to bring innovation and create new markets for spectrum access. MMW spectrum is also anticipated to combine emerging technologies for 5G, capable of facilitating spectrum reuse [21].

2.3 Performance Requirements for 5G

Future 5G network standards are desired to address the capacity issues, suitability for short-range communication to attain minimal attenuation, the capability to handle the path loss limitations and connectivity to multiple users with low latency. It has been discussed that MMWs have a significant impact of weather attenuations, rain droplets

and even absorptions due to oxygen molecules. Fig. 2.1(a) shows the statistics of the rain attenuation against frequency at various rainfall rates. It is observed that a heavy rainfall of 25 mm/hr causes an attenuation of 7 dB/km at 28 GHz. However, if the coverage cell area is restricted to a radius of 200 m, the rain attenuation interprets to about 1.4 dB. In Fig. 2.1(b), attenuations due to atmospheric absorptions are demonstrated over a distance of 200 m, and clarifies that atmospheric absorption does not create a substantial increase in path loss at certain MMW frequencies. For instance, path loss figures are 0.012 and 0.016 dB at 28- and 38-GHz respectively, also, frequency bands of 70–100 GHz and 125–160 GHz show small loss [22, 23].

Based on the statistical analysis reported in Fig. 2.1, the proposed solution to deal with above-mentioned effects is to reduce the cell area as the attenuations become more critical with the distance. Heavy rainfall is not obvious is most of the parts of the world and radio links can be developed to minimise the attenuations due to rain effect [24]. The proposed architecture is based on coverage cell size of 200 m or less by adopting the concept of highly dense picocells and that will also multiply the number of installed devices at repeatable distances and ultimately increases the system cost. High gain antenna arrays should be utilised to overcome signal fading due to bad weather conditions in both LOS and NLOS scenarios. Antenna arrays with high directionality are preferred to incorporate if beam steering is the desired choice to tackle the path loss issues. LOS communication can provide high spectral efficiency, low latency, error-free signal detection and faster connectivity. With such arrangements, there is a need of suitable MMW 5G antennas capable to deal with challenges of future.

The radio latency and data throughput both are of crucial importance for advanced communication systems to inspect the performance of wireless networks. Latency refers to the transit time during the signal transmission, and defines the speed of the transmission, while data throughput governs the number of packets being transmitted, and it further depends on the bandwidth available to maximise the amount of data being sent. With interactive applications like online gaming, video, connected health, remote

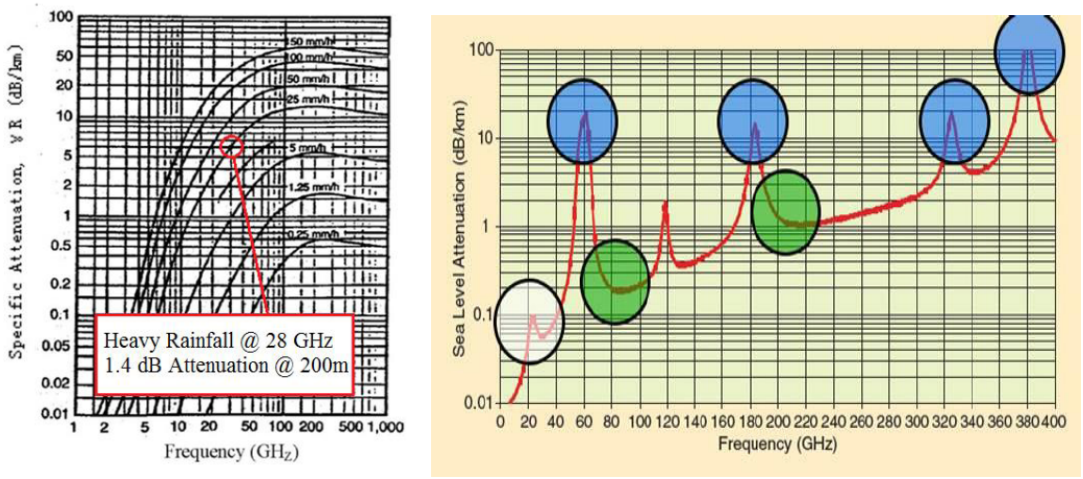

(a) (b)

Figure 2.1: Rain and atmospheric absorption statistics of the propagation model with a cell area of 200 m, (a) Rain attenuation in dB/km vs. frequency at various rainfall rates [23], (b)Atmospheric absorption vs. frequencies in dB/km [taken from 18, 22].

healthcare and multimedia ones, high latency can result in performance's degradation. Therefore, deploying highly efficient coding schemes as part of the real-time wireless applications; i.e., withstanding the introduced delay for maintaining the quality of service; would intrinsically enhance the system performance [25, 26]. The huge demand of interactive applications is expected in future and 5G is expected to be capable of providing ultra-low latency in this regard. Integration of smaller simplified buffers in radio link will reduce the latency as well as system's cost. Low latency is also helpful in improving the energy efficiency of the network. For instance, fast transitions between sleep and active state of the mobile phone, a short active time with high data rates and lower sleep-mode power consumption will increase the energy efficiency of the device. Device battery consumption is also an aspect of improvement. As the MMW cell size is very small, so the transmitted power required to cover the cell range will be much smaller than the power needed by currently used BS units. 5G will bring an efficient air-interface design, which does not involve continuous transmissions towards every carrier for the purpose of detection. It will permit Tx and Rx to be switched off even at the smallest interval of zero traffic to provide an energy efficient performance [27].

2.4 Challenges and Mitigation

Although the concept of introducing MMWs for future networks is widely accepted at many forums, still it is observed that this technology is not sufficiently mature to be deployed in commercial cellular networks. A thorough investigation on demands of 5G infrastructure and some fundamental advancements is essential to be done in the existing cellular networks to deal with challenges of high frequencies. One of the concerns is, much higher pathloss for the same communication distance, as it is increased by 3 dB with twice the transmission frequency. This requires sophisticated antennas to deal with the severe attenuations and path loss. The attenuation due to extreme weather conditions should also be taken into account. For instance, the communication is drastically affected by scattering at the times of heavy rainfall, where raindrops are of the diameter of 3 mm, which is of the order of MMW wavelength. Additionally, mechanical motions due to wind or storms could change the placement of antenna arrays in the order of hundreds of MMW wavelengths, and can cause severe alignment issues especially in the case of narrow beam antenna arrays [28]. Furthermore, various ground obstacles are also responsible of causing losses in links between the BS and access points [29].

MMW cellular networks are more suitable for a short-range LOS communication due to much shorter wavelengths, to minimise the influence of surrounding obstacles like buildings, trees etc. Indoor MMW communication is comparatively simpler as LOS links could be easily established within a building. Instead, for outdoor scenarios, highly directional antennas and steerable antenna beams are required to overcome the path loss effects and to fulfil the user mobility demands for MMW cellular communications. Advancement and upgradation in fundamental beam steering methods is needed based on MMW environmental conditions to accomplish more precise beam alignment [28]. It is expected that the severe path loss circumstances can be well handled by utilising an appropriate beam steering antennas. LOS signals suffers from signal blockage due to obstacles in the transmission path and these effects become more critical where high mobility is required. The LOS signal is attenuated due to shadowing, multipath fading

and even results in packet loss. In order to ensure high mobility at user end, anti-blockage techniques are essential to realise seamless connectivity. These techniques are capable of providing an adaptive control to switch the signal transmission from LOS mode to NLOS mode and thus guarantee an effective coverage. It is suggested that utilising cooperative relay techniques and distributed antenna arrays in 5G could facilitate many new possibilities to deal with blockage and enable effective coverage and unobstructed service at the expense of some additional design challenges. Highly directional antennas are supportive in establishing LOS channels with insignificant shadowing or multi-path components. These advancements ensure the high capacity of the prospective MMW system architecture with negligible interference from nearby users [30].

2.5 5G Antenna Design Requirements

Design and implementation of a mobile network at MMW spectrum is an unprecedented and huge challenge. The declaration of prospective 5G frequency bands by FCC and Ofcom has provided much-needed clarity towards the future research objectives of the development of 5G architecture. FCC has suggested a reserved bandwidth of 3.25 GHz for licensed access, i.e. 27.5–28.35 GHz, 37.6–38.6 GHz, 38.6–40 GHz, and a 7.6 GHz bandwidth for shared and unlicensed access, i.e. 37–37.6 GHz and 64–71 GHz [14]. It is highly desired that the deployed antenna is capable to operate at multiple bands for 5G licensed access in the range of K_a–band. Wideband, multiband and reconfigurable antennas are useful to cover such a high range of frequencies. In comparison to the currently deployed sub-6 GHz spectrum, several factors such as signal attenuation with respect to propagation, atmospheric effects and dielectrics properties become much more crucial at MMWs. The attenuation issues can be handled by increasing the gain of the 5G antenna, which is typically 5–6 dBi for a conventional patch, and 2–3 dBi in omnidirectional patches. Moreover, substrates with lower dielectric constant and loss tangent should be implemented in the antenna design and fabrication. In addition,

higher radiation efficiency of above 60 %, compact size, conformity and low cost are also significant features to address while proposing an antenna design for 5G devices [31].

2.6 Antenna Design Techniques for 5G Networks

Antenna is the centralised unit of communication networks and the advancement of 5G is greatly influenced by the performance of the antenna integrated in the network including the BS units and handsets. It is essential to understand the 5G demands for smart phones and other wireless devices, and utilise promising technologies to develop diversified antenna solutions. Many antenna configurations have been reported including planar wideband MMW antennas [32], reconfigurable antennas [33], planar phased-arrays [34], grid-array antennas [35], substrate integrated waveguides (SIW) [36] and MIMO topologies [37]. Efforts have been made in the progress of MMW cellular handset antennas addressing critical design aspects like cellular handset effects, radiation coverage, antenna gain, hardware implementation, and cost. Although exponential rise has been observed in the development of 5G cellular antennas, still there is a lack of systematic antenna design approach and design criteria. A great deal of research work is required to fill the gap and to provide a number of feasible antenna designs that can fulfil 5G demands in different areas. Among several promising topologies for the efficient antenna design, the following three techniques are investigated in this research.

- Wideband antennas in MIMO configurations,
- Frequency reconfigurable antennas,
- High gain antenna arrays

The purpose of choosing these configurations is their contribution in smart applications due to high performance particularly high bandwidth to ensure high capacity and high gain characteristics to deal with issues related to propagation losses.

2.6.1 Wideband and MIMO Antennas

The demands of high data rates and capacity can be accomplished by deploying wideband antennas for 5G. The capacity can be further enhanced with the MIMO technology which suggests simultaneous operation of multiple antennas [38]. Integration of wideband antennas in a MIMO assembly is anticipated as an integral part of advanced wireless networks for higher data rates, capability to mitigate multipath fading, improved transmission quality, better coverage and many other features. This implies to an increase in the demand of novel high-bandwidth MIMO antennas that can be suitably integrated in cellular devices. Incorporation of multiple antenna elements within the limited space of portable devices of a small form factor is a challenging task especially for sub-6 GHz bands, because the antenna size is big and compact arrangement usually comes with effects of mutual coupling. In MMW spectrum, the smaller antenna size has facilitated MIMO deployment and considered as one of the instrumental factor in 5G systems [39].

A two-element MIMO array comprising of metamaterial antennas is designed to operate at 5.8 GHz in [40]. The mutual coupling is reduced using DGS between two antennas. The antenna offers -45 dB of coupling isolation with a size reduction of more than 50%, while the disadvantage of using metamaterials is narrow bandwidth. An integrated antenna for wireless handheld devices is proposed in [41]. The design is well-fitted for both current 4G standards as well as upcoming 5G high data-rate communications. An arrangement combining microwaves and MMW antenna arrays is suggested to construct a MIMO system comprising of two reactive loaded monopoles to cover 1870–2530 MHz for 4G, and planar 2 $\times$ 4 slot antennas at 28-GHz for 5G applications. Measurements show that a bandwidth of 1.7 GHz at 28-GHz, the peak gain of 3.86 dBi and efficiency of 83% have been achieved. However, it has a limited operation only to one of the 5G bands and other prospective 5G bands have been ignored in this design. Another compact configuration reported in [42] presents a MIMO dual-band antenna array operating at 28 GHz and 38 GHz for 5G systems. Each subsector consists of an antenna array with gain above 12 dBi at each resonating band. The proposed BS design comprises of

six sub-sectors arranged along the azimuth plane, while each covering 40° and 30° spans at 28- and 38-GHz respectively, with the limitation of design complexity.

A compact dual-polarised 5G MIMO antenna configuration of quasi Yagi-Uda antennas is demonstrated in [43]. The antenna is designed for MMW wireless applications with potential integration in a mobile terminal and demands high fabrication complexity. Dual-port dual-polarised antennas are effectively deployed for both corner and lateral positions to provide polarisation diversity and compact area. The lateral topology is also extended to a 1 × 4 array in order to achieve high gain of 11 dBi, efficiency above 80% and phased-scanning characteristics. Experimental results show the impedance bandwidth of above 25% in both of the scenarios covering approx. 30–40 GHz and radiation pattern along the end-fire direction. A compact wideband MIMO antenna with operational bandwidth of 3–30 GHz is presented in [44] for miniaturised 5G devices. The proposed antenna design and reflection coefficient profile of two-element MIMO array is shown in Fig. 2.2. The high bandwidth is achieved due to insertion of slotted structures in the patch geometry. An additional radiating patch is incorporated at the antenna back to reduce back lobes. The compact antenna with dimensions of 25 × 25 mm^2 in oriented in such a way to offer orthogonal polarisation, reduced mutual coupling and high isolation within a compact design, though limited in gain performance.

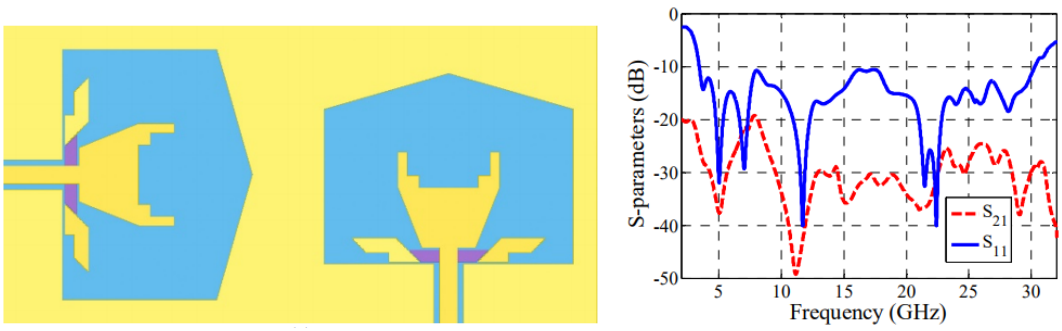

(a) (b)

Figure 2.2: Two-element MIMO antenna for 5G: (a) MIMO antenna design, (b) S-parameters of the designed MIMO antenna [taken from 44].

2.6.2 Frequency Reconfigurable Antennas

The massive increase in demand of highly efficient cognitive radio systems and wireless services has encouraged the implementation of multifunctional or reconfigurable antennas. Communication networks are at high risk of crosstalk interference at the user end as the same channel is employed in multiple access communication systems. In order to mitigate the interference, spread spectrum signalling is deployed due to its high efficiency. This technique offers the advantages of lower susceptibility to multipath fading and better data security, yet requires relatively large bandwidths [45]. This aggravates the requirement of an antenna with high bandwidth profile. The performance of an antenna can be greatly diversified by incorporating reconfiguration mechanism. This dynamic response enable the antennas to alter the characteristics of radiation pattern, polarisation and frequency to adapt with the changing circumstances in a controlled and reversible way [46, 47]. Frequency reconfigurable antennas are considered as efficient solution for bandwidth requirements. The functionality of antenna system is enhanced without any increase in size or complexity, as the reconfigurable antenna is not bound to cover all the desired bands simultaneously, thus results in a cognitive approach of selecting the desired frequency on demand [48, 49].

Design and implementation of reconfigurable antennas have gathered huge success in bringing versatility and adaptability by providing tuneable characteristics in the current wireless transceivers. It is anticipated that future wireless networks and particularly 5G will be highly reliant on adaptable antennas capable to tune the operating frequency while filtering out the interfering signals [50]. Advanced cognitive radio systems demand smart antenna systems rather than conventional wideband and multiband antennas, to deal with different situations and applications. Antenna reconfigurability is traditionally associated with controlling the effective radiating length to select a variable frequency of operation among the range of accessible wireless bands. A frequency reconfigurable antenna is usually designed with the flexibility to operate as a standalone narrowband, wideband or even multiband configuration. Several frequency reconfigurable antennas

have been proposed capable to switching among different narrowband configurations [51, 52], as well as wideband to a narrowband mode of operation [53, 54]. Reconfigurable antennas offer superior out-of-band rejection than wideband antennas and avoid the use of additional filters. A reconfigurable antenna capable of switching among multiband and single-band operations is reported in [55]. Kang and Lim [56] proposed a dual-band frequency reconfigurable antenna provided with a single band tuning while the other resonance remains intact due to miniaturised substrate-integrated waveguide (SIW). A switched beam dual-band antenna is designed by Li *et al.* in [57], a pattern reconfigurability in proposed in [58], and a polarisation reconfiguration is performed in [59].

2.6.2.1 Switching Schemes for Reconfigurable Antennas

Frequency reconfiguration is performed by changing the geometry of the radiating element by including or excluding a fractional radiating area by means of electronic switches. The switch is selected based essentially on the desired switching speed and the signal power level. Moreover, impedance characteristics, biasing requirements and activations conditions, form factor, cost and packaging technology are also important while selecting a switch [60]. Several switching mechanisms have been introduced and efficiently deployed for this purpose. Surface mount switches, such as PIN diodes [61, 62], FETs [63], and RF MEMS [64, 76] are extensively used to reconfigure the geometry of planar as well as conformal antennas. These switches belong to mature technologies and commercially available in market, but the performance is restricted due to the requirement of biasing circuitries. Many other switching techniques are also developed to overcome issues related to biasing effects by incorporating varactors [65], optical switches [66], or by altering the substrate permittivity [67] or permeability [68] to perform frequency tuning. PIN diodes offer reasonable linearity with low ON-state loss and OFF-state capacitance with the drawbacks of high DC power consumption and complex biasing network. FETs are more advanced and efficient in power consumption than pin diodes with better linearity but more expensive. MEMS switches provide high linearity with a

compromise on reliability and slow switching speed due to mechanical actuation mechanism [69]. Varactors provide low DC power consumption but highly nonlinear and analog bias voltages are required [70]. Optical switches are good choice as the biasing circuits are avoided, but requires a long way of research and advancement.

A. Reconfigurable antennas by using PIN Diodes

A number of frequency reconfigurable antennas are reported with different switch-configurations and tuning techniques. A slot-ring antenna capable to reconfigure 1.76/5.71 GHz bands based on the state of PIN diodes have been reported in [71]. However, performance is limited due to variation of gain magnitudes of 0.1/4.2 dBi as well as radiation efficiency of 66.6%/80.7% in two configurations. A planar inverted-F MIMO antenna (PIFA) is discussed in [72] and presented in Fig. 2.3, where a quarter-wave slot line is inserted between two antennas to achieve high isolation greater than 30 dB. The operating frequency and isolation reconfigurability for the bands at 3.5, 2.6, and 2.35 GHz is achieved by adjusting the PIN-diode configurations mounted on the antenna and the slot. Besides, the antenna has limited performance in terms of magnitudes of realised gain and radiation efficiencies, such as 2.78 dBi with 73.9%, 1.99 dBi with 48.43%, and 1.39 dBi with 43.71% at modes I, II, and III, respectively. A reconfigurable multiband antenna for WiMAX/WLAN applications is presented in [73] with two PIN diodes. The compact antenna of 50×45 mm^2 is capable to reconfigure ten frequency bands between 2.2 and 6 GHz. Furthermore, reconfiguration of linear polarisation in six different angles and at five discrete bands is performed by implementing PIN diodes in [74]. PIN diodes are also implemented to perform frequency and pattern reconfiguration in [75]. However, the efficiency is a limiting factor in these antenna designs due to the internal resistance of the tuning devices, and also complexity has also increased due to dc-biasing.

B. Reconfigurable antennas by using Varactors

Another promising technique is variable reactive loading (typically capacitance) implemented by varactor diodes to reconfigure the resonant frequency. The frequency is tuned

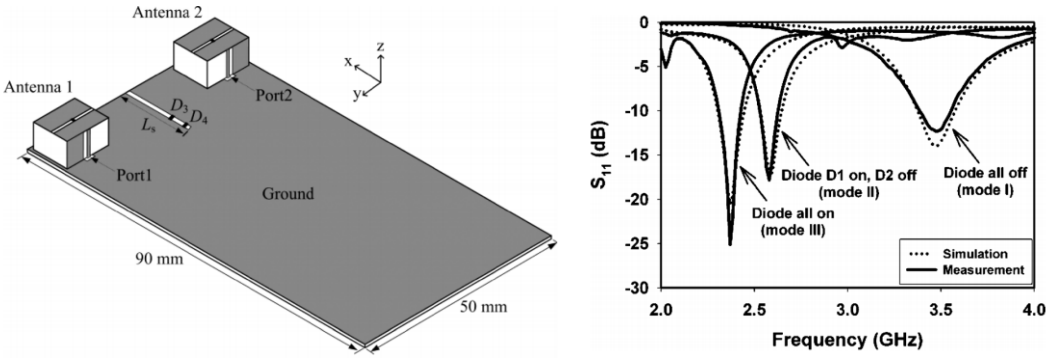

(a) (b)

Figure 2.3: Reconfigurable MIMO antenna: (a) Proposed schematics, (b) S_{11} of the reconfigurable antenna in three modes [taken from 72].

by changing the value of capacitance. A frequency tuning H-shaped antenna using varactor diode has been discussed in [77]. Qin *et al.* [78] proposed reconfiguration in three states of linear polarisation by using varactors. This work is further elaborated and presented in [79] with an additional capability of switching to two circularly polarised states, and more extended in [80] with a distinct feeding network. A frequency- and pattern-reconfigurable antenna in frequency range of 2.68 to 3.51 GHz is designed in [81]. The antenna incorporates varactors loaded with open-circuited stubs to perform reconfiguration. The proposed antenna is capable to switch its operation between two distinct radiation configurations, i.e. broadside radiation in microstrip patch mode and an omnidirectional pattern in the monopole configuration. A low profile monopole omnidirectional antenna provided with slots arrangement to offer dual-band response is discussed in [82]. Fig. 2.4 shows that the design is made reconfigurable by using two sets of varactors capable to control the resonant frequencies of individual bands independently. Tuning ranges of 31% and 22% are achieved, at the resonant frequencies of 0.9 and 1.7 GHz, respectively, as depicted in Fig. 2.5.

2.6.2.2 Reconfigurable Antennas for Cellular Communication

Reconfiguration mechanism is highly desirable in mobile communication as the electrical size of an antenna has an impact on the bandwidth and efficiency [83, 84]. As the mobile communication comprises of frequency bands distributed into various channels, and instead of all the channels to be simultaneously active, the efficient approach is to tune the antenna to a specific channel, which will reduce the bandwidth requirements. Different techniques have been proposed to carry out an efficient reconfiguration with the feasibility to be integrated in the mobile handset. For instance, varactors are extensively

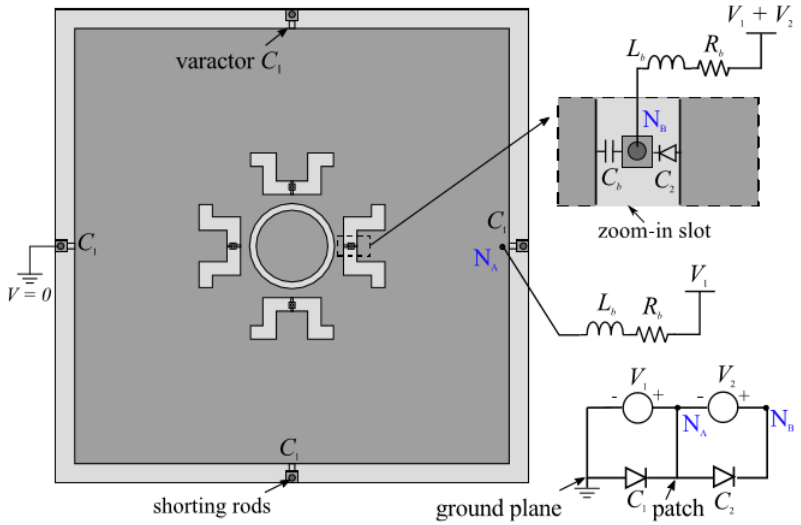

Figure 2.4: Proposed dual-band reconfigurable antenna with varactors [taken from 82].

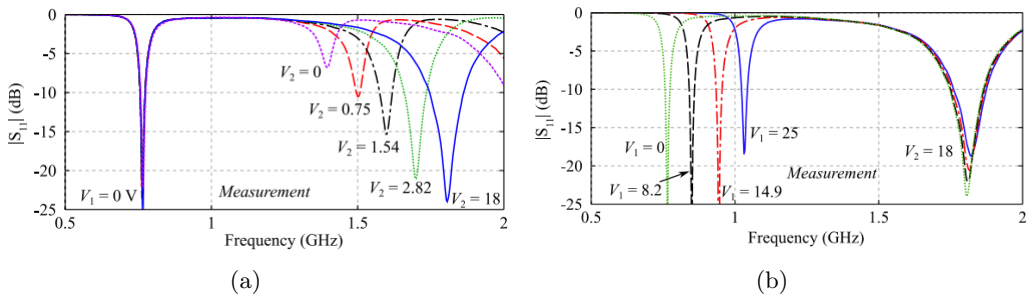

(a) (b)

Figure 2.5: S_{11} plot of proposed antenna: (a) S_{11} plot for fixed V_1 and varying V_2, (a) S_{11} plot for fixed V_2 and varying V_1 [taken from 82].

employed for digital video broadcasting-handheld (DVB-H) reception, but the application is limited to the Rx due to low RF power handling [85, 86]. PIN diodes solve the limitation of varactors with a compromise on high DC power consumption [87]. MEMS offer high power handling; small insertion loss and lower DC power consumption but are more critical in design complexity and switching speed [88]. A frequency reconfigurable antenna of dimensions $15 \times 15 \times 1.6$ mm^3, covering bands of 1.7–2.7, 3.3–4.5, and 5.475-–6.425 GHz with an efficiency of 90%, for potential mobile applications is demonstrated in [89]. A cluster of mutually coupled antennas is designed and excitation is provided with the frequency-dependent weights by implementing a multichannel transceiver with adjustable phase and amplitude in each branch. Another configuration of reconfigurable antenna for mobile terminals is presented in [90]. The design is incorporated with a digitally tuneable capacitor (DTC) to provide communication at current allocated spectrum as well as an extended band coverage for future 5G spectrum reallocations.

In [91], novel contribution in reconfiguration mechanism suggests a potential application of graphene. Two multiband designs have been proposed, where first configuration operates at WIFI frequencies (i.e. 2.4, 3.6, and 5 GHz), and the second suggests cellular LTE (covering bands of 1.8, 2.5, 2.6, and 3.6 GHz). The working principle suggests that graphene surface impedance can be tuned by a DC bias, and results in the ON and OFF states of switch at two extreme conditions. This switching mechanism is responsible of modification in the electrical length and consequently determines the resonant frequency of the antenna. The concept is evaluated based on the performance trade-offs. Furthermore, the results show that the proposed hybrid metal–graphene frequency reconfigurable antennas can provide a tuneable bandwidth as well as antenna matching simultaneously. Fig. 2.6 shows the proposed antenna design as well as the impedance bandwidth along with the mechanism of reconfiguration.

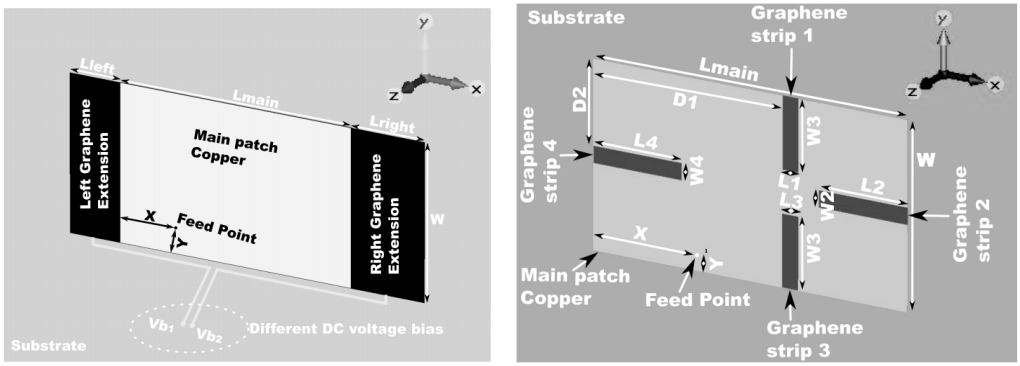

(a) (b)

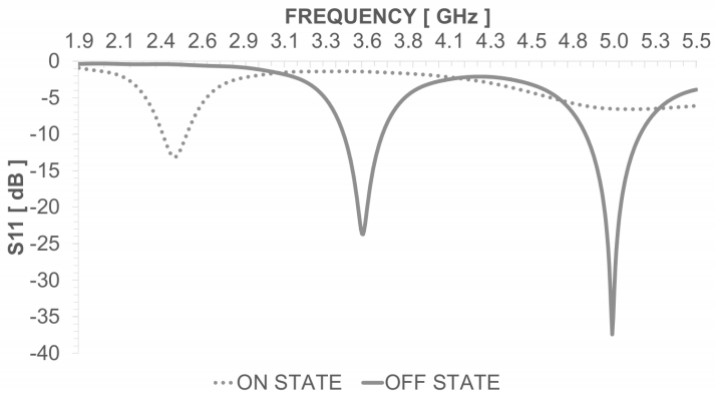

(c)

Figure 2.6: Graphene-based frequency reconfigurable antennas (a) Schematics at WIFI applications, (b) Schematics at LTE applications, (c) S_{11} plot at two switch configurations [taken from 91].

2.6.2.3 Reconfigurable Antennas for 5G Networks

In [92], a pattern reconfigurable antenna is proposed for 5G handset devices covering 36–40 GHz. The designed structure is a multi-antenna system consisting of RF switches and a reconfigurable power divider capable to excite one or multiple antennas based on system's requirements. The versatile combination of antenna excitation provide fifteen different radiation patterns to facilitate the functionality of 5G mobile handsets. A polarisation reconfigurable MMW antenna suggested in [93] for future 5G applications. As shown in Fig. 2.7 (a) and (b), the antenna design incorporates a cost-effective 3D printed polariser, which can be rotated to change the polarisation state from linear to

circular or from circular to linear. The proposed antenna offers a wide bandwidth with lower insertion loss and high gain up to 16 dBi. In two modes of circular polarisation, the antenna achieves an axial ratio (AR) bandwidth of 30% and a gain of 15 dBic as shown in Fig. 2.7 (c) and (d); while for the linear polarisation, the antenna bandwidth is 50% with the gain of 16 dBi as shown in Fig. 2.7 (e).

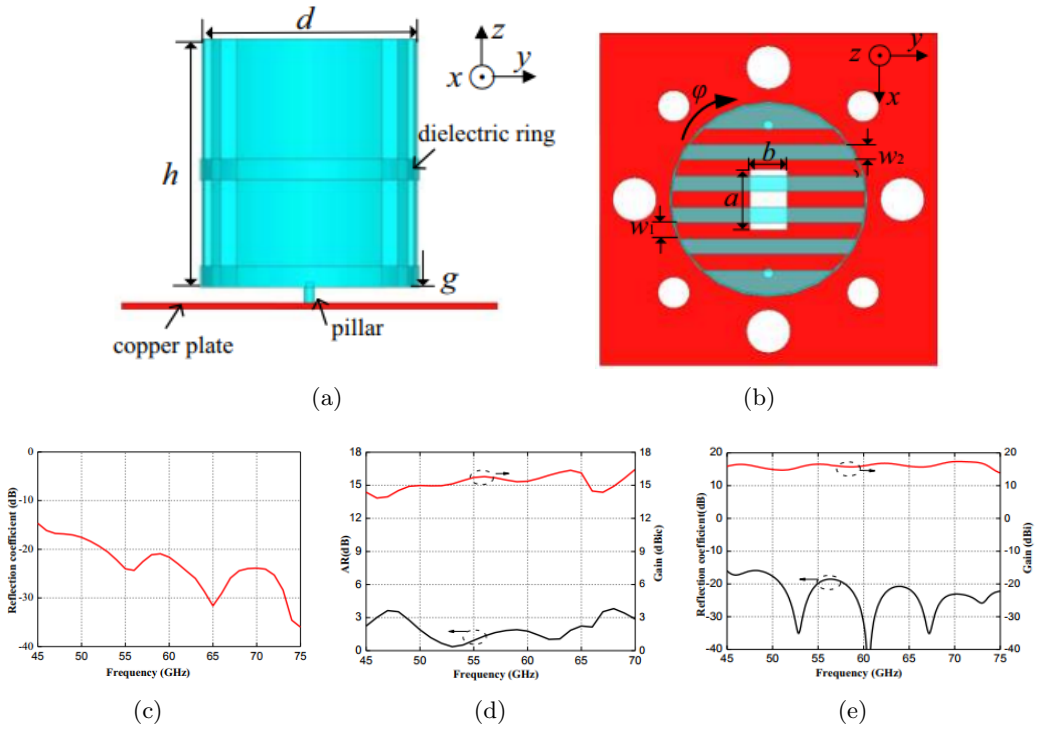

Figure 2.7: Polarisation reconfigurable antenna: (a) Side view, (b) Front view, (c) S_{11} at CP mode (d) Gain at CP mode, (e) S_{11} and gain at LP mode [93].

Fig. 2.8 (a) shows a quasi-Yagi patch antenna proposed in [94], which operates at high attenuation band of 60 GHz. The antenna offers a high bandwidth of 55–65 GHz with a radiation pattern reconfiguration of +20° to -20°. Another antenna design suggesting pattern reconfiguration for 5G communications is presented in [95]. A reconfigurable parasitic layer technique is employed comprising of a driven dipole antenna placed along the central axis of a 3D hexagonal prism-like structure of parasitic layer surrounding it. PIN diodes are used to reconfigure the geometry of the parasitic surface. The antenna offers a bandwidth of 4.8–5.2 GHz, and capable to steer the beam in both the azimuth (0°

$\leq \phi \leq 360°$) and elevation planes (-18° $\leq \theta \leq$ 18°). A phased array antenna solution with beam steering capability at 28 GHz for 5G cellular networks is presented in [96]. The arrangement comprises of four identical ultra-thin quasi-Yagi sub arrays along the edges of the mobile handset. The direction of coverage could be reconfigured by switching the feed of the desired sub array. The antenna offers high-gain and efficiency. An aperture-coupled magneto-electric (ME) dipole antenna is presented in [97] for 5G applications. The antenna is designed to reconfigure switches states between square patches and an additional strip of the ME dipole, which results in reconfiguration among linear and two circular polarisation states. The peak gain of 8.2 dBi and a radiation efficiency of 85% are achieved in the proposed antenna design.

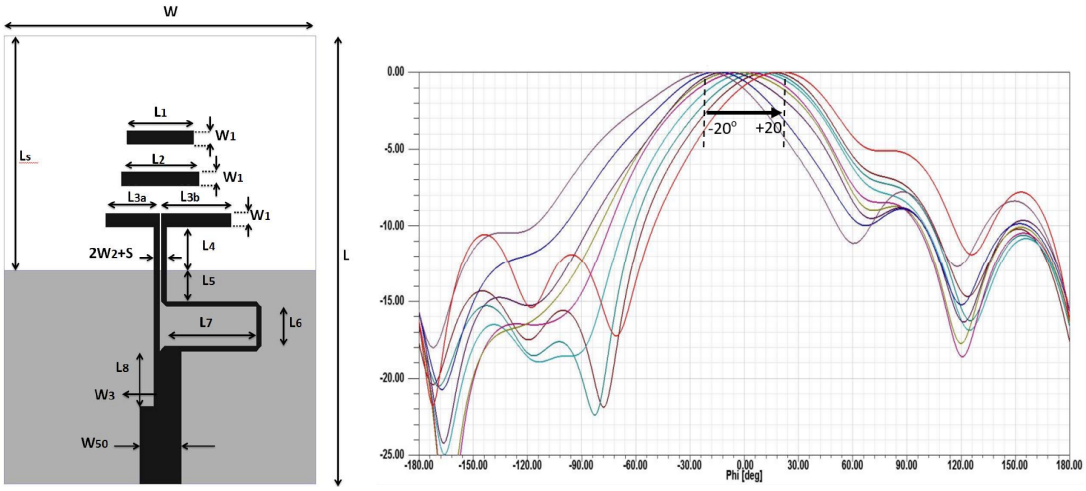

(a) (b)

Figure 2.8: Proposed MMW antennas: (a) Quasi-Yagi pattern reconfigurable antenna, (b) Beam steering from +20° to -20° at the step size of 5° [94].

2.6.3 High Gain Antenna Arrays for Cellular Networks

Patch antennas offer several advantages of planar structure, lightweight, low profile, and low cost of fabrication. However, there are some limitations like low bandwidth and low gain of a traditional patch antenna geometries. To improve the antenna performance, various methods have been developed. Antenna arrays are well-known for improving

the gain performance by collimating the individual radiation of antennas in a combined beam with high gain. Compact size and ease of fabrication make the microstrip antennas suitable to be deployed in the array assembly. Antenna arrays are also occasionally combined with other techniques for further improvement. For instance, antenna performance is fairly enhanced by using air as a substrate, or cavity-backed patches [98–100]. In [98] a circularly polarised array is proposed where dielectric loss is reduced by using air as dielectric. It is observed that the arrays comprising of 4, 16, and 64 elements constitute peak gains of 15.3, 21, and 25.4 dBic, respectively. In [99], cavity backed patch antenna is used to establish an array configuration to achieve relatively high bandwidth and efficiency. An efficient high gain 2×2 array is proposed in [100] by using multilayer structure comprising of air dielectric and parasitic patches. The efficiency of array is approximately 80% with the peak gain of 14.9 dBi. Another patch loaded with slot antenna for circular polarisation is proposed in [101] where the parasitic patch improves the antenna gain. Desired bandwidth profile could be achieved by insertion of slots, which can effectively generate a multiband response. U-shaped slots are embedded on the patch geometry in [102] to achieve a multiband antenna. Moreover, radiation efficiency is improved by means of metamaterial [103], also by using multilayer substrates deployed in antenna array demonstrated in [104]. Another array design for high gain mobile satellite communication applications is proposed in [105].

2.6.3.1 Millimetre-wave Arrays for Future 5G Networks

MMWs offer much shorter wavelength than the sub-6 GHz bands, which permits compact antenna sizes and can fit a massive number of antenna elements within a small area. This efficient utilisation of space enable MMW antennas suitable for integrated circuitries in smart phones and many other wireless devices. High-gain MMW antenna arrays can easily manage transmission of multi-Gbps over short indoor distances. A considerable amount of work has been reported to discuss the feasibility of utilising multiband antennas designed at MMWs for effective operation in potential 5G bands. A MMW antenna

with broadband (i.e. 20–40 GHz) as well as dual-band mode of operation covering 28 and 38 GHz is suggested in [106]. The antenna gain is 4 dBi in the broadband mode, and 3.5 and 4.5 dBi at 28 and 38 GHz, respectively in the dual-band mode.

Fig. 2.9 shows a 7-element microstrip linear antenna array designed with a stacked arrangement of parasitic patches at 28 GHz. A high gain of 14.71 dBi and a side-lobe level of 18.81 dB is achieved at 28 GHz [107]. A 4-element antenna array based on substrate integrated waveguide (SIW) structure is designed to achieve high gain and a dual band response in [108]. The peak gain profile suggests 11.9 and 11.2 dBi at 28- and 38- GHz, respectively. Another work presents a 4-element, dual-band, printed slot, antenna array with gain of 10.58 dBi at 28 GHz, and 12.15 dBi at 38 GHz [109]. In [110], a versatile fixed-beam grid array structure at 28 GHz band for 5G cellular applications has been reported. The operating range of 23.8–31 GHz, radiation efficiency of 86.27% at 28 GHz, and a peak gain of 12.7 dBi at 29.2 GHz are distinct features, as well as the design is also embedded on 30 × 50 mm^2 PCB board to address the performance after the antenna placement on the cellular phone's body.

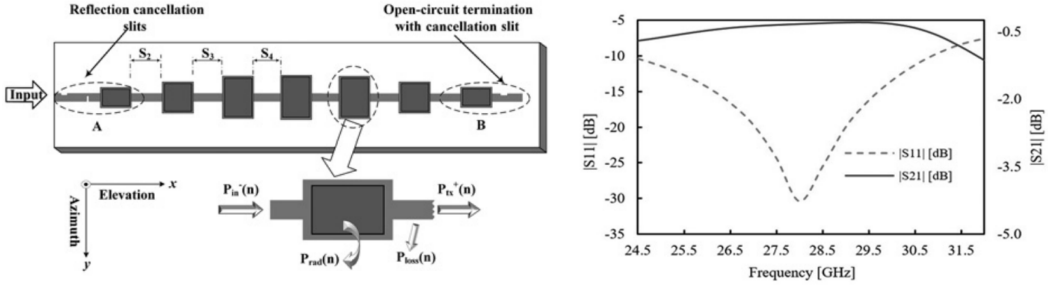

(a) (b)

Figure 2.9: Linear antenna array with stacked parasitic patches: (a) array design, (b) S-parameters of the proposed antenna array [107].

A broadband antenna array comprising of four elements and provided with an electromagnetic bandgap (EBG) ground structure-feeding network, is presented in [111]. High bandwidth is attained in the proposed structure at the expense of high design complexity and large array size. This tapered slot configuration of antenna array offers an end-fire radiation pattern, where a peak gain of 20 dBi is achieved at 30 GHz. Moreover,

another EBG ground based array prototype is developed in [112] where four circular dense dielectric (DD) patches are assembled in an array, as shown in Fig. 2.10. The impedance bandwidth of 27–32 GHz and beyond is achieved targeting 5G cellular applications. Yet the biggest drawback of this structure is its high complexity due to Wilkinson power divider and stacking of multiple layers. Moreover, the radiation efficiency of the designed structure is also relatively low.

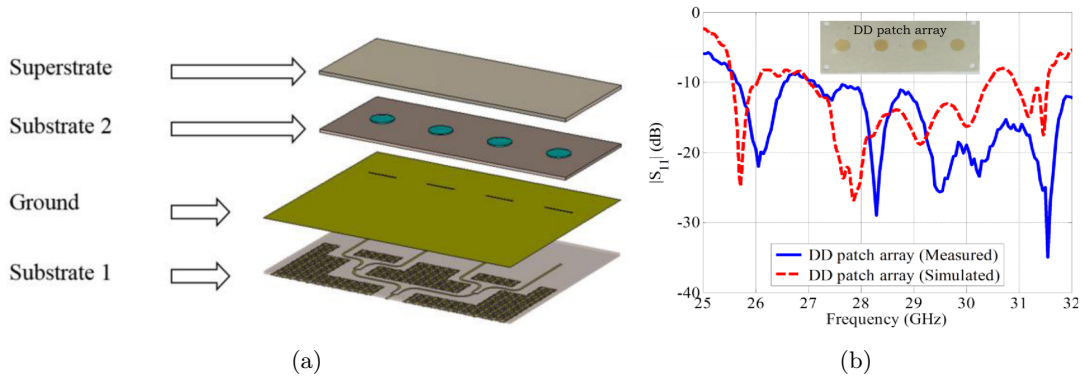

(a) (b)

Figure 2.10: EBG based DD patch antenna array: (a) Multilayer antenna model, (b) Simulated and measured S_{11} plots of the array [112].

Mutual coupling between adjacent antenna elements is of high importance in the array design process as it determines the antenna performance, i.e. the lower the mutual coupling the better the overall system's performance [113]. Many techniques have been developed to reduce mutual coupling in the closely packed array geometry. Defected ground structure (DGS) is capable of reducing mutual coupling effects and widely used in filters, amplifiers, coplanar waveguides, and antennas for this purpose [114]. DGS is famous for size reduction of the RF components, bandwidth improvement, gain enhancement, and capable of suppressing higher order harmonics as well as unwanted crosspolarisation [115, 116]. DGS technique mainly works on hit-and-trail method of introducing different shapes in the ground plane. The dimensions of DGS are then optimised based on the frequency of interest, the required bandwidth, or desired application [117, 118]. A 2 × 2 planar array comprising of aperture-coupled antennas is suggested for 5.8 GHz operating frequency in [117]. DGS structures of dumbbell-like shape are introduced in antenna

ground for back radiation reduction. A recent contribution is a novel antenna array of 4×4 elements, suggested in [118] to operate at 28–38GHz for 5G mobile networks. Fig. 2.11 presents the designed geometry of array comprising of corporate feeding network integrated on the same side of substrate. Radiation performance of array is improved by introducing a c-shaped DGS, which is also responsible of improving radiation efficiency by 17.14%. Moreover, the impedance bandwidth is increased to 69.2% and the realised gain is increased by 2.44 dBi due to DGS.

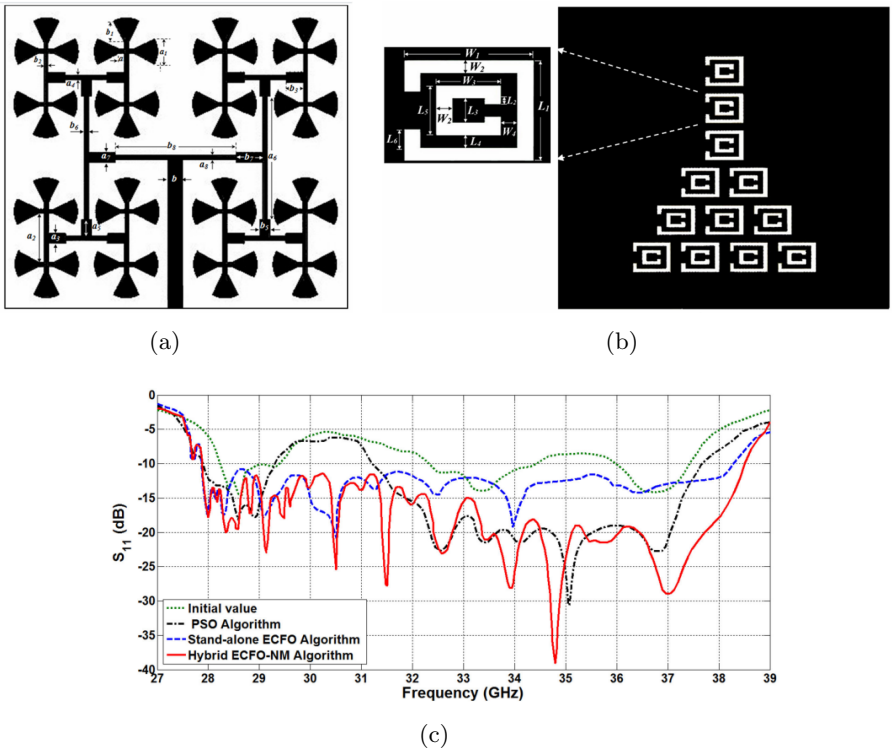

Figure 2.11: 4 × 4 DGS based array: (a) Top, (b) Bottom, (c) S_{11} plots [118].

The key challenges of 5G, the associated antenna requirements and on-body radiation effects of MMW antennas are discussed in [119]. A 32-element antenna is suggested for a cell phone to achieve a nearly spherical coverage. The proposed geometry consists of two arrays each containing sixteen elements, allocated on top and bottom edges of the cell phone with the slant of 50° at the corners of the PCB. The antenna operates at 28 GHz and offers a directional fan-beam radiation pattern. In addition, a human head phantom is included in simulation to compute specific absorption rate (SAR).

2.7 Fabrication Considerations for MMW Antennas

Planar antennas are the most attractive choice in integrated circuits and cellular devices due to their compact and robust structures. Designing and incorporating MMW patch antenna in a cellular device could be very demanding, and require precise analysis of necessary considerations. A number of factors that can affect the antenna performance such as, choice of a substrate, the accuracy of fabrication method, reliability and robustness of the fabricated prototype. Some of these issues are briefly discussed here:

2.7.1 Choice of Substrate

Conventional patch antennas are planar structures, and require a dielectric substrate material usually provided with a conductive patch and a ground at the top and bottom surfaces of the substrate respectively. Choice of a substrate is very instrumental as the antenna design is highly dependent on substrate properties. Several rigid substrate including FR4, Rogers RT/Duroid and Taconic are available in the market with the desired range of permittivity and low-loss characteristics, suitable for antenna design at MMW frequencies. Numerous structures are reported in the literature for cellular antennas and wireless devices by using the above-mentioned rigid substrates because of the availability and low cost. Furthermore, flexible substrates are also point of interest to provide an ease of antenna integration on a non-planar or conformal surface, which enables the antenna to be integrated into wearable devices to perform on-body communication, which is cost-effective. Different types of flexible films are commercially available varying in thickness, coating, texture and dielectric constant and a best possible selection can be made depending on the demands of antenna design [120, 121].

Paper based substrate is one of the common choices among the ultra-thin, inexpensive and flexible substrates suitable for antenna design. Many other textile-based materials such as cotton, jeans, and leather are also used in wearable antennas. Synthetic polymers such as LCPs, Kapton sheets, polyurethane (PU) coated stretchable textile

and pre-treated 65/35 polyester/cotton textile (PET film) have been used in flexible antenna design [122]. PET is a very useful thermoplastic polymer resin belongs to the polyester family, and is widely used in the manufacture of synthetic fibres, food containers, thermoforming applications, and engineering resins often combined with glass fibre. Depending on its mechanical and thermal properties, PET exists both as an amorphous (transparent) and as a semi-crystalline polymer. The semi-crystalline material is usually transparent (particle size $<$ 500 nm) or opaque and white (particle size up to a few microns). Its appearance is generally dependent on its crystal structure and particle size [123]. PET films are available with varying permittivity and loss tangent offering the advantages of low cost, high flexibility, harmless to human body and resistive towards environmental effects. PET has been implemented as an antenna substrate in many reported research articles [123–125].

2.7.2 Fabrication Processes for MMW Antennas

The size compactness at MMWs requires a high fabrication accuracy, as the radiating length is directly proportional to the resonant frequency and any error in dimensions due to fabrication can shift the resonant band. There are several manufacturing methods such as inkjet printing, photolithography, etc. to precisely manufacture compact structures operating at high frequency, and some of these processes are discussed here.

A. Inkjet Printing

Printed circuit technology has evolved as a low-cost, fast and precise way of antenna fabrication on flexible substrates and well suited for mass production [126–128]. Advanced high-resolution inkjet printers are capable of depositing ink droplets of a size of few pico litres and therefore, compact fabrication provided with tiny details can be realised accurately. The earliest inkjet printers were based on continuous stream mode in which the printheads incorporated with a single jet ejects a continuous flow of air-drying or heat-cure ink. Continuous inkjet is a high-speed printing technology but lacks high-quality

printing. Recent inkjet printers are equipped with drop-on-demand printing technology in which a piezo or thermo-component is integrated in the printhead of the printer to generate pressurised pulses to control the ink discharge from the nozzle. Most of the modern printed electronics manufacturers utilise the piezo pulse-type equipment [121].

Several types of conducting inks are available in the market for inkjet printers [128]. Inkjet printing involves three basic steps; printing, sintering and characterisation. Printing is done by a printer consisting of a set of nozzles provided with conductive ink and an automated system, where the printer provides a freedom to the user to control the jetting of ink, feature size and resolution, thickness of the printed layer, drop spacing and accuracy of the printed pattern. Dimatix Materials Printer (DMP) is one of these printers designed to achieve the accuracy of up to 50-μm. Jetting frequency, temperature of the nozzle and plate, voltage waveform, drop spacing and several other parameters are adjusted to achieve desired printing quality. Conductive inks based on silver or copper nanoparticles are available with variable viscosities and conductivities. The ink composition is very important as the viscosity and conductivity of nanoparticle ink are directly related to the number of nanoparticles in the net volume of ink.

After printing, the next step is to sinter the printed pattern. Sintering is the process of breaking the sheath of polymer to release the encapsulated conductive nanoparticle. The conductivity of the printed layer increases after the sintering process. Laser sintering and heat sintering are two most commonly used methods, where high-energy laser beam or heating at high temperature will melt the polymer coating and the conductive ink particle. The molten ink particles combine together to form a layer of metal. Laser printing is time efficient with a risk of defects if the intensity and time of exposure are not well regulated. Heat sintering requires curing of the samples in a heating oven at the set temperature for several minutes. Temperature and time of exposure are key parameters that determine the desired conductivity. Unusually, the conductivity of printed layer is smaller than the actual conductivity of metal because of very thin layer deposition of approximately 0.5 μm. The conductivity can be improved by successive printing and

sintering of multiple layers to enhance the thickness of a printed layer. Another way of sintering the printed layers is by chemical treatment. Specialised surface treated films are commercially available provided with a micro coating of sintering chemical at the surface of the film. This micro-porous coating speeds up the process of drying and chemically reacts with the polymer coating of nanoparticle to dissolve it and provides a conductive layer. The third step is to characterise the deposited pattern in terms of conductivity, surface roughness etc. and crack analysis is performed in case of bending to analyse the potential of the print towards conformal structures. The complete inkjet printing process from layer deposition to characterisation is demonstrated in Fig. 2.12.

B. Photolithography

Photolithography is the process of transferring the pattern with the help of light and usually referred as light writing [131]. A single iteration of the process involves several steps and requires specialised clean rooms to avoid contaminations. The first step involves cleaning the wafer/substrate with a wet chemical treatment such as acetone or methanol. The substrate is heated on a hot plate to remove the residuals of cleaning chemical. Then the photoresist is applied by spin coating where the number of

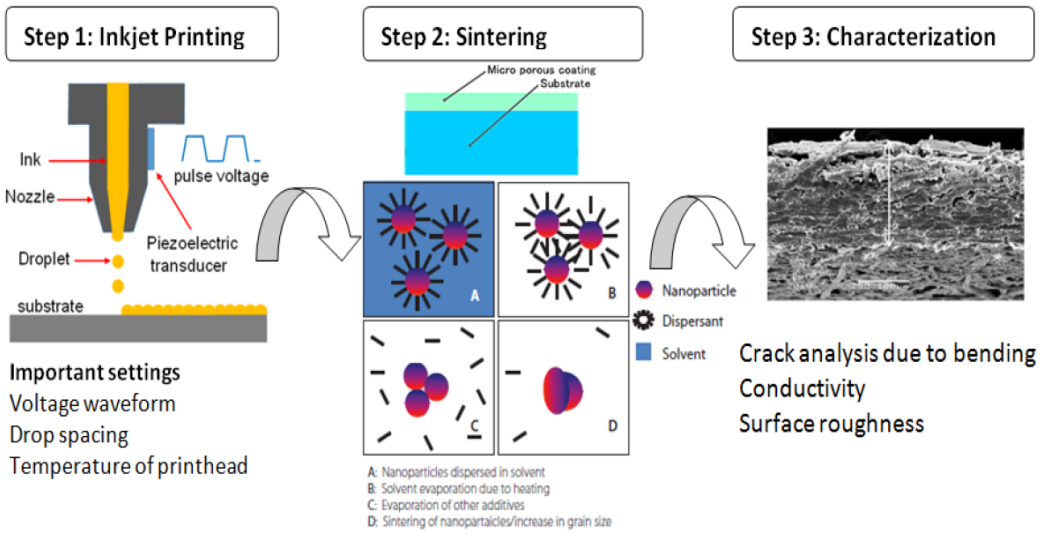

Figure 2.12: Inkjet printing process for the fabrication of MMW antennas and circuitries [taken from 129–130].

spins controls the thickness of the deposited layer followed by baking of the substrate. Temperature, viscosity of a photoresist, time intervals and spinning speed are important parameters to control at this stage. After this, the photoresist is exposed to intense light by means of a specified mask to make a certain pattern of photoresist dissolvable in some special solvents. The process is called developing of photoresist in which the exposed light changes the properties of photoresist and makes it soluble in the solvent. The sample is hard-baked to solidify the remaining photoresist, which then acts as a mask to expose desired area of substrate for ion implantation, vaporisation, sputtering or plasma etching. The layer of metal is deposited and the photoresist mask is removed afterwards leaving behind the desired pattern. The photolithographic process of fabrication of small circuitries and antennas can achieve high degree of accuracy. Antennas at MMWs with requirements of precise manufacturing are often fabricated by photolithography and this technique is applicable on both rigid and flexible substrates.

C. Laser Milling and PCB Prototyping

Electronics circuits and antennas are usually fabricated by using PCB milling machines provided with an automated system (consisting of mill/drill/router bits) to remove copper in a particular pattern from the surface of copper cladded PCB board. This technology has been advanced by implementing extremely precise UV laser source to direct a beam for etching-off copper instead of metallic tools. The laser beam avoids the use of hazardous chemicals, needs no masks and holds minimum expense of manufacture. The laser probe in such machines works contact-free from an appropriate height above the substrate and therefore can be easily employed on sensitive materials. These laser-milling machines are highly efficient in prototyping on metal-laminated sheets of both rigid and flexible substrates and provide fast and reliable fabrication with high accuracy [132]. A wide variety of rigid and flexible substrates with quite a large variation in the thicknesses of substrate and copper cladding are commercially available and can be used directly in laser milling machine to achieve precise fabrication of MMW antennas.

2.8 Summary

Wireless standards have experienced a drastic progress, and in 4G LTE several devices are interconnected to provide an ultra-fast, high-speed and efficient communication to its users. It is expected that 5G will be utilising MMW spectrum and according to FCC 28 GHz, 38 GHz and 64–71 GHz are potential candidates, while Ofcom suggests 26 GHz band suitable for 5G. Observations based on several antenna designs proposed on MMW, suggest that antenna should be offering high bandwidth to support high-speed communication, high gain to overcome attenuations, preferably flexible enough to be incorporated in both planar and non-planar geometries; additionally, the antenna should be simple, compact, cost-effective and feasible for bulk fabrication.

A thorough literature review on 5G antenna requirements has been conducted in this chapter followed by the investigation of possible design methodologies to handle challenges involved in designing MMW antennas. High bandwidth 5G spectrum could be accessed by deploying wideband antennas, and throughput could be further enhanced with MIMO antenna systems. Reconfigurable antennas could also be deployed for high bandwidth requirements. Thus, the gain of antenna in reduced while achieving high bandwidth due to gain-bandwidth trade-off. Antenna arrays have been found useful for gain increase, but are usually narrow band. The design of efficient antenna with high gain and bandwidth is highly challenging and one of the major considerations of the 5G evolution. There is a need to extensively exploit the MMWs spectrum and massive efforts are needed to perform the task of an efficient MMW antenna design for 5G. This research contributes in the progress towards the implementation of highly efficient 5G antenna solutions by using advanced antenna techniques at MMWs, which are discussed in the next chapters.

Chapter 3

Wideband Antennas and Multiple-input-Multiple-output Solutions for 5G Applications

3.1 Introduction

The increasing number of wireless devices has raised concerns related to bandwidth scarcity in frequencies below 3 GHz. The communication spectrum is on its threshold limits of maximum utilisation and requires more bandwidth allocation for further upgradation. MMWs are promising candidates to realise the demands of future wireless networks, but there is a need of extensive research and development to transfer the traditional communication on higher frequency bands. Antenna design is a key factor that governs the performance of wireless networks. 5G is defining ways of utilising efficient antenna design techniques at MMWs that are also capable of dealing with the critical limitations of signal fading, path loss, and atmospheric effects. In current wireless systems, MIMO antennas are favourable choice to solve capacity issues without any additional bandwidth or transmitted power. MIMO antennas are capable of delivering

multi-Gbps throughput and can perform an efficient communication at higher data rates [133]. Smaller antenna dimensions at MMWs are an additive advantage of integrating MIMO systems with more antenna elements in the same limited space. It is desired that the 5G antennas should offer flexibility towards MIMO architecture, reliability to achieve high spectral efficiency, as well as lower multipath fading [134, 135].

The integration of wideband antennas in MIMO systems will increase the system's overall throughput. In such systems, each antenna acts individually with much wider channel bandwidth, and the simultaneous functioning of several antennas eventually provides high throughput to drive numerous services. Moreover, high gain antennas are required to deal with the high-frequency attenuations. MMW designers are keen to present high gain and bandwidth antennas with structural simplicity suitable for MIMO systems. Also, the antennas should be compact to be part of handheld mobile devices. Lower mutual coupling and high isolation is required in between narrow-spaced antennas to reduce the effect of adjacent elements in MIMO assembly. Coupling effects can be handled by increasing the spacing between the antennas, which is itself a difficult task due to limited space assigned for antenna placement in the mobile phones. Several articles have suggested ways of lowering the mutual coupling between MIMO antennas [136–139]. MMW based MIMO systems are expected to incorporate much larger number of antennas with reduce mutual coupling due to smaller antenna size.

In this chapter, two novel MMW antennas have been suggested by utilising rigid and flexible substrates. K_a–band is selected for antenna design to cover 28- and 38-GHz for 5G cellular networks. MIMO assembly comprising of four antenna elements in a linear arrangement is also presented and examined in terms of isolation and mutual coupling. The performance suggests that the proposed MIMO antenna is suitable for installation in cellular phones and BSs for 5G communications. Inkjet-printed antennas on flexible films recommend a much faster and low cost fabrication and can lead to mass production, if combined with reel-to-reel process. The potential of inkjet printing on PET has been highlighted for MMW antennas in many articles [140–141]. In the second

proposed design, an effort to develop a MMW antenna on a PET film is made to utilise the idea of printed electronics on flexible films. The conformal geometry of antenna can be mounted on windows and doors as well as can be made part of uniform or clothing.

3.2 Wideband Antennas with Defected Ground Structures

Patch antennas have secured enormous success because of the planar geometry, robust designs, compact structure and ability to be utilised in integrated circuits. The performance of traditional patch geometries is usually affected by lower gain and bandwidth characteristics, and various methods have been developed to overcome these limitations. For instance, one such technique is defected ground structures (DGS), which involves creating a 'defect' in the planar geometry of the antenna ground [142]. These defects are responsible of causing induced perturbations to disturb the uniformity of the metallic ground plane and generate discontinuity in the path of surface currents. These structures are usually designed as symmetrical and well-aligned structures added directly under or on each side of a feed line to allow efficient coupling with the feeding network. DGS acts as resonant gaps and changes the shield current distribution in the ground depending on the shape and size of the defect. This results in a controlled excitation and wave propagation through the antenna substrate and consequently alters the capacitive and inductive properties of the transmission line.

It has been observed that the presence of DGS in the ground plane increases the effective capacitance and inductance and generate resonances in a multiband antenna [143], or can also enhance the band notching capability of an antenna or a filter [142, 144]. The resonant bands of DGS based antenna can be adjusted on suitable frequency by appropriate selection of defect geometry and position. A number of wideband and multiband antennas have been developed by employing DGS as symmetrical/asymmetrical arrangements, single/periodic structures [145–147], and also incorporated as slots/apertures within the radiating patches or ground plane [148, 149]. Majority of the reported DGS

based antennas are presented for low frequency or single band MMW operation [150], and further exploitation of DGS concept is needed for MMW wideband operation.

This chapter presents a novel wideband DGS-based geometry of MMW MIMO antenna for high capacity demands of 5G networks. Split-ring slots are loaded as DGS in the bottom ground to create additional resonances. The MMW antenna offers high bandwidth without any compromise in gain and efficiency. Another design of MMW antenna is demonstrated on a flexible substrate and covers K_a–band (26.5–40 GHz) with reasonable gain. The antenna design incorporates DGS as symmetrical slots into a T-shaped patch, which is positioned inside the rectangular aperture cut into the ground. The major differences in both of the proposed MMW antenna designs are, first design incorporates symmetrical DGS slots in the ground plane and has been designed for rigid substrate (Rogers RT/duroid), while the second antenna implements symmetrical slots into the patch geometry and uses a flexible substrate to add conformity.

3.3 K_a–band Antenna with Defected Ground Structures

3.3.1 Antenna Design and Fabrication

The antenna is designed to fulfil the requirements of high bandwidth which covers 28- and 38-GHz bands, reasonable gain above 4 dBi, design simplicity that avoids multilayer-stacking, vias or complex feeding, and ease of integration in MIMO configuration due to lower mutual coupling with transmission coefficient below -20 dB. A systematic antenna design consisting of T-shaped patch provided with coplanar waveguide (CPW) feed is proposed, incorporated with the DGS at the bottom ground of the antenna. Rogers RT /duroid 5880 ($\varepsilon_r = 2.2, tan\delta = 0.0009$) of dimensions 12.0 $\times$ 12.5 $\times$ 0.8 mm^3 is selected as a substrate due to its low-loss characteristics. Antenna patch is designed on the top surface of the substrate and a partial ground loaded with two iterations of slots is constructed at the bottom. The design procedure is initiated with a simple

CPW-fed T-shaped patch designed for a single frequency operation. For the purpose of bandwidth improvement, the bottom ground is then modified as a partial ground plane. Split-ring slots each of width 0.2 mm are periodically loaded in the bottom ground as DGS to alter the current distribution in the ground plane. Computer Simulation Technology (CST) Microwave Studio software is used for antenna designing, modelling, and parametric study, as well as analytical evaluations. CST is regarded as a reliable tool in order to design, analyse and optimise performance, electromagnetic compatibility and signal/power integrity in RF and microwave components and devices.

The first iteration is initiated by incorporating a slot along the terminating edge of partial ground exactly in the centre, which couples directly with the top layer radiating patch and feed line. Two more slots are also positioned along the edge of the ground on either sides of first slot at an optimised distance 'r', as shown in Fig. 3.1 (b). The numerical estimation of the designed structure indicates that the radiating slots are responsible of generating resonances at this point. Second iteration of integrating slots is carried out for further improvement in resonant response. Two split-ring slots are loaded at diagonal arrangement and equidistant to slots of first iteration, though truncated in the opposite direction to conserve the design symmetry.

The proposed slot arrangement acts as DGS and introduces disturbance in the mean current paths at the ground plane. The surface current distribution in the bottom ground is altered due to these slots and results in multiple resonances. Slot width, ring diameter, the fraction of ring to be split and position of slots are important factors, which govern the impedance bandwidth of the proposed antenna. Multiple resonances accomplished by insertion of DGS are combined under a continuous bandwidth due to the partial ground. Antenna fabrication is carried out by LPKF milling machine, and 35 μm thick copper cladded substrate is used for the prototyping. Jyebao K–connector (K864N5–00AB) is selected for measurements due to its thinner inner conductor pin compatible with smaller dimensions of the transmission line. Fig. 3.1 (c) presents the fabricated prototype and Table 6-B illustrates the design dimensions of the proposed MMW antenna.

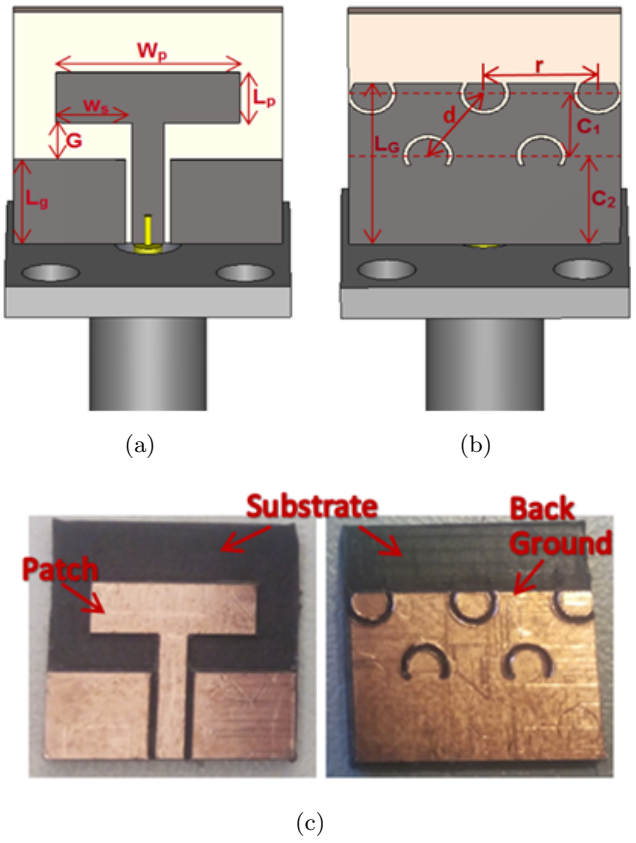

Figure 3.1: A MMW DGS-based antenna: (a) Top view; (b) Bottom view, (c) Top and bottom views of fabricated prototype.

Table 3-A: **Optimised Dimensions of MMW Antenna with DGS**

Parameters	**Symbols**	**mm**
Patch width	W_p	8.0
Patch length	L_p	3.1
Width of one side	w_s	3.3
Gap	G	1.9
Length of CPW ground	L_g	4.35
Length of partial ground	L_G	8.35
Distance between two centres	C_1	3.25
Distance from centre 2 to edge	C_2	4.6
Gap between adjacent slot centres	r	5.0
Diagonal gap between slot centres	d	4.1
Radius of each slot	R	0.9

3.3.2 Results and Discussion

The antenna performance is investigated based on the S-parameters, radiation patterns, realised gain, and radiation efficiency. Parametric analysis is carried out in software to attain the optimised coordinates for the placement of split-ring slots. The effect on the mean currents due to slot loading is inspected from the current density plots. It is observed that measurements show a good agreement with the numerically estimated results. Negligible variances between the simulated and measured results could be due to the variations in substrate properties at high frequency, connector mounting errors, and unavoidable fabrication tolerances. However, the differences are insignificant and do not cause substantial deviation from the proposed response of the MMW antenna.

A. Impedance Bandwidth

Fig. 3.2 (a) depicts the results of proposed antenna based on numerical evaluation and experimental work. The S_{11} plot of fabricated prototype shows the measured bandwidth of 25.1–37.5 GHz at a reference of –10 dB. A slight shift is observed in measurements towards lower frequencies due to fabrication intolerances. Fig. 3.2 (a) also shows the bandwidth with and without DGS incorporation in the design, which validates the claim of additional resonances due to DGS. Parametric analysis of the design parameters is performed in the simulation, and only the analysis involves optimised slot placement for attaining desired bandwidth is presented at this point. The distance between the axes of orientations of split-ring slots' centres while performing the second iteration needs to be adjusted to realise optimal coupling between the slots at the bottom and the feed on the top surface of the substrate. Optimisation of the position of slots is carried out to attain an operating bandwidth of 12.4 GHz. The analysis of C_1 in Fig. 3.2 (b) shows optimised distance of 3.25 mm between slots' centres of two iterations (C_1).

B. Radiation Characteristics

Near-field scanning set up (i.e. NSI Near-field scanner) has been used which mea-

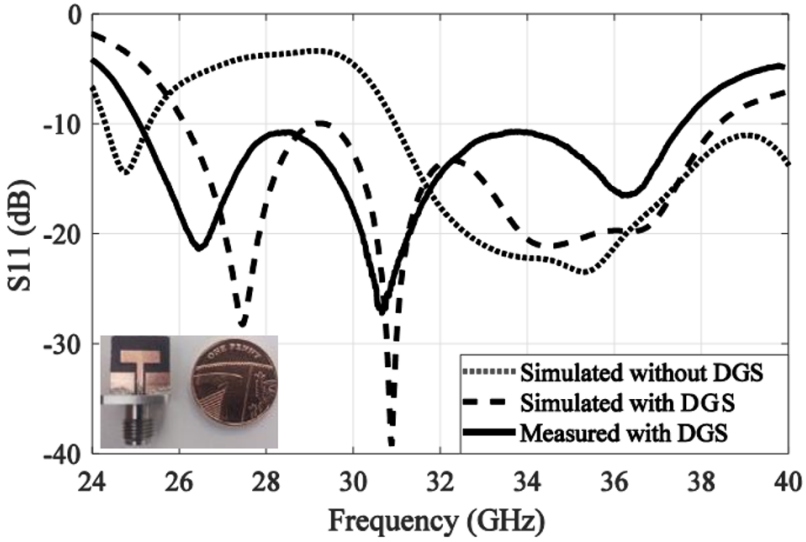

(a)

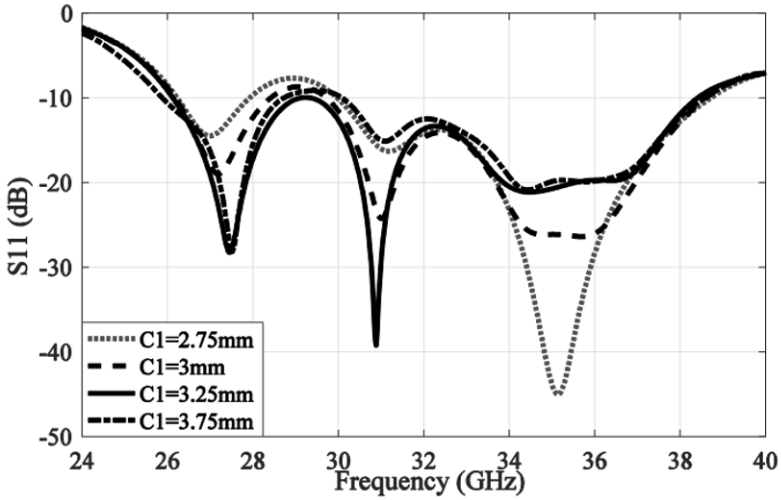

(b)

Figure 3.2: Impedance bandwidth of MMW DGS based antenna: (a) Simulated and measured S_{11} plots, (b) Parametric analysis based on C_1.

sures the radiation characteristics of the antenna under-test by means of a scanning probe placed in its near-field region. The set up is equipped with a precise near-to-far-field algorithm which computes the far-field radiation pattern by deploying the near-field results. It is observed that the maximum radiation of the antenna is in broadside direction; however, somewhat tilted towards end-fire direction due to presence of CPW ground

on top surface acting as a reflector to tilt the beam. Simulated and measured normalised radiation characteristics at distinct frequencies of bandwidth at $\phi = 0°$ and $\phi = 90°$, show the close agreement as presented by dotted and solid lines, respectively, in Fig. 3.3.

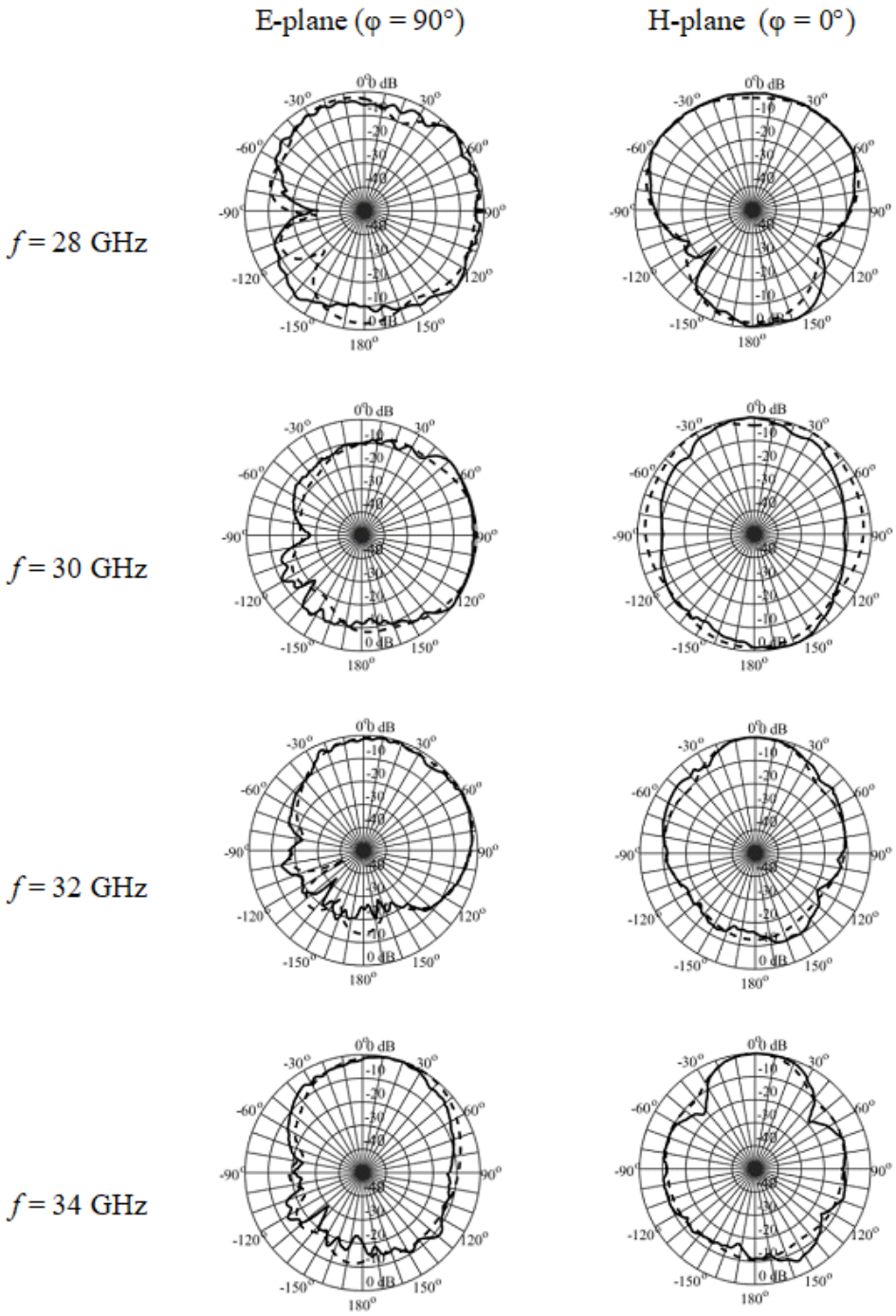

Figure 3.3: Normalised radiation patterns of MMW DGS based antenna at distinct frequencies of the bandwidth.

C. Realised Gain and Efficiency

Measurement results show similar gain profile as estimated in the simulations, though gain plot is also experiencing the same slight shift as observed in S_{11} plots. The plot in Fig. 3.4 validates that the measured gain is 5 dBi or above in complete range of 25.1–37.5 GHz, and the peak gain is 10.6 dBi at 36 GHz. In addition, the numerically estimated efficiency of the single DGS based antenna is above 80% which justifies high performance claim of the designed prototype.

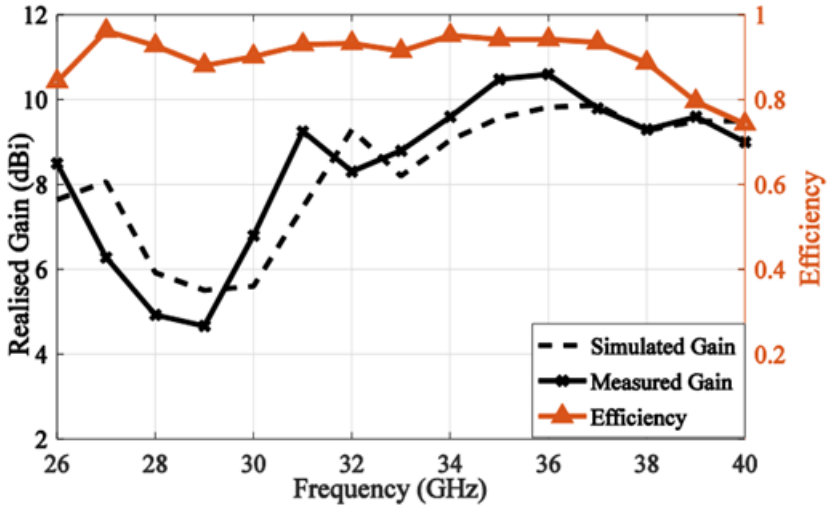

Figure 3.4: Simulated and measured realised gain and numerically estimated efficiency of MMW DGS based antenna.

D. Current Density

Although it is significant to examine the surface current distribution in the complete operating range to comprehend the radiating response of designed antenna, but for the simplification of the analysis the current distribution only at 36 GHz is presented in Fig. 3.5, where the antenna gain is maximum. It is observed that the current density is higher at the DGS slots' edges then the radiating patch which validates the radiating response of slots. The radiating slots also demonstrate the high coupling with the feed line, which generates added resonances as additional bands. These resonances are eventually combined in a wide bandwidth by the partial ground.

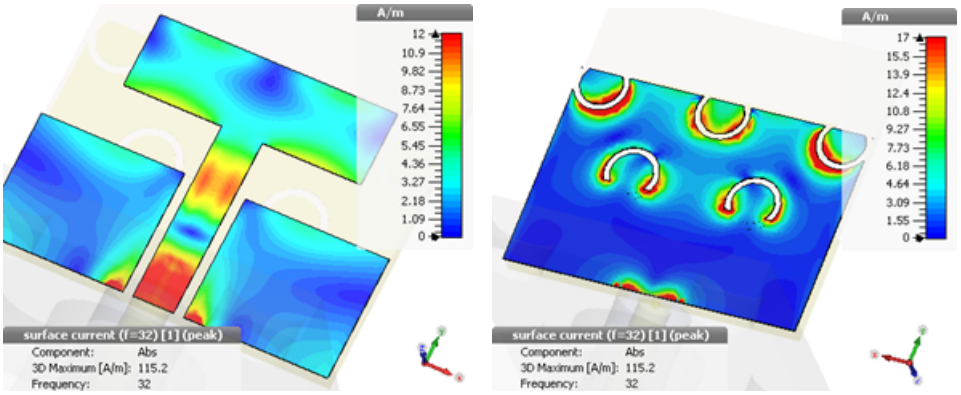

(a) (b)

Figure 3.5: Surface current distribution of MMW DGS based antenna: (a) Top surface; (b) Bottom surface.

3.3.3 Design and Fabrication of MIMO Antenna Array

The suggested MMW antenna design is further proceeded with the developement a four-element MIMO array configuration to be integrated in cellular BS units, as well as PCB layouts of a number of wireless devices. All the four antennas have been designed and fabricated on a single substrate of dimensions (L × W) 12 × 50.8 mm^2. The antennas are positioned in a linear arrangement as recommended by the conventional array design which requires minimum spacing between the patches 'S', that should be $\lambda/2$ or more (i.e., to reduce mutual coupling). Based on the width of the selected K–connector which is 12.7 mm, the antenna width is deliberately increased from 12 mm to 12.7 mm so that the same K–connector assembly can be implemented for measurement purposes. This modification makes sure that all the four connectors can fit adequately on a single substrate comprising of four antennas. It is worth noting that only the substrate width has increased in this case, while all other dimensions of patch and ground remain intact. This placement approach delivers a segmented ground structure by creating a gap of 0.7 mm between adjecent antennas, as top or bottom ground of adjacent antennas are not connected together. Each antenna works individually, therefore, the overall return loss profile of the antenna remain conserved. This also increases the spacing between two neighbouring antennas, and thus improves the isolation characteristics of the proposed

MIMO configuration. Fig. 3.6 (a–d) demonstrates the layout and prototype views of the suggested MMW MIMO antenna array.

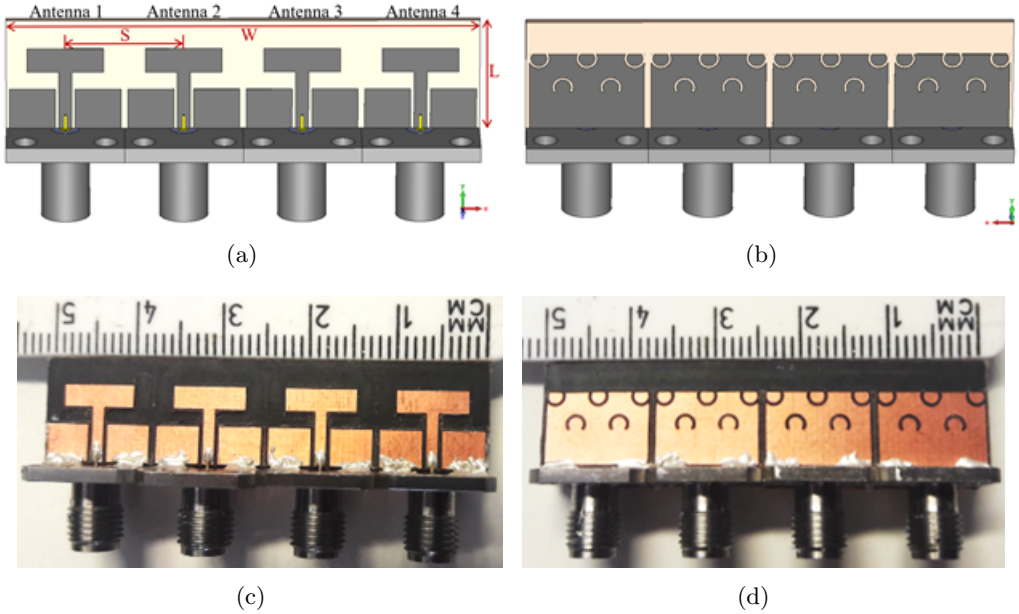

Figure 3.6: MMW DGS based 4-element MIMO antenna array: (a) Simulated model top; (b) Simulated model bottom; (c) Fabricated prototype top, (d) Fabricated prototype bottom.

3.3.4 Characterisation of MIMO Antenna Array

In this stage of evaluation, the performance of the proposed 4-element MIMO antenna array is analysed by investigating the *S*–parameters characteristics including reflection and transmission coefficients. The proposed bandwidth of each individual antenna is provided along with the isolation between the adjacent elements of the MIMO array. The functioning of MIMO as a multichannel unit as well as the impact of one element on the adjacent elements is demonstrated based on the surface current distribution.

A. *S*–parameters

The measured reflection coefficients of the designed MMW wideband antenna and its MIMO array topology are presented in Fig. 3.7 (a). The results show similar profile for all the four antenna elements constituting the bandwidth of 25.1–37.5 GHz with -

10 dB reference, and cover a complete K_a–band with -6 dB reference. It is essential to ensure the isolation below -10 dB among the array elements to lower the mutual coupling for the satisfactory performance of the MIMO configuration. The measured results of transmission characteristics, which determines the isolation between the elements are presented in Fig. 3.7 (b). It has been observed that the mutual coupling between two adjacent elements is significantly lower, as the transmission coefficients are below -22 dB that confirms a good isolation among the array elements.

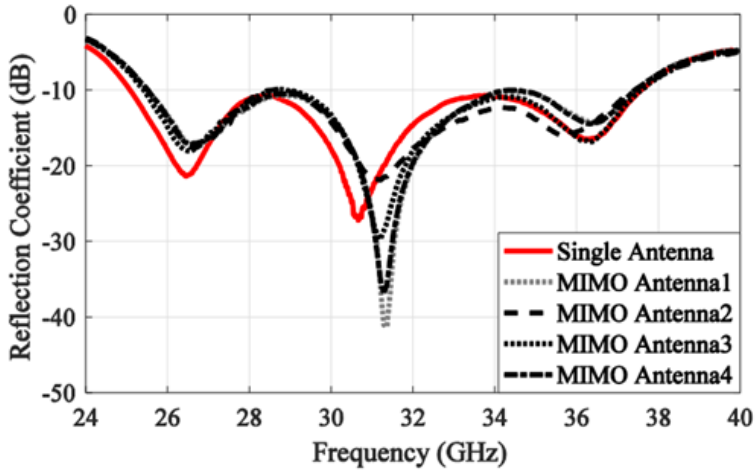

(a)

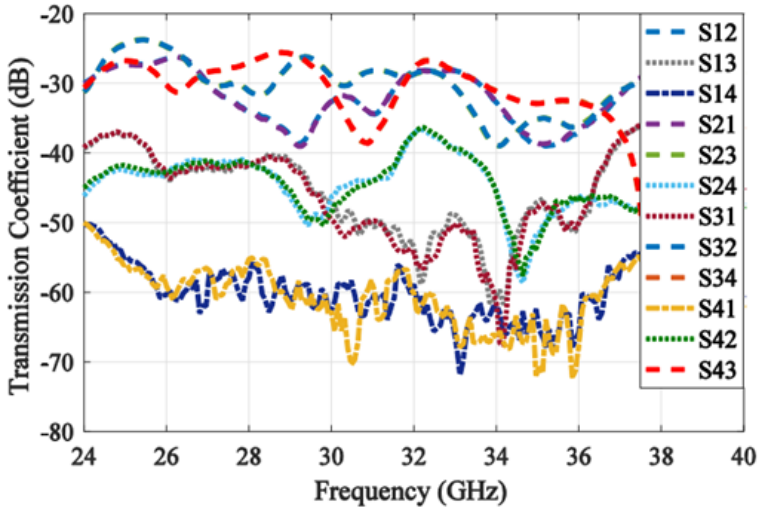

(b)

Figure 3.7: S–parameters of MMW DGS based 4-element MIMO antenna array: (a) Reflection coefficients of individual antenna elements; (b) Transmission coefficients of MIMO antennas.

B. Current Density

Surface current distribution of the MIMO antenna has been analysed in the simulation. Fig. 3.8 shows the current density plot when only antenna 1 of the MIMO array is excited and confirms less impact on the adjacent antennas during MIMO operation.

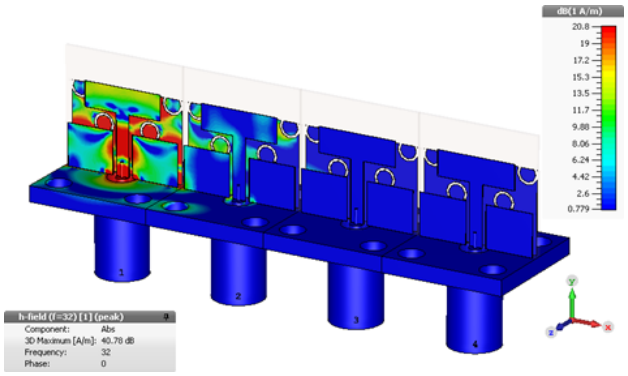

Figure 3.8: Current density of the MMW 4-element MIMO antenna array.

C. Envelop Correlation Coefficient

Envelope Correlation Coefficient (ρ_e) is a measure to estimate antenna's independence from its adjacent element and calculated based on S–parameters. ρ_e also takes into account the radiation pattern, polarisation, and relative phase between any two antennas of MIMO. Numerically computed ρ_e in Fig. 3.9 for the antenna ports is very low and close to 0 which shows low correlation between antennas and good isolation.

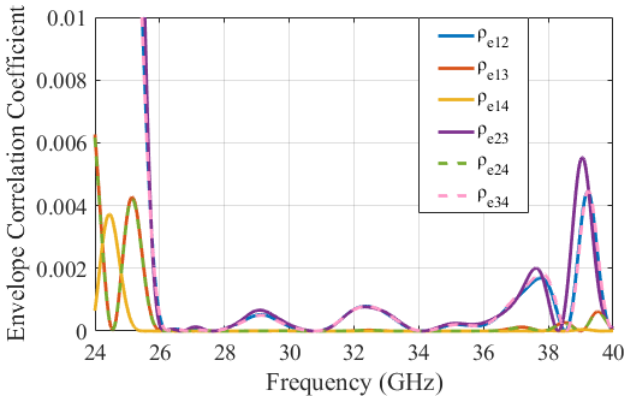

Figure 3.9: ρ_e between ports of the MMW 4-element MIMO antenna array.

3.4 K_a–band Flexible Inkjet-Printed Slotted Antenna

3.4.1 Antenna Design and Fabrication

In order to achieve conformity along with the desired performance in MMW 5G systems, a DGS based antenna is developed. The antenna is designed to cover 5G bands with gain above 4 dBi and should be adaptable with the integration in any irregular or non planar surface. In this section a CPW-fed T-shaped patch antenna to cover K_a–band is presented. The antenna is made on a low-cost flexible film of PET material. CPW ground is extended and antenna patch is positioned inside an aperture cut out from the ground. Unlike the antenna geometry from the previous section, symmetrical slot arrangements are inserted in the patch instead of the ground. The slots act as DGS and generate multiple resonating bands in the range of 20–40 GHz. Selected PET film of thickness 135 $\pm 12\mu$m, dielectric constant (ε_r) of 3.2 and a loss tangent (tanδ) of 0.022 at 10 GHz is used for antenna design. The antenna can fit within the dimensions of 16 $\times$ 16 mm^2. The aperture cut inside the ground for the placement of patch is also acting as DGS slot to alter current distribution at the edges of patch geometry. Right-angled slots, each of 2 mm width and placed at 5 mm distance apart are loaded in the two sides of the patch at parametrically optimised locations, as shown in Fig. 3.10 (a). Numerical modelling and analysis is carried out by using CST software.

Precise fabrication of antenna is carried out by using Dimatix Materials Printer (DMP-2831) and silver nanoparticle conducting ink has been used for printing purpose. Inkjet printing is an anisotropic deposition process that performs patterned writing without any need of a mask. It is a low cost process as compared to industrial manufacturing based on lithography, with comparatively less complication and highly material-conservation due to controlled consumption of ink. However, several issues need to be handled to achieve a precise and reliable fabrication from this process. The two determining factor of print quality are resolution, measured in dots per inch (dpi), and the minimum feature size that can be fabricated accurately, which is measured in

μm. Usually, higher number of dots confined precisely in a small area of print justify the overall print quality. The ink properties also impact the printing quality. Flow properties and specially wettability of dilute inks are of essential importance while carrying out inkjet printing process. The contact angle of nozzles which controls falling drops of ink for printing is associated with fluid viscosity and surface tension of the ink.

Fig. 3.11 (a) presents the in-house DMP-2831 used for antenna printing. The printer is provided with piezo-electric transducer which permits greater control over the shape and size of the released ink droplet. The cartridge used in DMP comprises of a set of sixteen nozzles and the ejection of ink from the nozzles can be controlled easily by adjusting the voltage waveform, jetting frequency and several other parameters. Ink is discharged from nozzles while the printhead moves over the substrate. The operation of DMP could be easily visualized as a liquid conductive nanoparticle ink being precisely sprayed onto substrate, like polymer or plastic film and creates a pattern. A substrate film is placed on the platen and printhead scans and ejects ink drops on the page in horizontal strips, using the printer's motor assembly to move it from left to right and back again. In this way a strip (or row) of the pattern is created, then the printhead moves back and ready for the next strip. The printhead not just print a single row of pixels in each pass, but a vertical row of pixels at a time, depending on the number of nozzles employed simultaneously. The temperature of platen can be adjusted to enhance the ink deposition and drying on the substrate. Moreover, the temperature of printhead can also be adjusted to increase the wettability of ink. Optimised adjustment of these parameters yield a precise antenna fabrication by inkjet printing.

The printed prototype is further sintered to enhance the conductivity of the layer. The printing is performed on special sheets with chemically treated surface suitable for inkjet printing. The micro-coating of chemical on the surface helps in rapid drying and sintering of ink and also enhances the adhesion of PET material. The crack analysis after bending is also examined by using a microscope. The investigation determines the high quality of printing as the prototype shows uniformity, better adhesion and resistance

towards cracks. The printed prototype of the proposed MMW antenna is shown in Fig. 3.10 (b) and the details of the optimised dimensions are provided in Table 3-B.

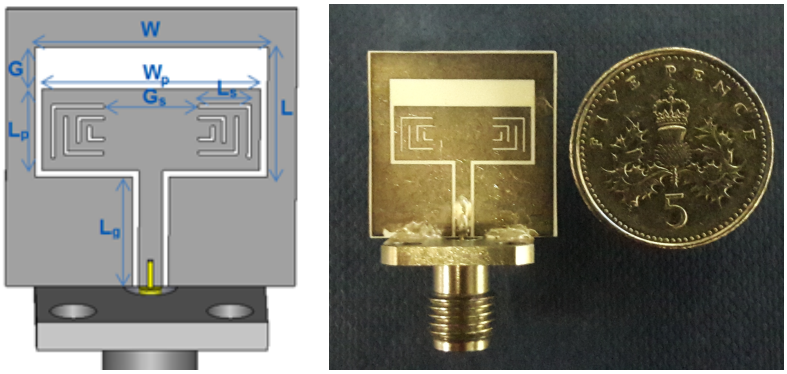

(a) (b)

Figure 3.10: MMW DGS based flexible antenna on PET film (a) Simulated model; (b) Fabricated prototype.

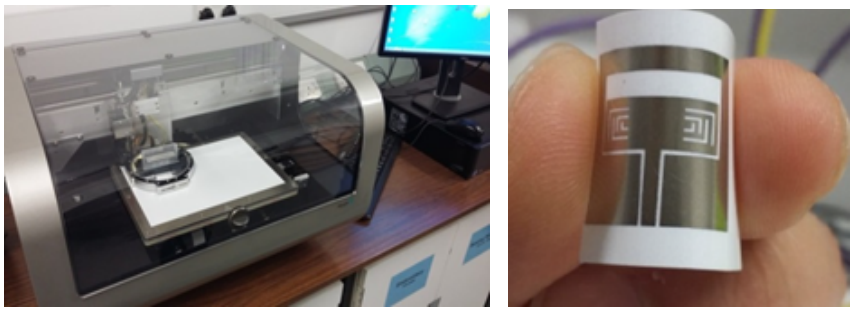

(a) (b)

Figure 3.11: Inkjet printing facility at QMUL: (a) In-house DMP-2831; (b) Inkjet-printed flexible antenna on PET film.

Table 3-B: **Optimised Dimensions of MMW flexible Antenna**

Parameters	**Symbols**	**mm**
Width of slot of ground plane	W	12.8
Length of slot of ground plane	L	7.5
Width of radiating patch	W_p	12
Length of radiating patch	L_p	4.7
Gap between patch and ground	G	2.4
Length of CPW ground	L_g	6.3
Length of the slot arrangement	L_s	2.9
Gap between two slot assemblies	G_s	5.2

3.4.2 Results and Discussion

The flexible antenna performance is characterised based on the S-parameters, radiation patterns and realised gain profile. Parametric study of a number of design parameters has been performed to achieve optimised geometrical dimensions of proposed MMW flexible antenna. Ultra-high bandwidth is achieved by merging the closely spaced resonating bands generated due to DGS slots in the patch geometry. The antenna performance is examined based on the agreement of simulated and measured results presented in this section. Omnidirectional radiation pattern, reasonable gain over the complete bandwidth of operation as well as flexible and planar geometry are distinguishing attributes of the proposed atenna for being a part of 5G wearables and body-centric devices.

A. Impedance Bandwidth

Simulated and measured results of S_{11} are presented in Fig. 3.12 (a) and the effect of fabric and human body is also included in the measurements. The parametric study of a number of parameter dimensions results in a continuous bandwidth covering K_a–band (26.5–40 GHz). Parametric analysis of length of slot arrangement (L_s) extended in the patch is examined where at 2.9 mm with a gap of 5.2 mm between the two slot arrangements a continuous bandwidth is obtained as shown in Fig. 3.12 (b).

B. Radiation Pattern

The far-field radiation patterns of the designed MMW flexible antenna at distinct frequencies of bandwidth are presented in Fig. 3.13. The antenna shows a steady omnidirectional radiation pattern in the complete operating bandwidth. Moreover, the results shows close match between the simulated and measured results.

C. Realised gain vs. Frequency

The simulated and measured realised gain of the MMW flexible antenna versus frequency, illustrated in Table 3-C show that the realised gain is above 4 dBi in complete

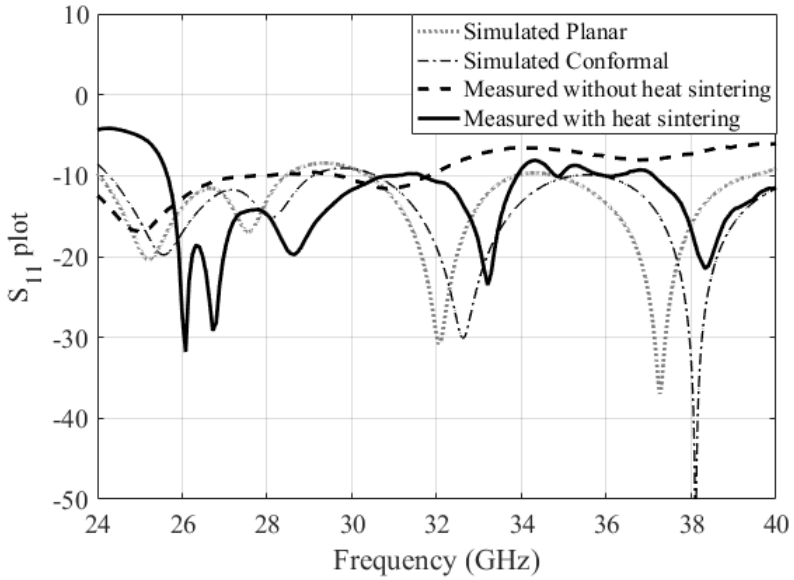

(a)

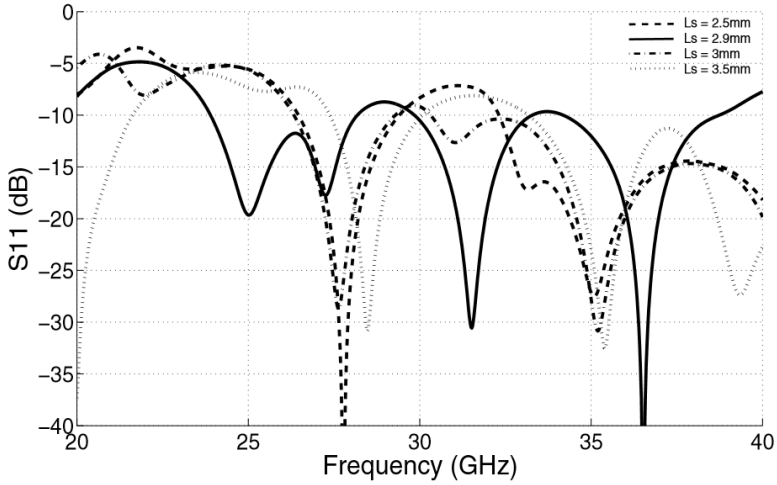

(b)

Figure 3.12: S_{11} of the MMW flexible antenna: (a) Simulated and measured S_{11} plots, (b) Parametric analysis of gap between the two slot arrangements.

operating range. The peak gain of 8.2 dBi is observed at 38.75 GHz. The higher gain magnitudes with an increase in frequency are due to an increase in the radiation directivity of the designed antenna. It is observed that the radiation pattern is omnidirectional at lower operating range, and becomes directive as the frequency increases.

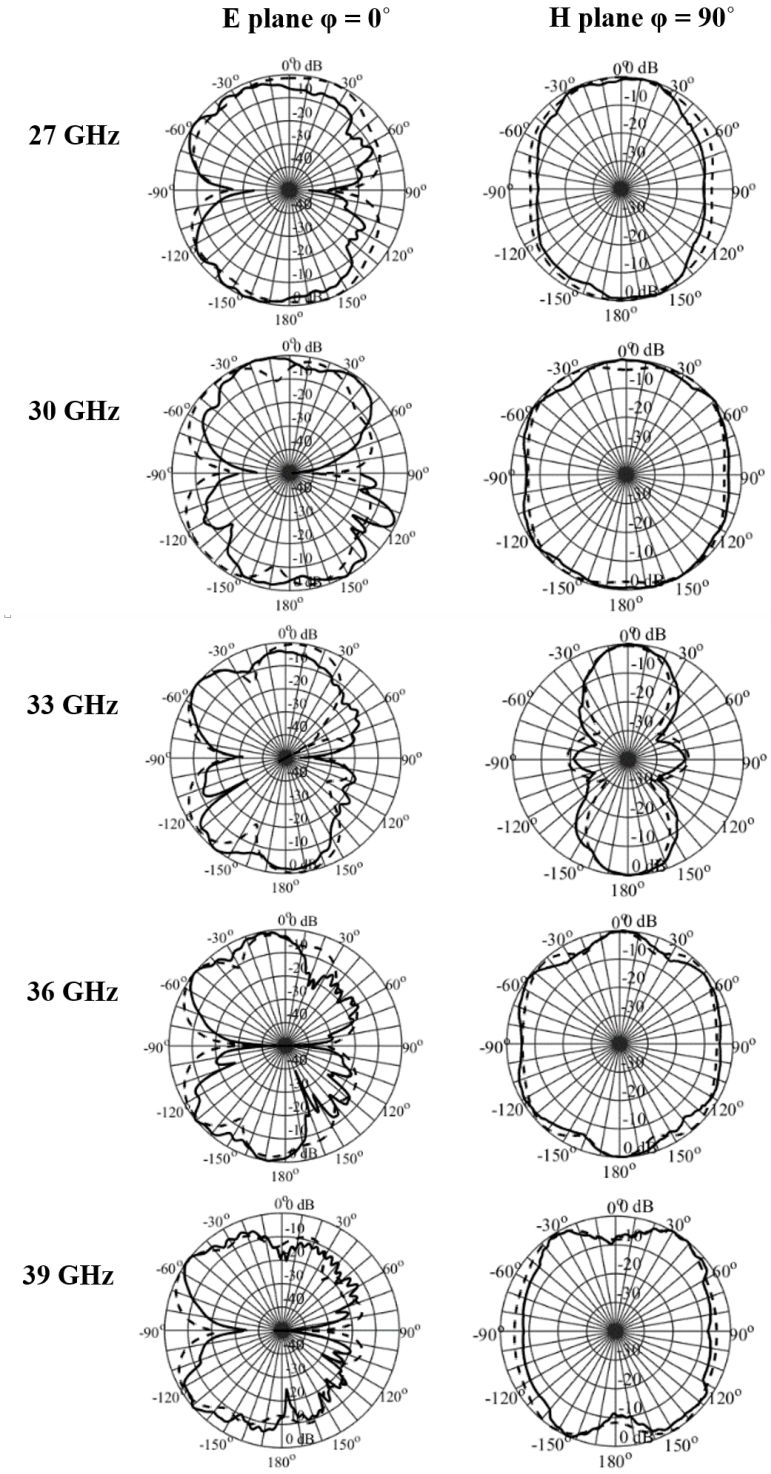

Figure 3.13: Far-field radiation patterns of the MMW flexible antenna.

Table 3-C: **Realised gain of MMW Flexible Antenna**

Frequency	**27 GHz**	**30 GHz**	**33 GHz**	**36 GHz**	**39 GHz**
Simulated Gain (dBi)	5.49	5.23	5.83	6.12	7.93
Measured Gain (dBi)	4.35	4.12	4.84	6.14	7.44

3.5 Conclusion

This chapter has covered the DGS based design, fabrication, and performance analysis of two wideband antennas. Both rigid and flexible substrates have been utilised for antenna fabrication and K_a–band (26.5–40 GHz) was selected as a design frequency for MMW 5G antennas. The first antenna design has accomplished high impedance bandwidth of 25.1–37.5 GHz, and a high gain profile with the peak gain of 10.6 dBi at 36 GHz. Performance of the antenna was further investigated for integration in MIMO systems by fabricating and testing a four-element MIMO array. The second slotted antenna has been designed on flexible substrate and well-suited for integration in wearable gadgets, and could also be made part of MIMO if required, similar to the first antenna. The proposed designs of MMW antennas have the advantages of simplicity, ease of fabrication, high performance attributes and potential towards future 5G and beyond applications. Though, the integration of wideband antennas in MIMO assembly has been suggested for high capacity and spatial diversity, yet this high bandwidth access by deploying the wideband operation has often resulted in degradation of the antenna efficiency. This limitation can be resolved with a more advanced antenna design topology to efficiently access the spectrum, addressed in the next chapter.

Chapter 4

Millimetre-Wave Frequency Reconfigurable Antennas

4.1 Introduction

Future wireless networks are expected to deliver an ultra-fast 5G infrastructure with high data rates and extended system capacity by deploying high effective bandwidth of the MMW spectrum [15]. In order to realise such systems, there is a need of efficient antenna front-ends to access the K_a–band, which is extensively emphasised for 5G networks at several research platforms [22]. Wideband antennas are one of the favourable choices to increase the system capacity but there are some issues related to degradation of antenna efficiency while accomplishing high bandwidth. Moreover, when efficient utilisation of spectrum is of crucial importance, frequency reconfigurable antennas dominate in performance over wideband antennas. In frequency reconfigurable antennas, the antenna functionality is diversified within the same electrical size, and antenna is capable to adapt its performance according to its surroundings. Unlike wideband antennas, a highly efficient utilisation of spectrum is performed with this adaptable frequency selection as the reconfigurable antenna is not bound to operate on all the bands simultaneously.

Frequency-reconfigurable antennas have substantial contribution in cognitive systems due the adaptive operation in more than one frequency bands because of the capability of physical structure alteration to shift the resonance towards the intended band [151]. This feature is highly instrumental in 5G wireless systems to enhance the data throughput due to an increase in the overall effective bandwidth and network capacity. Surface-mount switching schemes are usually deployed at the antenna's end to provide adaptive control required to perform reconfiguration. In many reported articles, PIN diodes [152], FETs [153], MEMS [154], varactors [155], and optical switches have been incorporated on planar patch antennas for this purpose. Choice of feasible switch type involves numerous aspects such as, insertion loss, isolation, linearity, reliability, size and cost.

Most of these switching technologies such as PIN diodes, FETs, etc. are well-established and commercially accessible at the MMW frequencies. PIN diode switches are available as discrete devices as well as integrated diode packages (MMICs) by manufacturers such as M/A-COM Technology Solutions. The recent products by M/A-COM Tech. are high power, multi-octave switches incorporating AlGaAs PIN diode HMIC devices. The switches offer high power handling of 50 Watt with insertion loss lower than 2 dB and isolation of 30 dB at 40 GHz. This class of AlGaAs/GaAs PIN-based switches [156, 157] offer probably the highest frequency and widest bandwidth (1 MHz to 75 GHz) as compared to any other state-of-the-art technologies. Another important feature of AlGaAs/GaAs based PIN diode switches is fast response which offers high switching speed of less than 500 picoseconds. It has been observed on low frequencies, the PIN diodes often require larger areas to comprehend the circuitries because of the passive components in the biasing circuit as compared to IC switches such as RF MEMS. This larger footprint is an important issue in compact designs and hand-held devices. However, in MMW frequencies the miniature size of flip-chip and beam-lead diodes and other passive components has made the realisation of compact devices more feasible.

After the successful deployment in the 4G networks, MIMO antennas are regarded as a promising technology for future networks as well. MIMO arrays encompass a number

of antennas acting as independent communication channels to support simultaneous signal throughput and desired level of communication [158]. Integration of frequency-reconfigurable antennas in MIMO systems is highly instrumental for efficient spectrum utilisation as it delivers an adaptability over the frequency selection as well as the signal throughput [159]. Another major emphasis of next-generation wireless networks is on the advancement of wearable electronics such as smart watches and health monitoring sensors, to ensure mobility, robustness, and flexibility. Conformal cellular devices and wearable gadgets are gaining massive attention at the user-end, which has aggravated the need of antenna design, conformal to the shape of the mounting surface or human body in case of body-centric networks. However, the impact of human body and surrounding objects are critical concerns related with the antenna performance in both on-body and off-body scenarios. The propagation distortions in body-centric antennas are mainly due to interferences and absorptions by the body tissues [160]. In addition, flexible antennas are highly applicable in conformal and light-weight implementations where shape can be a part of an aircraft, missiles and other high-speed vehicle.

This research suggests the aggregation of highly efficient technologies of MIMO and frequency reconfiguration on a flexible antenna for 5G hand-held as well as wearable applications. Material properties of flexible substrates are expected to influence critically the fundamental performance of antenna at MMW spectrum. Flexible antennas have been reported on a number of available flexible films such as textile, polymers, polyamides, and polyesters. PET is among the feasible choices of flexible substrates for printed antennas due to its suitable material characteristics and low cost [141]. LCPs have recently gained huge interest in the implementation of high-frequency wireless applications especially antennas [161]. LCP substrates offer outstanding electrical and mechanical properties such as low loss-tangent, moisture absorption, good flexibility, conformity, surface adhesion and capability to be part of multilayer structures. Moreover, inkjet printing has been reported as a suitable choice to accomplish a defined and accurate fabrication of the printed circuits and antennas on flexible films [140, 141].

In this chapter, four distinct designs of frequency reconfigurable antenna are presented at MMW spectrum for 5G applications. The design, fabrication as well as the numerical and experimental evaluations of the designed antennas are discussed in detail.

- The first antenna is designed on RT/duroid 5880 substrate and performs frequency tuning by using variable resistors. The intention here is to practice the reconfiguration concept on a standard rigid substrate by using numerical evaluation before moving towards the flexible reconfigurable antenna design.

- The second antenna covers frequency reconfiguration on 28/38 GHz and fabricated on a flexible PET film by inkjet printing.

- The third antenna is an extension of previous antenna with two additional states which covers an overall bandwidth of K_a–band. Two-element MIMO antenna configuration is evaluated to be part of 5G conformal devices. For the sake of simplicity, ideal switches by creating metal short or open-circuit have been used.

- The fourth antenna is developed on a flexible LCP substrate. Diode model along with biasing circuit is also presented. The antenna is well suited for 5G cognitive radio as its can scan the bandwidth and then select the desired band.

4.2 26-GHz Frequency Tuneable Antenna

4.2.1 Antenna Design

A frequency tuneable antenna at 26- and 28-GHz to cover both FCC and Ofcom standards for 5G, is presented in this section. In order to conserve the simplicity of the design, variable resistors are used for tuning. T-shaped patch geometry is selected, T-shaped though similar to rectangular patch but better in antenna bandwidth [162]. Several articles have proposed T-shaped patch antennas with structural modifications, as a part of multiband, wideband and ultra-wideband applications, though most of the

work is performed at low frequencies [162, 163]. In this section, T-shaped geometry is selected due to the prospective advantage of bandwidth, and an antenna design at high-frequency MMW spectrum is presented. A compact CPW-fed T-shaped antenna is designed with two stubs positioned on either sides of the strip-line at an optimised distance. Resonant frequency is tuned in the range of 23–29 GHz by integrating two variable resistors connected between the stubs and ground plane. The change in resistance value is responsible of altering the voltage and current densities of the stubs. The stubs are parasitically coupled with the antenna feed and the change in current distributions results in a change in resonant frequency of antenna. The proposed geometry is provided with the simplicity of uniplanar structure which requires only single-sided copper cladding. Rogers RT/duroid 5880 ($\varepsilon_r = 2.2$) with dimensions of 12 × 12 × 0.8 mm^3 is used as an antenna substrate. Patch dimensions are 6.4 × 1.55 mm^2 with a 35 μm thick copper cladding. A CPW feed of 6 mm length and 1 mm thickness is designed to provide 50 Ω impedance matching. Two stubs are placed parallel to the patch at the gap of 0.2 mm from the feed line while the resistors are inserted between the stubs and CPW ground plane as shown in Fig. 4.1.

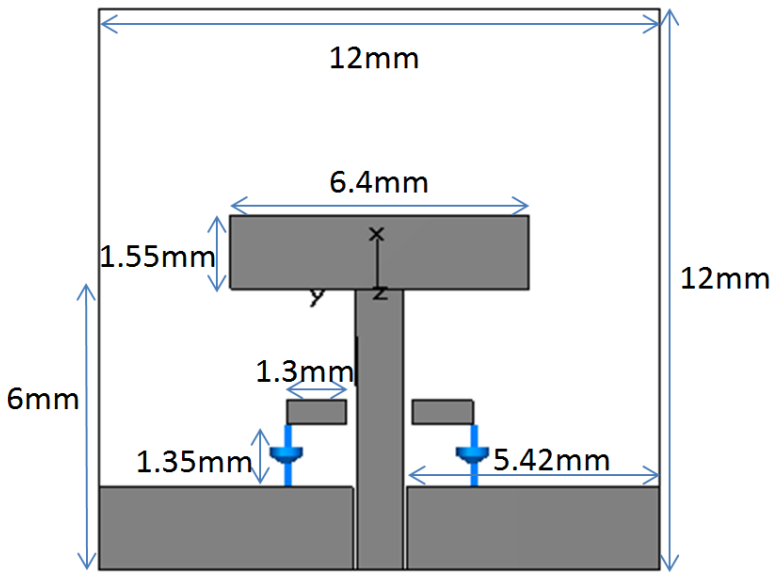

Figure 4.1: MMW frequency tuneable antenna with variable resistors.

4.2.2 Results and Discussion

T-shaped antenna geometry involves a horizontal metallic patch distributed on both sides of the feed and generates an end-fire radiation with two beams of same radiation intensity. Frequency tuning over 23–29 GHz is achieved by varying the resistance while the 3 dB beamwidth remains conserved over the range of operation. Simulation of the proposed antenna is performed in CST software. The antenna is equipped with the advantages of compactness, fabrication ease, frequency tuning capability and stable 3 dB beamwidth in the operating range. Additionally, the realised gain of each beam is suitable for short range wireless networks. The dual beam response provides a radiation diversity in narrow passages, corridors, underground mines and tunnels. These advantages make the proposed antenna suitable for 5G indoor wireless systems.

A. Impedance Bandwidth

Fig. 4.2 shows the simulated refection coefficient profile of antenna at different values of resistors. In order to preserve the symmetry of the antenna design, same values for both resistors are used at a time as different resistor values would result in an unsymmetrical beam shift. It is observed that the resonance is tuned towards higher frequencies when resistors' value is varied from 100 Ω to 10 KΩ. As high resistance shows an open-circuit or isolation in the current path, no significant frequency tuning has been observed above 5 KΩ due to the open-circuit state achieved at this point. Table 4-A illustrates the resonant frequencies corresponding to different values of resistors.

Table 4-A: **26-GHz Frequency Tuneable Antenna with Variable Resistors**

Resistance (Ω)	**Frequency (GHz)**	S_{11} **(dB)**
100	24.55	–11.89
250	25.28	–21.45
500	25.87	–40.34
1 K	26.3	–24.1
5 K	26.74	–19.8
10 K	26.88	–19.45

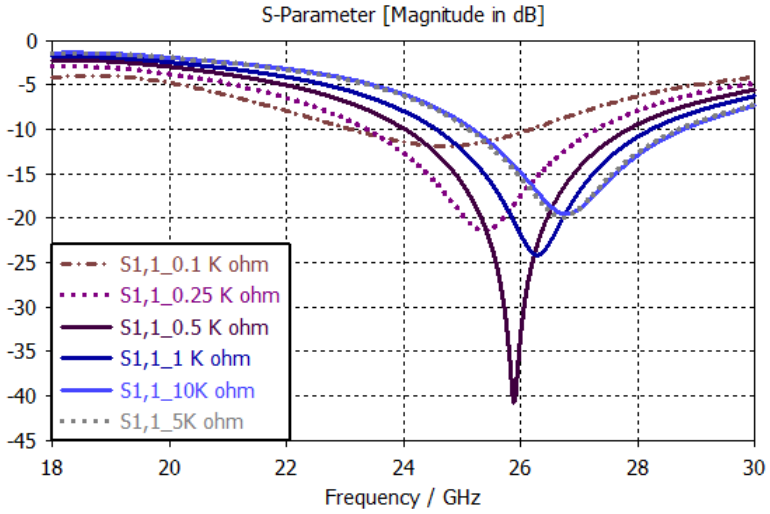

Figure 4.2: Simulated S_{11} plot of 26-GHz frequency tuneable antenna.

B. Radiation Pattern

The antenna design results in a symmetrical distribution of radiation into a dual beam along the end-fire direction. Each beam holds a narrow beamwidth and pointed at an angle of $\pm 30°$ from $\phi = 0°$. Fig. 4.3 presents the simulated patterns at different resonant frequencies where 3 dB beamwidth remains conserved during the entire range.

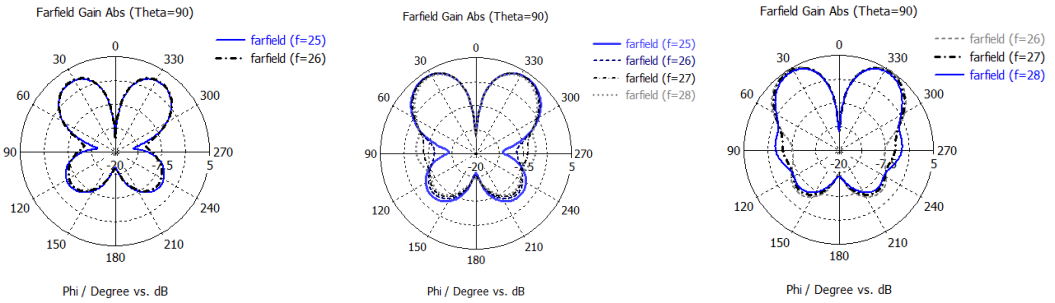

(a) (b) (c)

Figure 4.3: Simulated radiation pattern of the MMW frequency tuneable antenna at (a) R = 250 Ω, (b) R = 1 KΩ (c) R = 10 KΩ.

C. Realised Gain

Fig. 4.4 presents the simulated realised gain of the proposed MMW antenna. It is observed that the peak gain of antenna increases with the increase in resistance value

and sufficient for the short-range MMW wireless applications.

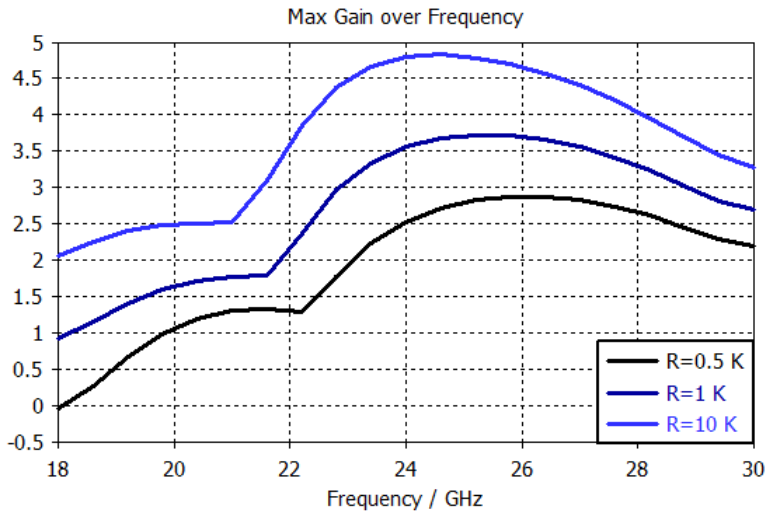

Figure 4.4: Simulated peak gain of the MMW frequency tuneable antenna.

4.3 28/38 GHz Frequency Reconfigurable Antenna

4.3.1 Antenna Design and Fabrication

In this section, the previous design is improved with more mature geometry in which two 5G bands (i.e. 28 and 38 GHz) can be accommodated within a conformal antenna. A flexible antenna comprises of a slotted T-shaped patch with CPW feeding is presented. The ground is provided with a rectangular aperture and antenna is placed at an optimised position inside the aperture. Two slots integrated with switches, i.e., *S1* and *S2* as shown in Fig. 4.5 (a), are designed to implement frequency reconfiguration. The switches act in a pair and state of switches determines the frequency of operation. When both of the switches are OFF, the slots act as an open-circuit, as shown in Fig. 4.5 (b), which results in an increase in the radiating length and the antenna resonates at 28-GHz. However, when both switches are ON, the slot edges act as a short circuit, as depicted in Fig. 4.5 (c), the radiating length of antenna is trimmed off and the resonance is shifted to 38-GHz. Variable resistors are also suggested as a switching mechanism and incorporated

in the simulation model. Fig. 4.5 (a) indicates the designed antenna modelled in CST, while the details of design parameters are illustrated in Table 4-B.

Antenna is fabricated on a thin and flexible surface-treated PET film, (i.e., h = 135 μm, ε_r = 3.2, tanδ = 0.002). DMP-2831 has been used for the printing process and performs an additive prototyping of 0.5 μm thin conductive layer with the pattern resolution of $\pm$20 μm. The primary setup adjustment of parameters including drop spacing, jetting frequency, firing voltage of ejecting nozzles, printhead temperature, and waveform characteristics is carried out to realise a precise fabrication. The composition of nanoparticle ink used for printing contains silver particles encapsulated in polymer sheath to avoid oxidation and dispersed in an inert solvent of suitable viscosity. Post-printing drying/curing, sintering and characterisation are of critical importance to attain desired performance. If proper sintering is performed, the conductivity of approximately $0.3 \approx 0.7 \times 10^7$ S/m can be accomplished from a printed layer. The chemically active microporous coating on the surface of PET films sinters the printed ink pattern. The microporous coating is also useful in improving ink adhesion by bonding the ink chemically with the substrate surface and holds the ink intact in a precise and definite pattern. Figs. 4.5 (b) and (c) present the fabricated inkjet-printed antenna prototype in the two possible switch states (i.e., ON- and OFF-states).

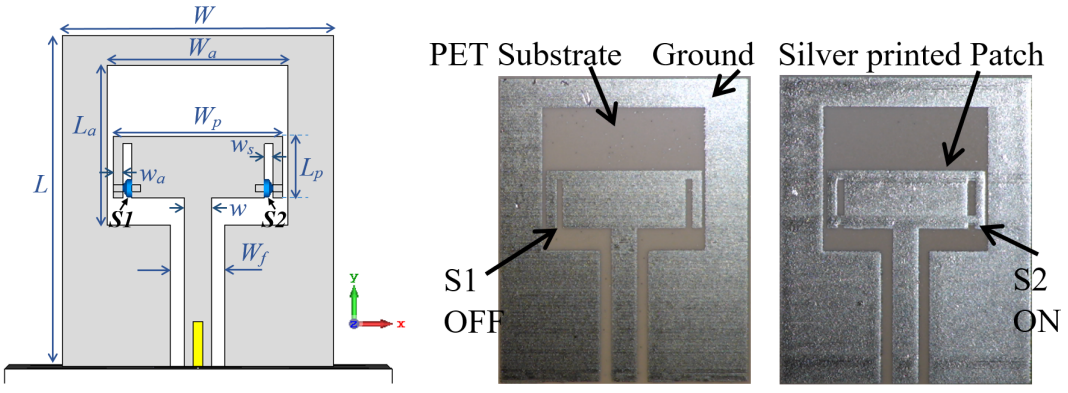

(a) (b) (c)

Figure 4.5: 28/38 GHz flexible frequency-reconfigurable antenna: (a) Simulated model; (b) Fabricated prototype when switches are OFF; (c) fabricated prototype when switches are ON.

Table 4-B: **Optimised Dimensions of 28/38 GHz Flexible Frequency-Reconfigurable Antenna**

Parameters	**Symbols**	**mm**
Antenna width	W	9.0
Antenna length	L	11
Ground aperture width	W_a	6
Ground aperture length	L_a	5.3
Patch width	W_p	5.6
Patch length	L_p	2.05
Slot width	w_s	0.3
Width of patch arm	w_a	0.3
Width of CPW feed ground	W_f	1.8
Width of CPW feed line	w	0.9

4.3.2 Results and Discussion

The analytical study of the presented antenna suggests that several aspects such as the substrate properties, ink specifications, adjustment of inkjet printer, and other fabrication tolerances could affect the performance. The results of S-parameters, radiation pattern, gain and efficiency are provided to justify the scope of designed antenna.

A. Impedance Bandwidth

The ideal switches (i.e., open-circuit at OFF-state and short-circuit at ON-state) are used for the proof of concept, and the reconfiguration mechanism is also inspected by proposing a variable resistor as a switch. The plot shows simulated results of S_{11} when the resistance is low (i.e., 10-Ω, ON state), and when it is high (i.e., 10-KΩ, OFF state). The antenna is fabrication with ideal switch configuration and measured results are presented in Fig. 4.6, along with the simulated plots.

B. Radiation Pattern

The radiation pattern plots on both 28 GHz and 38 GHz bands depict that radiation is converged along the z-axis, orthogonal to the antenna plane. The antenna ground

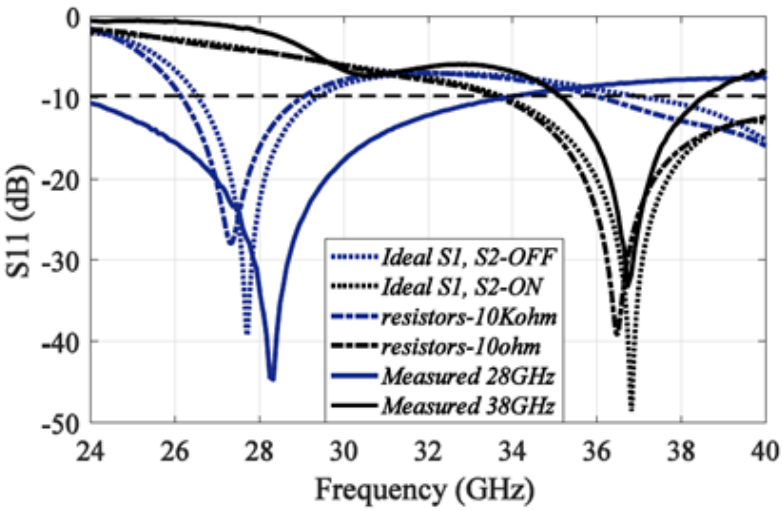

Figure 4.6: Simulated and measured S_{11} plots of the 28/38 GHz frequency-reconfigurable antenna.

is designed with a rectangular aperture that acts as a loop to converge the radiation of the patch into two radiating beams, oriented at top and bottom of the antenna. This radiation response is advantageous for both on-body and in-body applications and health-monitoring devices. Fig. 4.7 shows two vertical cuts (i.e., $\phi = 0°$ and 90°) of the 28/38 GHz frequency reconfigurable antenna.

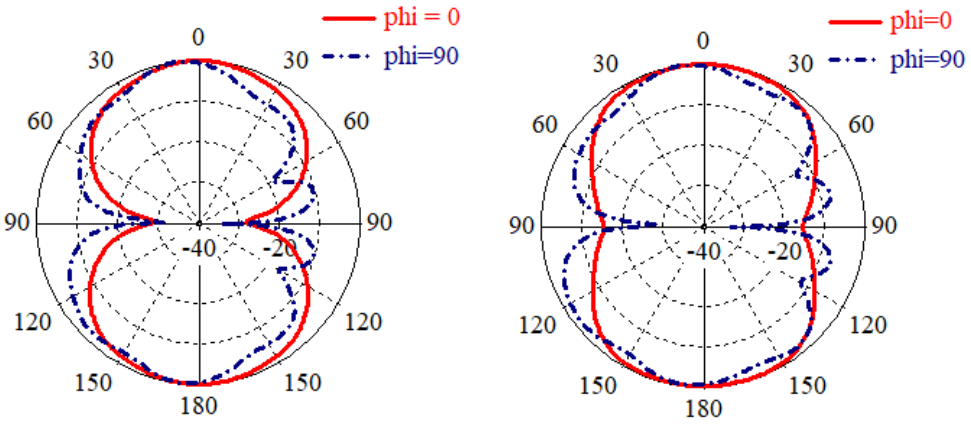

(a) (b)

Figure 4.7: Simulated radiation patterns of the 28/38 GHz frequency-reconfigurable antenna (a) $\phi = 0°$ and 90° at 28-GHz; (b) $\phi = 0°$ and 90° at 38-GHz.

C. Realised Gain and Efficiency

Simulated results of designed antenna show that magnitude of the realised gain fulfils the requirements of short-range communication links. Table 4-C illustrates the simulated gain versus frequency over the targeted bands of operation. Numerical analysis shows an efficiency of above 75% in the two operating bands of MMW reconfigurable antenna which is quite reasonable considering high dielectric loss of flexible substrates.

Table 4-C: **Realised Gain of 28/38 GHz Frequency-Reconfigurable Antenna**

28-GHz band	**Frequency (GHz)**	**26**	**27**	**28**	**29**	**30**
	Gain (dBi)	3.45	2.5	2.62	3.33	4.2
38-GHz band	**Frequency (GHz)**	**36**	**37**	**38**	**39**	**40**
	Gain (dBi)	4.68	4.01	4.39	4.59	4.69

4.4 Flexible Frequency-Reconfigurable MIMO Antenna

4.4.1 Antenna Design and Fabrication

In order to enhance the adaptability of the 28/38 GHz flexible antenna, the antenna design is made more versatile by the addition of two more reconfiguration states, and a two-element MIMO configuration is also implemented for multichannel communication. These characteristics enable the proposed antenna to tune the two antenna elements on different frequencies and can support communication at two different bands simultaneously. Moreover, the flexibility adds another degree of freedom, i.e. to place the antenna on planar or non-planar surfaces. Design is initiated by extending the previous antenna with the integration of two more slots. The initial two slots are terminated with x-pair of switches to reconfigure the antenna frequency based on the state of switches. Antenna resonates at 28-GHz when both of the switches are OFF, as the slots edges act as an open-circuit. While the resonant band shifts to 38 GHz when both switches are ON, the

radiating length is trimmed off as the slot edges act as a short-circuit.

The further modification with another pair of slots provided with y-pair switches is carried out which allows the antenna to operate in four distinct operating modes. In order to diversify the antenna functionality as a standalone Tx/Rx, two-element MIMO assembly is proposed, where both elements are independent of selecting their desired frequency of operation. Fig. 4.8 (a) presents the proposed flexible MIMO antenna model in the CST software, while the optimised dimensions of design parameters are illustrated in Table 4-D. Designed MIMO antenna is fabricated on surface-treated PET film (i.e., $h = 135$ μm, $\varepsilon_r = 3.2$, tan$\delta = 0.002$) with dimensions of 11×25.4 mm^2. DMP-2831 has been used for prototyping and silver nanoparticle ink (i.e., Colloidal Ag-J solid Ag) is employed in the printing process. The printer is calibrated and suitable adjustment of the key parameters is carried out. Drop spacing of 15 μm (i.e., 1693.33 dpi), firing voltage of 15V, and jetting frequency of 5 KHz have been set to print the designed antenna prototype. The selected PET films are provided with a self-sintering capability due to surface treatment. Printed prototype of MIMO antenna is presented in Figs. 4.8 (b) while four switch configurations have been also fabricated by the electrically-short/-open conducting paths, where the electrically-short depicts the ON switch mode, and the open one shows the OFF switch mode, as in Figs. 4.8 (a) to (d).

Table 4-D: **Dimensions of MMW Flexible Frequency-Reconfigurable MIMO Antenna**

Parameters	**Symbols**	**mm**
Length of patch	L_p	5.7
Width of patch	W_p	2.05
Length of ground slot	L_s	5.3
Width of ground slot	W_s	6.1
Length of MIMO antenna	L	11
Width of MIMO antenna	W	25.4
Distance of slot-1 from the feed	a	1.05
Distance of slot-2 from the feed	b	1.8
Length of CPW ground	L_f	4.7
Distance of ground slot from CPW	w	2.15

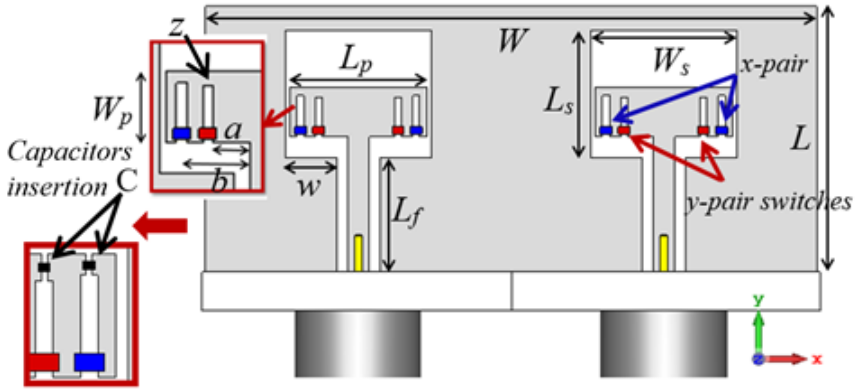

(a)

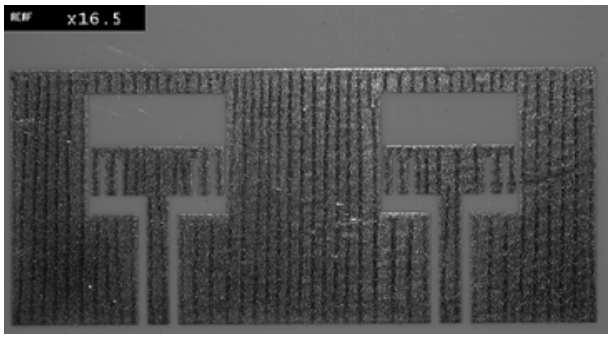

(b)

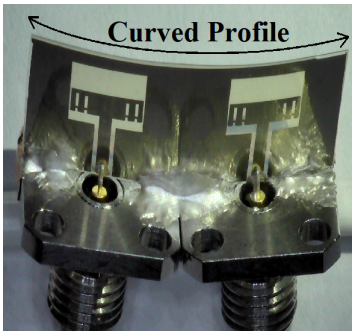

(c)

Figure 4.8: Proposed flexible frequency-reconfigurable 2-element MIMO antenna: (a) Simulated model; (b) Fabricated prototype, (c) Curved MIMO antenna.

4.4.2 Results and Discussion

The performance of the MIMO antenna is evaluated by the parametric study, and is validated by the measurements of the realised prototype. The analysis based on the results of S-parameters, radiation pattern, and realised gain shows that the measurements are similar to the simulated results, with the exception of some mismatches mainly due to the fabrication intolerances and the connector and cable losses.

A. Impedance Bandwidth

Fig. 4.9 (a–d) depicts the reflection coefficients of the designed MIMO antenna for four switching states, illustrated in Table 4-E. It is observed that the measured results

are close to the simulations in both planar and conformal configurations of the two-element MIMO antenna, which ensures a robust antenna performance even if it is not mounted on a flat surface. The measured transmission coefficients between the two antennas mounted in a planar configuration of the operating modes are below -20 dB, as depicted in Fig. 4.10. The optimal level for lower mutual coupling and high isolation suggests that the S_{12}/S_{21} should be atleast below -10 dB. The results show that the overall bandwidth of 23.3–40 GHz is covered in the combined operation of the four distinct modes. Furthermore, plots of Fig. 4.11 show the respective envelope correlation coefficients are approaching to 0 value in four operating modes, which states capability of a highly independent individual operation.

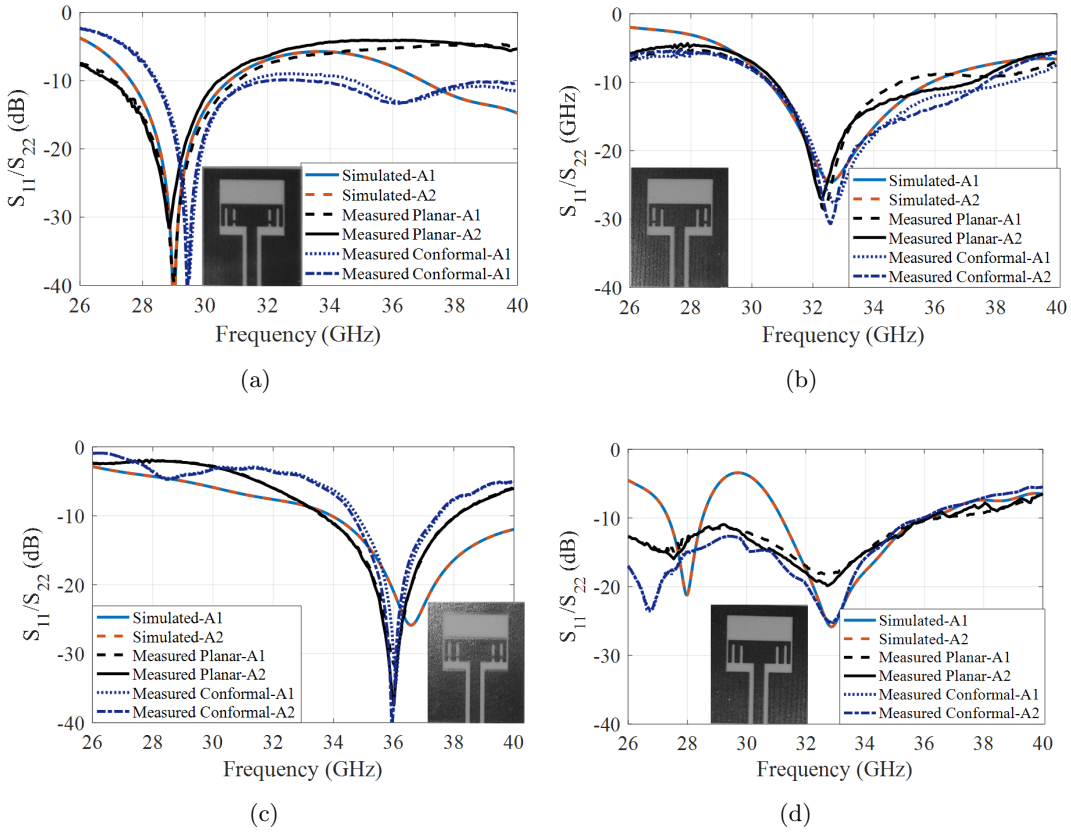

Figure 4.9: Simulated and measured S_{11} plots of the flexible frequency-configurable 2-element MIMO antenna: (a) mode-I: 28-GHz band; (b) mode-II: 32-GHz band; (c) mode-III: 36-GHz band; (d) mode-IV: dual-band.

Table 4-E: **Switching Modes of MMW Flexible Frequency-Reconfigurable MIMO Antenna**

Mode	**SW-x**	**SW-y**	**Band**	**Bandwidth**
Mode-I	OFF	ON	28-GHz	27.4-30.1 GHz
Mode-II	ON	OFF	33-GHz	30.5–35.9 GHz
Mode-III	ON	ON	37–39 GHz	34–40 GHz
Mode-IV	OFF	OFF	dual band	27.3–28.5 GHz and 31.1–36 GHz

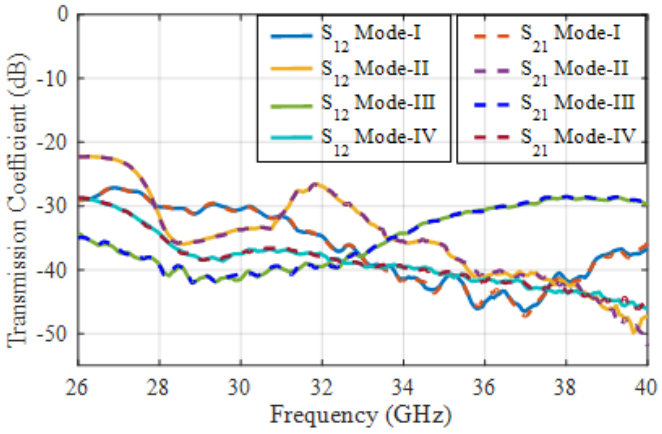

Figure 4.10: Measured transmission coefficient (S_{12} and S_{21}) plots of the flexible frequency-reconfigurable 2-element MIMO antenna.

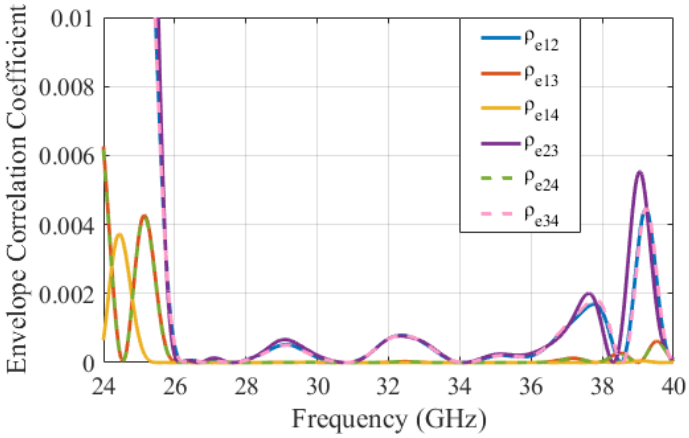

Figure 4.11: Simulated envelope correlation coefficient of the flexible frequency-reconfigurable 2-element MIMO antenna.

B. Radiation Pattern

The radiation patterns of the proposed antenna exhibit a radiation distribution on top and bottom surfaces of antenna. Fig. 4.12 shows the simulated and measured results of a single antenna element (unit cell of MIMO) at $\phi = 0°$ and $\phi = 90°$ at distinct frequencies of the operating modes I-IV. As the patch is placed in the aperture cut inside the metallic ground, this leads to more radiation directivity orthogonal to the antenna plane (i.e. along the top and bottom direction) while the radiation is trimmed off along the antenna plane, as shown by the E- and H-plane plots.

C. Realised Gain

The simulated and measured results of the realised gain for a single antenna element of the proposed MIMO configuration in the operating frequency range of 28–40 GHz have been tabulated in Table 4-F for the modes I–IV. As in MIMO, each antenna element operates individually, so the single element gain is important to determine than the collective array gain of the overall MIMO arrangement.

Table 4-F: **Realised Gain of Flexible Frequency-Reconfigurable MIMO Antenna**

Frequency	**(GHz)**	**28**	**30**	**32**	**34**	**36**	**38**	**40**
Mode I	**Simulated**	2.7	3.8	–	–	–	–	–
	Measured	2.5	3.4	–	–	–	–	–
Mode II	**Simulated**	–	–	4.6	3.7	–	–	–
	Measured	–	–	4.4	3.4	–	–	–
Mode III	**Simulated**	–	–	–	6.5	4.7	4.2	4.4
	Measured	–	–	–	6.2	4.6	4.1	4.2
Mode IV	**Simulated**	2.7	–	4.3	3.7	5.24	–	–
	Measured	2.5	–	4.2	3.5	4.9	–	–

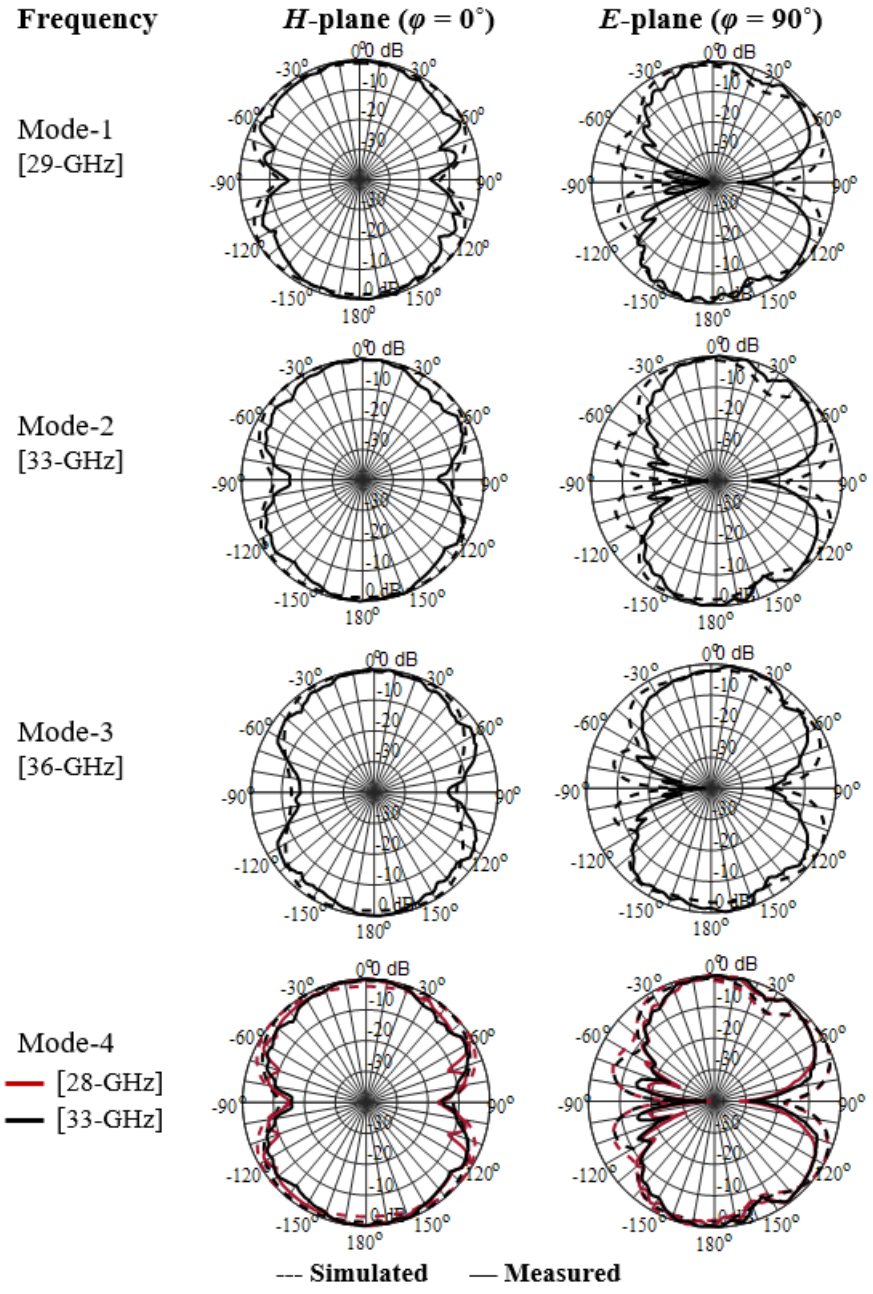

Figure 4.12: Simulated and measured radiation patterns of the single antenna element of flexible MIMO configuration.

4.5 Reconfigurable Antenna with PIN Diodes

The antenna design work performed till this stage provides an understanding of implementing the reconfiguration mechanism on a thin and flexible film; though, only ideal switch configuration is used up to this point for the sake of simplicity. Moreover, the cognitive radio is anticipated as a potential feature of 5G, which is comprised of spectrum sensing and then choosing the appropriate band for communication. The antenna design is further extended in this section with a conformal MMW reconfigurable antenna suitable for 5G cognitive radio. Practical switches i.e. PIN diodes, have been implemented and a complete biasing circuit is developed in this regard, which delivers a practical insight of implementation of reconfigurable antenna at high-frequencies. LCP has been selected as substrate due to low loss-tangent. Two potential fabrication methods, inkjet printing and laser etching have been suggested for the antenna prototyping.

4.5.1 Antenna Design and Fabrication

The proposed antenna is single-sided printed monopole comprising of a structure similar to a tuning fork with two prongs of different lengths. The antenna has two additional stubs on either side of the radiating patch at an optimised distance which can be included in the antenna geometry by means of switching. Prong 1 of longer length L_{p1} is connected with a stub 1 by means of a switch 1 (SW1), while prong 2 of length L_{p2} is linked with stub 2 via switch 2 (SW2). The reconfiguration mechanism can be performed by altering the radiating area of the patch by connection and disconnection of stubs based on the switch state, which eventually changes the corresponding resonant frequency. The CPW feeding is provided to the antenna and 50Ω matched K-connector is included in the RF numerical analysis performed in CST software.

A flexible sheet of LCP Rogers ULTRALAM 3850 (ε_r = 2.9, tanδ = 0.0025) of dimensions 16 × 14 × 0.1 mm^3 is used. In the first fabrication, inkjet printing process has been suggested by using silver nanoparticle ink. While in second fabrication, laser

etching on copper laminated LCP sheets has been recommended due to its high accuracy of prototyping. The next stage demonstrates the implementation of switches, where PIN diodes have been selected due to the mature technology and ease of availability. Bias voltage is applied at the diode terminals in order perform its operation. PIN diode works like a simple switch as in OFF state, diode acts as an open-circuit, and blocks all the RF current to pass through. Ideally S_{21} specifies no transmission due to high isolation and S_{11} should be 0 dB to allow complete power reflection. On the other hand, when the PIN diode is operating in ON state, it works like a short-circuit, and allows maximum current to transfer through. Ideally, S_{11} should be low at this state to attain better impedance matching while S_{21} should be 0 dB for 100% power transmission. However, in practical switches complete power transmission or reflection could not be achieved due to losses. S-parameters characteristics are important considerations for switch selection.

Two commercially available switches, Al/Ga/As beam lead (MA4AGBLP912) and Al/Ga/As flip-chip diodes (MA4AGFCP910) from M/A-Com Technology Solutions, have been inspected in the simulated antenna design for switching purpose. Diode MA4AGFCP910 offers an ON-state series resistance (R_s) of 4.2 Ω at 10 GHz and maximum series inductance of 0.5 nH, while switch at OFF-state offers capacitance of 20 fF and shunt resistance of 3 KΩ. Diode modelling based on the specifications mentioned in data sheet is performed in simulation and touchstone files from the vendors are also imported to validate the results based on the diode model. The touchstone files include the measured data of the actual diode response that can be imported in simulation to achieve close approximation of switch performance.

DC bias circuit is of critical importance in reconfigurable antenna design implemented by switches to achieve desired functionality. Incorporation of passive elements in circuit is tricky and challenging in terms of designing and fabrication of antenna prototypes. The switching loss in biasing circuit should be minimal by choosing the appropriate values of passive components like resistors, inductors etc. The width of DC-bias lines should also be minimised to control the effect of radiation from the lines, as the lines could act as

parasitic elements due to close proximity of antenna. If the bias line-width is too thick, it will couple with the antenna's geometry and contributes in radiation. On the other hand, if the bias line is too thin, it might not be able to handle the required value of bias currents. It is preferable that the width of bias lines should be as low as 0.1–0.2 mm. In order to see the impact of DC bias on the antenna, the biasing circuit is constructed in simulation using thin bias lines of 0.2 mm width; and inductors of 0.22 μH as the RF-chokes. Fig. 4.13 (a) presents the layout of the MMW frequency reconfigurable antenna design and the equivalent circuit models of PIN diode in ON and OFF states while Table 4-G illustrates the optimised dimensions of the proposed antenna. Simulated model with touchstone files in schematics window of CST is illustrated in Fig. 4.13 (b).

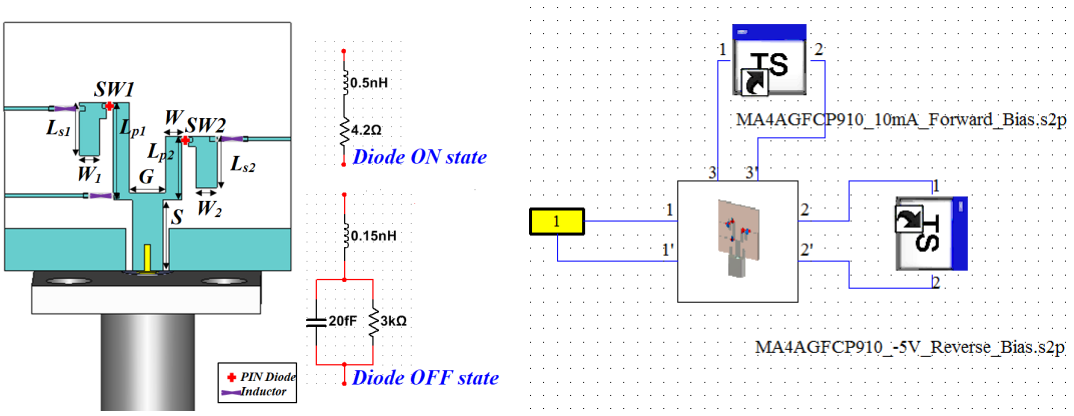

(a) (b)

Figure 4.13: MMW frequency reconfigurable antenna with PIN diodes: (a) simulated model with equivalent diode circuit, (b) simulated model with touchstone files.

4.5.2 Results and Discussion

It is observed from the simulated results of implementing PIN diodes with equivalent circuit model and with the touchstone files (experimental data of the switch performance) from the vendors, that both cases show approximately same operating bandwidth in each mode as referred in Table 4-H. However, the radiation pattern, realised gain and efficiency results with lumped model are presented in this section for performance evaluation.

Table 4-G: **Dimensions of MMW Flexible Frequency-Reconfigurable Antenna with PIN diodes**

Parameters	**Symbols**	**mm**
Length of prong 1	L_{p1}	5.5
Length of prong 2	L_{p2}	3.6
Length of stub 1	L_{s1}	3.0
Length of stub 2	L_{s2}	2.9
Width of each prong	W	0.9
Width of stub 1	W_1	1.1
Width of stub 2	W_2	1.2
Length of strip feeding	S	4
Gap between two prongs	G	2

A. Impedance Bandwidth

The MMW reconfigurable antenna operates in the frequency scanning mode and covers an impedance bandwidth of 20.7–33.2 GHz when both the switches are ON and incorporate both stubs in the radiating geometry (Mode 1). Frequency selection has been performed by altering switch configuration according to the states illustrated in Table 4-H. Fig. 4.14 depicts the four different modes of operation by means of S_{11} plots and represents the collective operating range of 20.7–36 GHz.

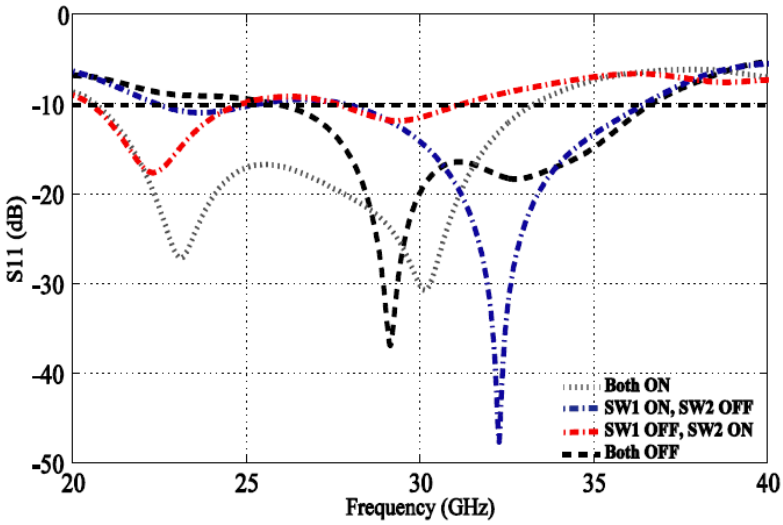

Figure 4.14: S_{11} of MMW frequency reconfigurable antenna with PIN diodes.

Table 4-H: **Switching Modes of MMW Flexible Frequency Reconfigurable Antenna with PIN diodes**

Mode	**SW-1**	**SW-2**	**Bandwidth-equivalent circuit model**	**Bandwidth-touchstone data**
Mode-I	ON	ON	20.7–33.2 GHz	20.2–33.0 GHz
Mode-II	ON	OFF	28–36.3 GHz	27.7–36.2 GHz
Mode-III	OFF	ON	20.5–24.7 GHz	20.2–24.3 GHz
Mode-IV	OFF	OFF	26–36.5 GHz GHz	26.1–36.3 GHz

B. Radiation Pattern

The radiation pattern of the antenna in the scanning mode (mode-I) is presented where maximum bandwidth is achieved. The E-plane and H-plane plots of Fig. 4.15 show a fairly consistent omnidirectional behaviour in the operating range of mode I. The radiation response observed in the other three modes of the designed antenna is shown in Fig. 5.16. The H-plane cut ($\phi = 0°$) is not perfectly circular in these modes due to an asymmetric patch geometry.

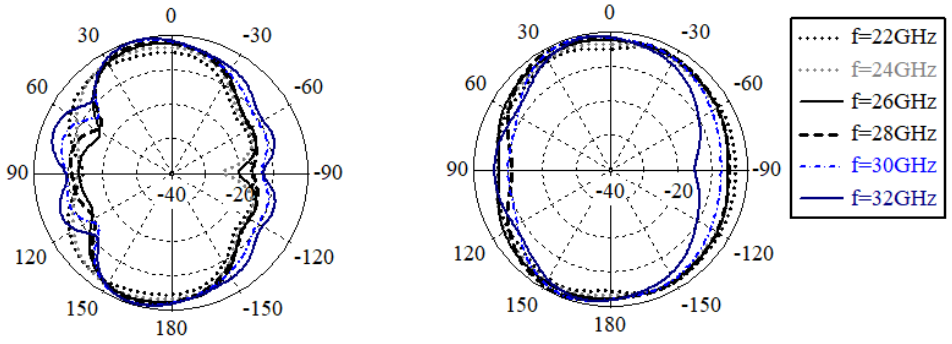

(a) (b)

Figure 4.15: Simulated radiation patterns of the MMW flexible frequency-reconfigurable antenna with PIN diodes in Mode I (a) $\phi = 90°$ and (b) $\phi = 0°$.

C. Realised Gain and Efficiency

Mode I is selected for presenting gain and efficiency profiles, as it is the spectrum sensing mode with the maximum bandwidth. The simulated results show that the peak

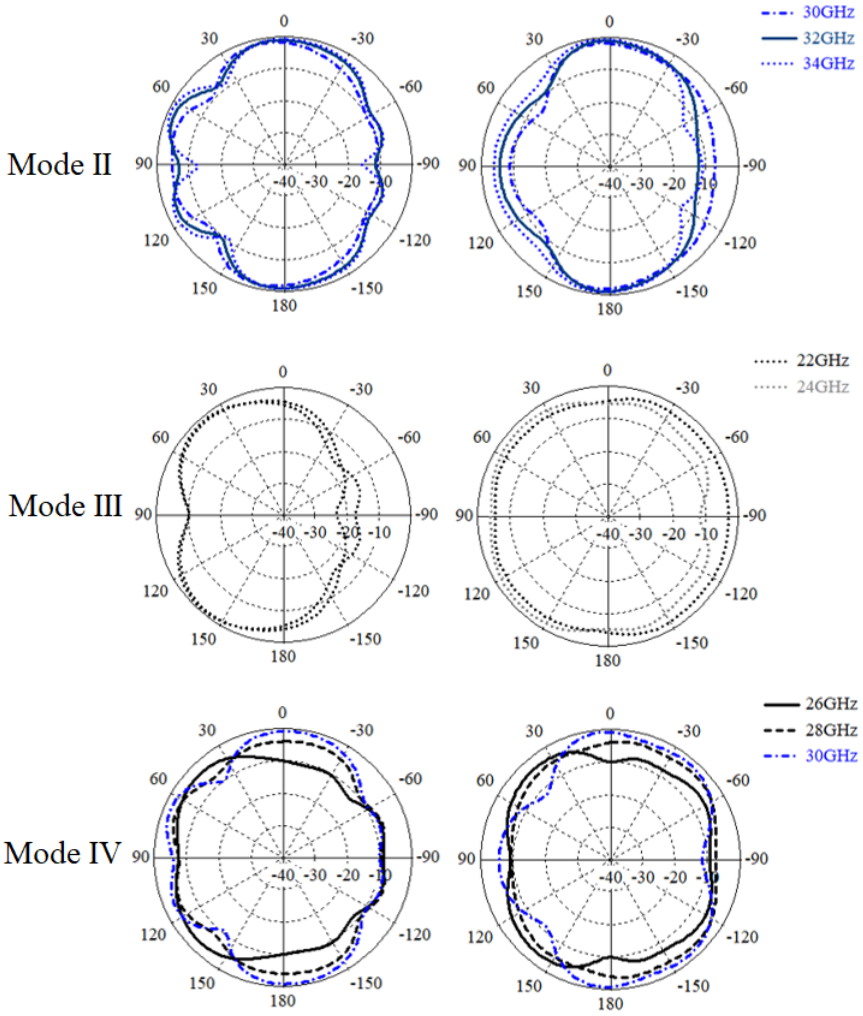

Figure 4.16: Simulated radiation patterns of the MMW flexible frequency-reconfigurable antenna with PIN diodes in Mode II, III, and IV at $\phi = 90°$ and $\phi = 0°$.

realised gain of the antenna is 5 dBi at 31.7 GHz in Mode I as shown in Fig. 4.16. Simulated efficiency of Mode I is above 75% in the operating range of 20.7–33.2 GHz.

4.6 Conclusion

This chapter has recommended an efficient spectrum utilisation approach by deploying MMW frequency reconfigurable antennas for 5G wireless networks. For this purpose, four

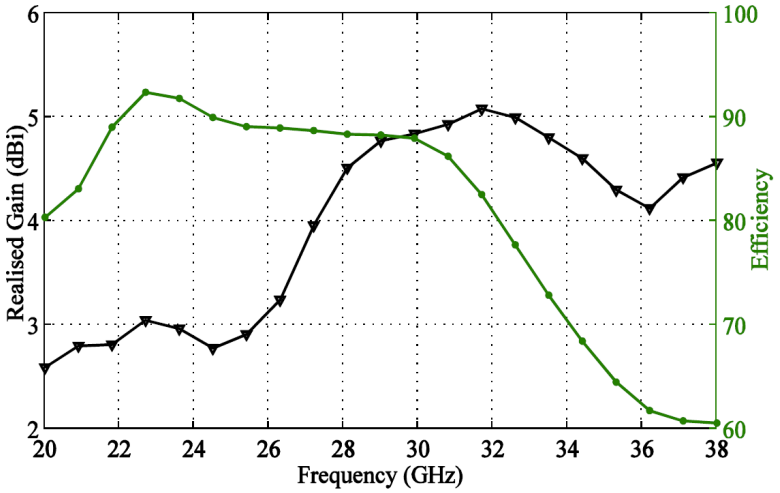

Figure 4.17: Realised gain and efficiency of the MMW frequency reconfigurable antenna with PIN diodes in Mode I.

distinct antenna designs have been presented, starting with a frequency tuning antenna on a rigid substrate. Then the flexible substrate was introduced in the antennna design for the frequency reconfiguration of 28/38 GHz bands. MIMO configuration was established along with the frequency reconfiguration of four distinct bands to enhance the spatial diversity in the third antenna design. The switching concept was implemented by means of open and short-circuit in the first three antenna configurations while in fourth antenna the actual PIN diode switches were integrated and complete biasing circuit was developed for the operation of switches. The features of compactness, light weight, structural conformity, as well as frequency reconfigurability, have suggested these antenna designs potentially suitable for 5G applications. However, single antenna elements though provide high bandwidth but have limited gain performance, which can be enhanced with the array configurations, discussed in the next chapter.

Chapter 5

5G Antenna Array based on Enhanced Franklin Model

5.1 Introduction

Antenna bandwidth is one of the fundamental requirements of 5G but there are several other parameters important to consider as well. For instance, in order to deal with the path loss issues related to atmospheric absorptions at high frequencies, high-gain antennas are required. Numerous techniques could be implemented to improve the antenna gain and directivity. As the size of antenna is small at MMW frequencies, integration of multiple antenna elements in arrays or grid assemblies would acquire a compact space and results in high gain and directive beam. Designing a simple, compact and efficient feeding network is challenging while incorporating antennas into arrays. Among shapes of microstrip antennas, the rectangular patches can be easily incorporated in series arrays [164] and grid structures [110]. Series arrays find their applications in fixed-beam arrays, frequency scanning antennas and leaky-wave antennas (LWA) [165].

Several novel 5G antennas and array at MMWs, especially at 28- and 38-GHz have been suggested in literature [166, 167]. However, the desired performance is limited due

to complexity of hardware integration, smaller form factor, installation and fabrication cost in most of the reported antennas. In this chapter, the main emphasis is to deploy the simplicity, compactness and relatively lower complexity of Franklin array for MMW antennas, and to diversify and extend the Franklin array concept with multiple resonant bands. This is accomplished by recommending an enhanced Franklin model, which offers a multiband and wideband operation in the FCC-suggested bands with high gain performance. At first, a multiband cellular antenna array based on the enhanced Franklin array model is developed providing a high-gain performance on the desired 5G bands. After that, a novel 2-dimensional (2D) antenna array targeting 5G bands is designed based on same strategy. Moreover, the concept of enhanced Franklin array is elaborated further to develop a wideband antenna on a flexible substrate.

5.2 High-Gain Franklin Antenna Array

Franklin array is developed on a collinear array (CoA) principle and composed of a series of patches provided with a well-matched in-phase feeding network between adjacent patches [168–170]. In the fundamental Franklin antenna, the dimensions of each segment are associated with wavelength of the design frequency, which restricts its operation to a single resonant band [171] (i.e., $f = c/\lambda$, where f = resonant frequency, c = speed of light, and λ = wavelength of resonant frequency). Two thin non-radiating transmission lines or stubs are inserted in between two adjacent half-wavelength (i.e., $\lambda/2$) long radiating elements. Each pair of stubs is folded and acts as a feed-line to the successive patch as well as a phasing network with 180° phase shift to minimise parasitic discontinuity at the junction. Franklin proposed that by employing non-radiating $\lambda/4$ stubs, the original out-of-phase currents could be transformed into an in-phase currents on each collinear segment (i.e., Fig. 5.1,) which provides one major broadside radiating beam [168, 171]. This configuration results in a compact arrangement of closely spaced patches with high gain and directivity, yet limited to narrow bandwidth.

Several modifications in high-gain Franklin antenna are suggested still the critical limitation is the narrowband operation [170, 172]. The CoA principle is also employed to propose a compact 2D antenna array in [173], offering high gain of 15.4 dBi, however, it is also restricted to a narrow bandwidth. Significant work has been done to increase the bandwidth of Franklin antenna, which either resulted in higher degree of design complexity [172], or influenced the compactness of the structure [174].

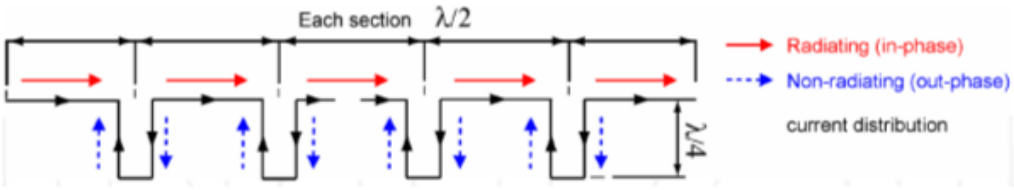

Figure 5.1: Franklin array; collinear segments provide in-phase current distribution [taken from 168, 171]

5.3 Enhanced Franklin Antenna Model

Enhanced Franklin antenna model introduced in this chapter is based on the geometrical modifications, and intentionally deviates the CoA principle to transform the narrow bandwidth of the Franklin array into a multiband. It is observed that the $\lambda/2$ length of the feeding network could be modified to generate additional resonances. If the stub length is changed such that it will not be a CoA anymore and not creating 180° phase shift, then the stub will no longer be non-radiating. The folded stub acts as a folded dipole-like antenna and its resonant frequency depends on the length of the folded dipole. This technique is implemented to design 1D and 2D antenna arrays offering multiband response at 5G bands. The proposed model is adaptable enough to offer successful tuning of any resonance of the multiband, while keeping the other bands intact.

The same concept is also utilised to develop a wideband flexible antenna for 5G wearable applications. The deviation of CoA principle by changing the stub length also results in a travelling-wave or LWA configuration, as the wave is not terminated at the end of each section. The LWA offers a wide bandwidth provided with a beam-sweeping,

which is helpful in wearable antennas, where larger scan area of radiation is more effective than a directive beam. The proposed array retains the high-gain of standard Franklin array with the additional features of beam steering over a wide bandwidth.

5.4 Millimetre-wave Multiband 1D Antenna Array

5.4.1 Antenna Design and Fabrication

This MMW antenna based on the enhanced Franklin array model is developed to achieve a reasonable gain of approx. 7–10 dBi, and a bandwidth which can cover 28- and 38-GHz bands suggested for 5G. In this 1D antenna with alternating patches and folded dipole stubs, the non-radiating stubs of length $\lambda/4$ are redesigned for the stub length of $\lambda/6$, where two folds of stubs act as a folded dipole antenna segment. This refers to a change in the total length of the folded stub from $\lambda/2$ (i.e., in the Franklin antenna) to $\lambda/3$ (i.e., in the proposed one). Here, the design frequencies are 5G bands (i.e. 28- and 38-GHz), therefore, the patch length is associated with $\lambda/2$ of 38-GHz, as the patch at 38 GHz will acquire lesser area than patch at 28 GHz. The other resonance is achieved by defining length of folded stub as $\lambda/3$ of 28-GHz. The resonant frequency of the folded dipole antenna is related with the mean-average length (i.e., L_{avg}) of the folded stub, which is computed by averaging the outer and inner lengths of the stub. The fringing field effects are also considered based on the transmission line model and incorporated as effective lengths in both patches and folded dipoles.

The proposed antenna consists of six unit cells arranged in a linear array configuration. Each unit cell is composed of two radiating elements, i.e., the patch and the folded stub. As each unit cell is repeated without any intermediate phasing network, this may cause an impedance mismatch at the terminating edges of each cell. The phasing mismatch can be improved by adjusting the patch width, gap between the folds, and width of the folded antenna. Fig. 5.2 (a) presents the simulated model of 1D array

of MMW multiband antenna of size 12.6 × 30 mm^2 designed by using the CST software. The design parameters of Fig. 5.2 (a) along with the optimised dimensions are tabulated in Table 5-A. The antenna is fabricated on a 0.8 mm thick Rogers RT/duroid 5880 substrate ($\varepsilon_r = 2.2$, tan$\delta = 0.0009$) with 17.5 μm thick copper cladding. A feeding strip of length 2.25 mm is provided at one end of the array of unit cells. The LPKF laser machine is used to achieve precise prototyping to avoid frequency shifts and the fabricated prototype is shown in Fig. 5.2 (b).

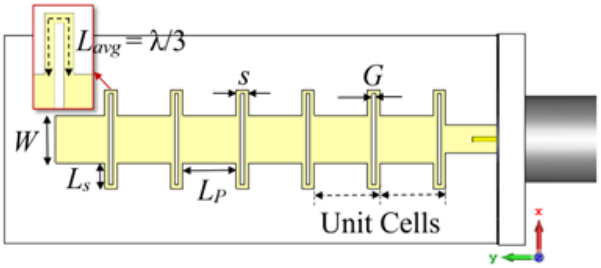

(a)

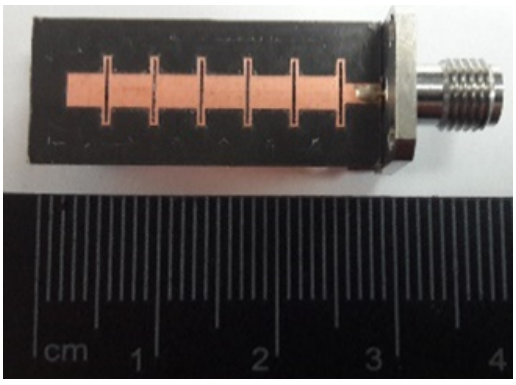

(b)

Figure 5.2: MMW multiband 1D antenna array: (a) Simulated model, (b) Fabricated antenna prototype.

5.4.2 Proposed Antenna Performance Analysis

The performance of the proposed 5G multiband antenna is examined by means of the scattering S–parameters, far-field radiation characteristics, and the realised gain profile. The measurements taken in the far-field anechoic chamber of the National Physical Laboratory (NPL) validate the numerical evaluations carried out in CST software.

Table 5-A: **Optimised Dimensions of Multiband 1D Antenna Array**

Parameters	**Symbols**	**mm**
Length of patch	L_p	3.26
Width of patch	W	2.9
Length of stub	L_s	1.65
Width of folded stub	s	0.74
Mean length of folded stub	L_{avg}	3.54
Gap of folded stub	G	0.24

A. Impedance Bandwidth

Simulated and measured S_{11} plots of Fig. 5.3 depict that at -10 dB reference the measured bandwidth of the proposed antenna is 27.9–33.2 GHz, and 34–39.1 GHz. Though, mismatches have appeared in the S_{11} plot magnitudes mainly due to connector and cable intolerances, but the resonant frequencies and the corresponding bandwidth remain conserved at the desired FCC-allocated 5G bands. Figs. 5.4 (a) and (b) present the parametric analysis performed in the CST simulation to identify the frequency tuning parameters of the two bands of interest. The analysis suggests that stub length L_s controls the resonant frequency of band I (i.e. 28-GHz), while band II (i.e. 38-GHz) can be tuned by changing the patch length, L_p.

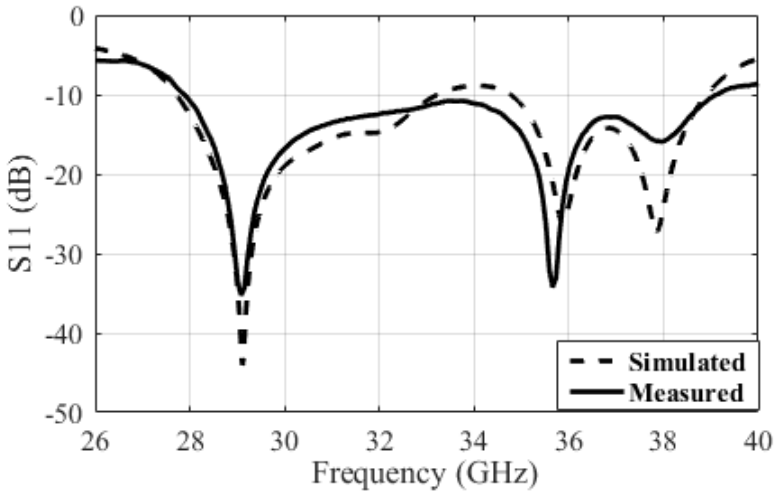

Figure 5.3: Simulated and measured S_{11} plots of MMW multiband 1D antenna array.

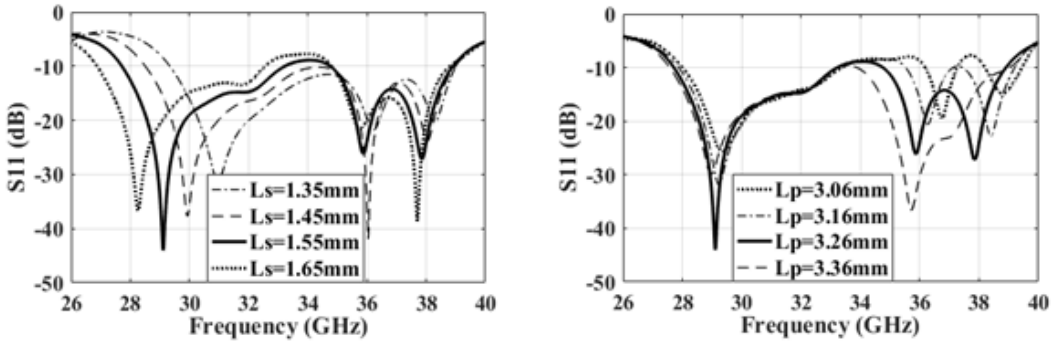

(a) (b)

Figure 5.4: Parametric study of the MMW multiband 1D antenna array: (a) Frequency of band I can be tuned by length of stub, L_s, (b) Frequency of band II can be tuned by patch length, L_p.

B. Radiation Characteristics

The co- and cross-polarised far-field radiation patterns of the proposed 1D antenna array are shown in Fig. 5.5 at three resonant bands. The results depict a close match between the simulations and measurements. The main beam in band I is along the boresight direction and tilted towards end-fire direction at an angle of 30°. In band II, the maximum radiation is along the end-fire direction in 36–38 GHz with grating lobes, and exhibits a response similar to a LWA. The LWA sweeps its radiation beams as the frequency sweeps. The compact linear arrays usually exhibit radiation characteristics like LWA if the wave remains continuous at the end of each segment.

C. Realised Gain

Table 5-B provides the realised gain computed by Two-antenna method at the distinct frequencies over the operating range. Reasonable gain profile has been achieved which covers a wide bandwidth of K_a–band. The results verify the high performance claim of multiband enhanced Franklin antenna as required by the advanced paradigm shift, which is currently undergoing for the K_a–band 5G-centric communication architectures.

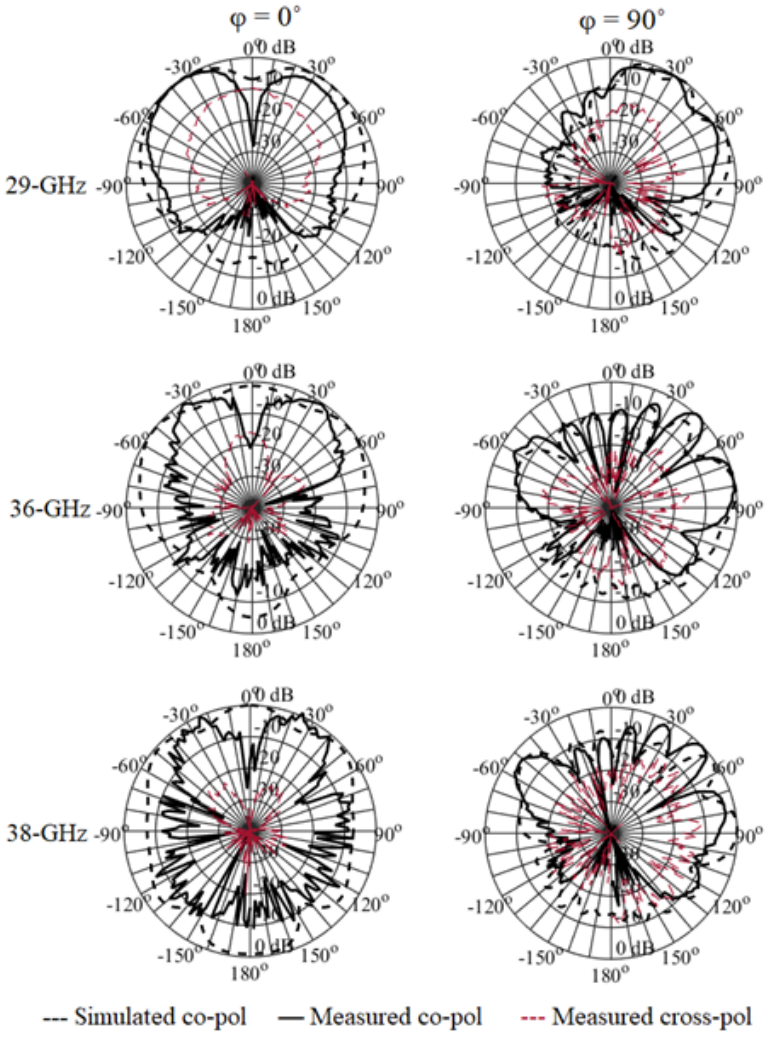

Figure 5.5: Co- and cross-polarised radiation patterns of the MMW multiband 1D antenna array.

Table 5-B: **Realised Gain of MMW Multiband 1D Antenna Array**

Frequency (GHz)	**28**	**30**	**32**	**34**	**36**	**38**
Simulated Gain (dBi)	7.15	7.91	8.19	8.81	10.09	9.9
Measured Gain (dBi)	7.2	7.64	7.94	8.68	10.23	9.8

5.5 Millimetre-wave Multiband 2D Antenna Array

5.5.1 Antenna Design and Fabrication

In this section, 2D illustration of the enhanced Franklin array is presented to achieve compactness, a multiband response at 5G frequencies, and a high gain of 10 dBi or above. Based on these objectives, a 2D antenna is developed at K_a–band by utilising the enhanced Franklin array concept. As discussed previously, multiple frequency bands are generated by altering the standard CoA principle and introducing new fractional length for folded stubs of the antenna. The fractional lengths for the standard CoA comprising of a series of patch elements and stubs constituting 180° phase shift are shown in Fig. 5.6 (a). The first geometric variation made at this point is the transformation of the standard non-radiating stubs into folded-dipole-like antennas as described by the enhanced Franklin model. The resonant frequency of folded dipole antennas is determined by the radiating length of the stubs. This transformation provides a simplicity to create additional resonance within the same compact area, though, there is a compromise of a slight detuning of main radiating beam as the phasing network has been removed. Thus, each unit-cell incorporates a rectangular patch, and a folded-dipole-like stub, both are designed for distinct radiating frequencies, as presented in Fig. 5.6 (b).

The layout of the linear Franklin array is extended in 2D, provided with a single feeding line. This novel antenna offers high-performance in terms of high bandwidth and compact footprint to integrate 3 × 3 unit cells. The 28-GHz band is attained in the proposed structure by using a stub length of $\lambda/4$ (i.e., at 28-GHz) instead of $\lambda/2$ as suggested in [168, 170], depicted in Fig. 5.6 (a). The stub is then folded from the centre like a folded-dipole-antenna, as shown in Fig. 5.6 (b). In this way, an additional resonance is generated in the former feed-line, which has been transformed into a folded-dipole-like antenna and is fed from the successive patches. Current distribution in Fig. 5.6 (c) explains the travelling wave in the designed antenna geometry.

The design frequency mid-way between 33-GHz and 38-GHz is selected for antenna patches and radiating length is fixed as $\lambda/2$. CST software has been used for the design, modelling and evaluation of results. It has been observed by the numerical analysis that a single resonance at 36.5-GHz can split into a dual-band by introducing an increment 's' in the length of the patches positioned at the terminating edge of the array, as shown in Fig. 5.6 (d). This additional length is incorporated in the patch length L_p of the terminating row to adjust the wave propagation as there is no interconnection between the patches at the far end of the designed grid layout. Parametric studies have shown that the 33-GHz and 38-GHz bands can be tuned by varying the parameter L_p along the y-axis, i.e., the greater the length, the lower the resonant frequency will be.

The distance between the centres of the two parallel patches is set as λ (i.e., at 38-GHz) to lower the mutual coupling. Concisely, the standard unit-cell in [160] suggesting a dipole arrangement consisting of two patches of length $\lambda/2$ and a $\lambda/2$-long feed line in the centre, has been changed in this 2D array of patches and folded-dipole-like antennas. Each element (i.e., patch or folded-dipole) acts as a standalone fully-matched antenna to minimise parasitic discontinuities without any additional feeding network inserted between antennas, and also each antenna is fed from the preceding antenna. Microstrip line of length 'l_f' along with the matching stub of width 'w_s' is designed to feed the array from the centre point of one terminating edge. The simulation layout of 2D antenna array along with the designed parameters and the fabricated prototype are presented in Figs. 5.6 (d) and (e), while the design parameters are demonstrated in Table 5-C. Rogers RT/duroid 5880 ($\varepsilon_r = 2.2$, and $\tan\delta = 0.0009$) of height $h = 0.8$ mm is used as a substrate with a metallic ground at the bottom.

5.5.1.1 Proposed Antenna Performance Analysis

The proposed 2D antenna array is analysed by the parametric study, and the performance is validated by measurements of the S–parameters, radiation pattern, and the realised gain. The measurements of radiation pattern are carried out at National Phys-

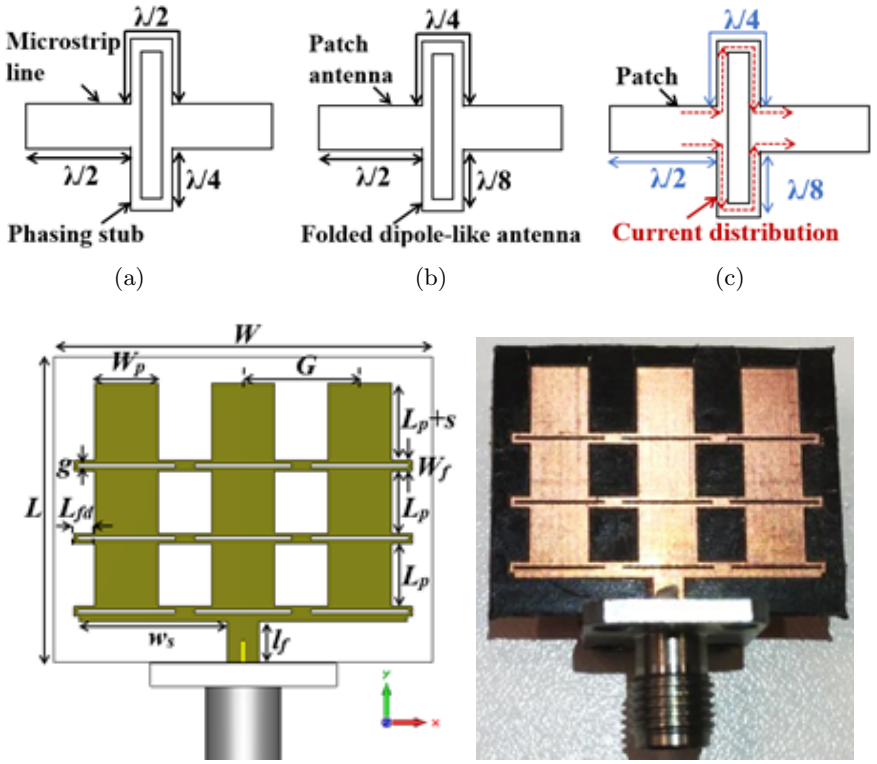

Figure 5.6: MMW multiband 2D antenna array: (a) Standard Franklin unit-cell; (b) Proposed array unit-cell; (c) Proposed array current distribution; (d) Simulated 2D array; (e) Fabricated prototype.

Table 5-C: **Optimised Dimensions of MMW 2D Antenna Array**

Parameters	**Symbols**	**mm**
Length of patch	L_p	4.3
Width of patch	W_p	4.34
Extended length of terminating patches	s	1.0
Gap between centres of two parallel patches	G	8.0
Length of folded-dipole	L_{fd}	1.4
Width of folded-dipole	W_f	0.7
Width of matching stub	w_s	10.15
Length of feed	l_f	2.8
Gap of folded-dipole	g	0.26
Length of array prototype	L	21.0
Width of array prototype	W	26.0

ical Labortory (NPL) by using the far-field anechoic chamber. Measurements agree with the simulations, despite of some mismatches mainly due to fabrication intolerances, connector, and cable losses etc.

A. Impedance Bandwidth

Fig. 5.7 presents the S_{11} plots of the 2D array, which depict multiple bands taking -10 dB as a reference. S_{11} magnitudes show relatively more mismatches with the simulation at 28-GHz band as compared to 33-GHz and 38-GHz bands due to lower resolution of the LPKF machine, which might have caused more obvious fabrication intolerances in the dipole structure than the patch dimensions. Several parameters such as, mutual coupling associated with the gap between the patch centres, dimensions of feed, and gap of the folded-stub are important to optimise the S_{11} profile of the antenna. Parametric study to determine the frequency tuning parameters depicted in Fig. 5.8 (a) shows that L_p controls the frequency tuning of 33-GHz and 38-GHz bands based on the principle of greater the length, lower the resonant frequency will be. The patch length at the terminating end of the array is set as L_p+s to compensate for the wave propagation, as the patches are not interconnected by means of folded-dipole assembly. It is observed that s is also capable of frequency tuning as it splits a single resonance at 36.5-GHz (i.e., when s = –0.55 mm) into a dual-band, as shown in Fig. 5.8 (b).

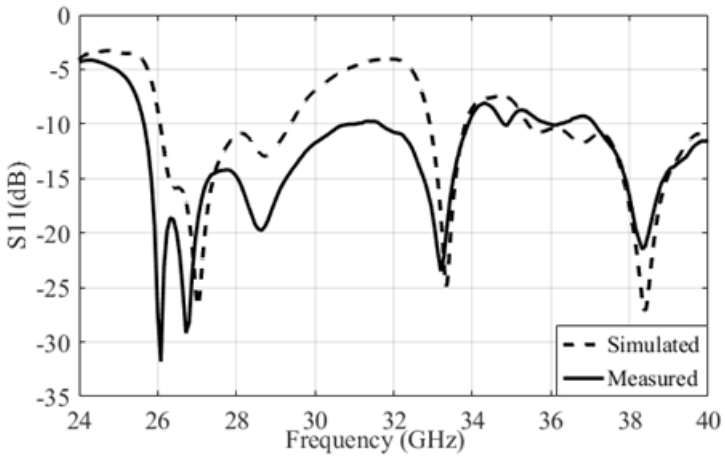

Figure 5.7: Simulated and measured S_{11} plot of the MMW multiband 2D antenna array.

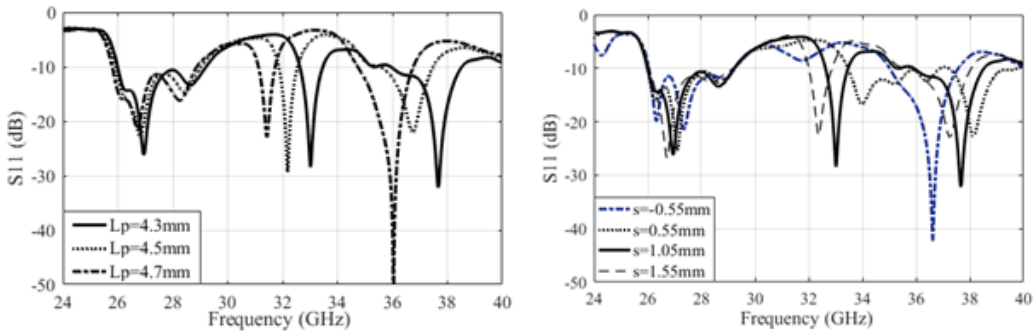

(a) (b)

Figure 5.8: Parametric analysis of the MMW multiband 2D antenna array: (a) Analysis by varying the length of patch L_p; (b) Analysis with incremental length s.

B. Radiation Characteristics

The far-field normalised radiation patterns of Fig. 5.9 show that the absence of phasing network results in the main beam shift from standard 0° of broadside direction in all the three bands. It is important to mention that the requirements of high gain and directivity at MMWs are generally to deal with the path loss attenuations in both the LOS and NLOS environments, which suggests that the observed beam shift would not affect the performance in NLOS links. Band 1 at 28-GHz offers maximum directivity at 29-GHz, where the main beam is at 50°. While in 33- and 38-GHz bands, the main beam is more dispersed and having lower directivity than 28-GHz band due to leaky-wave effect. As the length of unit cell is less than $\lambda/2$, wave is not truncated at the end of each unit cell, the designed array acts similar to a leaky-wave or travelling-wave antenna, which exhibits beam shift with the frequency sweep.

C. Current Density

Surface current distribution is analysed at different resonant bands and provides an insight of the designed multiband 2D antenna array. Fig. 5.10 (a) shows that at 29-GHz, a high current density is observed at the folded-dipole stubs. However, Figs. 5.10 (b) and (c), show the antenna patches are spots of high current density as compared to the

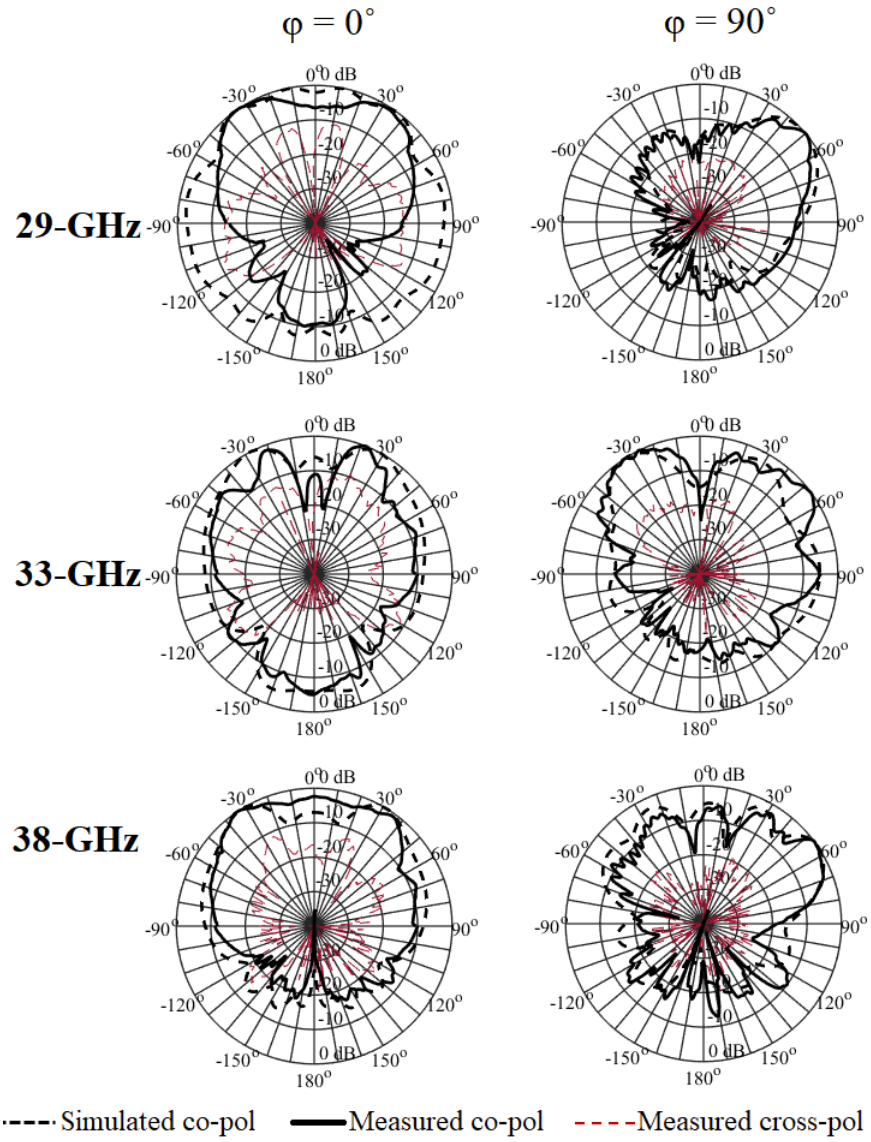

Figure 5.9: Simulated and measured normalized radiation patterns (at $\phi = 0°$ and $\phi = 90°$) of the MMW multiband 2D antenna array.

stubs, which explains that the patches are radiating at 33- and 38-GHz bands.

D. Realised Gain and Efficiency

Simulated and measured realised gain of the proposed antenna array is presented in Fig. 5.11. Two-antenna method is used for evaluation of measured gain which is above 7 dBi in the bandwidth of each band. The measurements show that the peak gain of

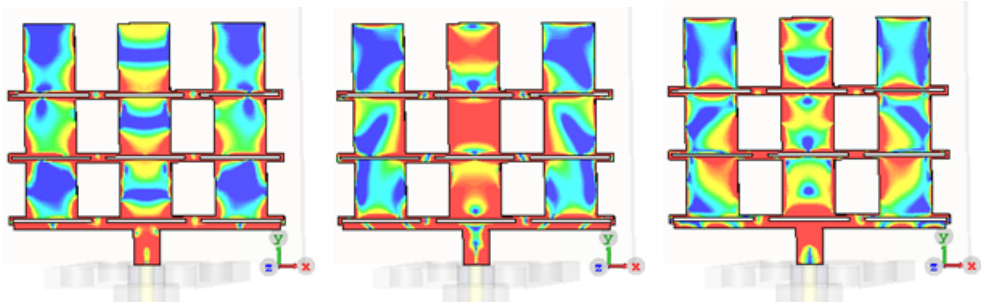

(a) (b) (c)

Figure 5.10: Surface current distribution of the MMW multiband 2D antenna array: (a) at 29-GHz; (b) at 33-GHz; (c) at 38-GHz.

13.5 dBi is observed at 29-GHz, while the other bands also offer reasonable gain, i.e., 8.33 dBi at 33-GHz, and 9.58 dBi at 38-GHz. The single resonance at 36.5-GHz, tuned from L_p, splits into dual-band by parametric analysis of s, which results in lowering the gain due to gain-bandwidth trade-off. The gain can be further improved with increase in number of the antenna elements. However, for compatibility of the integration in mobile handset PCB board of size 50 × 30 mm^2, the proposed dimensions are restricted to 3 × 3 array of the size 21 × 26 mm^2. Moreover, numerical results also present an efficiency of approximately 70% and above, in all of the MMW bands of the antenna.

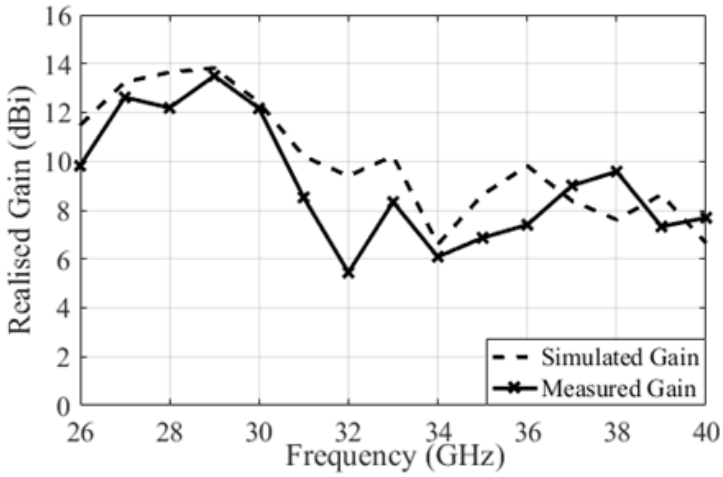

Figure 5.11: Simulated and measured realised gain of the MMW multiband 2D antenna array.

5.6 Flexible Enhanced Franklin Antenna Array

5.6.1 Antenna Design and Fabrication

In this section an attempt has been made to utilise the extended Franklin model in the antenna design for conformal applications. The objectives are to incorporate the gain of approx. 6–8 dBi, bandwidth of 5 GHz and beam-scanning capability into a flexible and bendable antenna. The antenna is suitable to operate on both Ofcom (26-GHz) and FCC (28-GHz) 5G standards. The fractional length of both patch and folded stub is altered in this case and both design frequencies are selected to be close enough to merge into a single wideband response. It is suggested that both the lengths are of quarter-wavelength ($\lambda/4$) at the desired operating frequency. In order to achieve a wider bandwidth the two radiating lengths are adjusted according to the lower and upper cut-off frequencies of the intended bandwidth. Hence, the two main variable lengths are modified, as follows:

a) Length of each resonant patch = $\lambda_L/4$ (where f_L = lower cut-off frequency)

b) Stub length = $\lambda_U/4$ (where f_U = upper cut-off frequency).

Parametric analysis shows that the width of the radiating patches controls the impedance matching while the width of stubs and the gap between the folded stubs affects the return loss. The dimensions of design parameters depicted in Fig. 5.12 (a) are tabulated in Table 5-D, to construct a wideband antenna array on a flexible substrate.

The numerical modelling of the PET based antenna is carried out using CST software. The six-element Franklin array is designed on the substrate of $12 \times 28.2 \times 0.4$ mm^3. The bottom part of the substrate is provided with a continuous ground. It has been observed by performing numerical analysis that the 'h' effects the antenna bandwidth, i.e. the greater the height, the wider the bandwidth, while similar findings are also reported in [175]. Contrary to this, the greater the 'h' will lead to thicker substrates with lesser flexibility and conformity. The 0.4 mm thickness is suggested based on the analysis to

achieve a reasonable reflection coefficient profile while retaining the desired flexibility of the substrate. Fig. 5.12 (a) shows the simulated prototype of the proposed flexible array.

The flexible antenna is fabricated on surface treated PET film ($\varepsilon_r = 3.2$, $\tan\delta = 0.022$ at 10-GHz). Inkjet printing process is employed by using DMP-2831 with silver nanoparticle ink. Surface treated PET film with the standard height (h) of 135 μm $\pm$ 12 μm is used. Height of substrate (h) of 0.4 mm is selected as an optimal choice in this regard, which is attained by bonding the three PET sheets. Thin layer of 0.5 μm of conductive silver ink is deposited on the surface with the pattern resolution of approximately $\pm$20 μm. Drop spacing, jetting frequency, firing voltage of ejecting nozzles, temperature of the printhead, waveform characteristics and other cartridge settings have been adjusted to an optimum level in order to achieve a highly precise fabrication [176, 177]. Silver nanoparticle ink (i.e., Colloidal Ag-J solid Ag) is selected for the printing process with a drop spacing of 15 μm (i.e., 1693.33 dpi), to achieve a good quality printing. The ink incorporates silver particles encapsulated in polymers to prevent oxidation and dispersed in an inert solvent. Post-printing drying, curing and sintering processes are essential to enhance the conductivity of the prototype. The reported conductivity of nanoparticle silver is $0.4 \approx 2.5 \times 10^7$ S/m, and is determined by the number of successive layers printed, as well as temperature and interval of the curing and sintering processes [176–178]. If properly sintered, the conductivity of approximately $0.3 \approx 0.7 \times 10^7$ S/m can be achieved from a single printed layer [178].

The selected PET films are processed with a microporous coating of chemically active components, capable to perform rapid drying and chemical sintering of the printed pattern of silver ink in order to facilitate reliable conductivity performance. The microporous coating is also useful in improving ink adhesion on the PET surface, as this surface treatment elevates the surface energy of PET surface and offers a capability to bond the ink chemically with the surface, which eventually holds the ink intact in a precise and definite pattern [179]. Fig. 5.12 (b) presents the fabrication of the proposed Franklin array obtained by the inkjet printing.

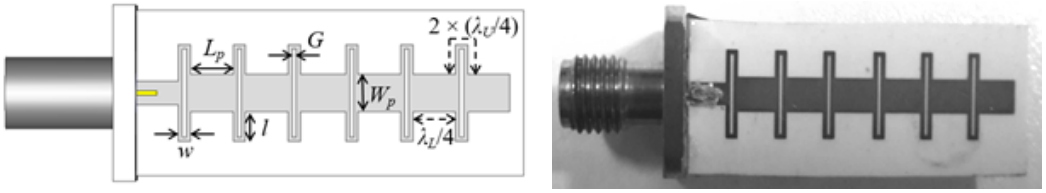

(a) (b)

Figure 5.12: MMW flexible enhanced Franklin array; (a) Simulation model, (b) Fabricated prototype.

Table 5-D: **Dimensions of the Flexible Enhanced Franklin Antenna**

Parameters	**Symbols**	**mm**
Length of patch = $\lambda_L/4$, where f_L = 24 GHz, λ_L = 12.5 mm	L_p	3.1
Width of patch	W_p	2.7
Length of stub $\approx \lambda_U/4$	l	2.15
Width of feed	w	0.9
Length of folded stub = 2 × ($\lambda_U/4$), where f_U = 30 GHz, λ_U = 10 mm	$2l + w$	5.2
Gap of folded stub	G	0.3

5.6.2 Proposed Antenna Performance Analysis

The conductivity of the printed layer affects the antenna performance especially magnitude of gain which can be improved by the repetitive multiple layer printing process, and also performing the appropriate heat treatment in order to enhance the surface current density by increasing the sheet conductivity.

A. Impedance Bandwidth

The S_{11} plots of Fig. 5.13 shows a good agreement between the measurements taken of the fabricated prototype and simulated results of CST, hence validating the proposed findings of the designed LWA. Measurements have shown that a bandwidth of 24.6–30 GHz has been achieved from the fabricated prototype with the substrate height of 0.4 mm. The slight shift in the measured S_{11} might have been caused by the possible variations in the dielectric constant, due to the tape bonding of PET substrate sheets.

Surface gradients of the printed layer may also be another cause of deviation from the expected S_{11} behaviour, as the printed nanoparticles are not heated to melt and combine in a form of a uniform layer. Bandwidth is improved by parametrical optimisation of patch and phasing stub dimensions. Fig. 5.14 shows a parametrical reduction in the substrate height (h) to an optimum level to retain the flexibility of substrate as well as to avoid a big distortion in impedance bandwidth, which results in achieving a high bandwidth without any compromise in gain of antenna.

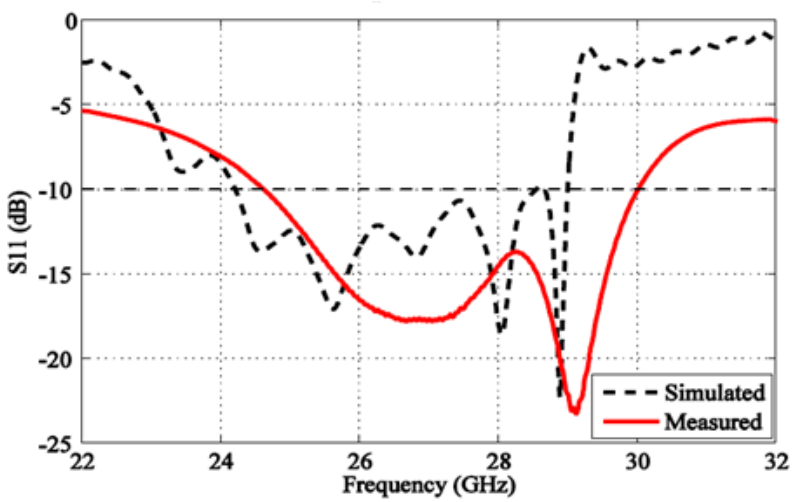

Figure 5.13: Simulated and measured S_{11} plots of flexible enhanced Franklin antenna array.

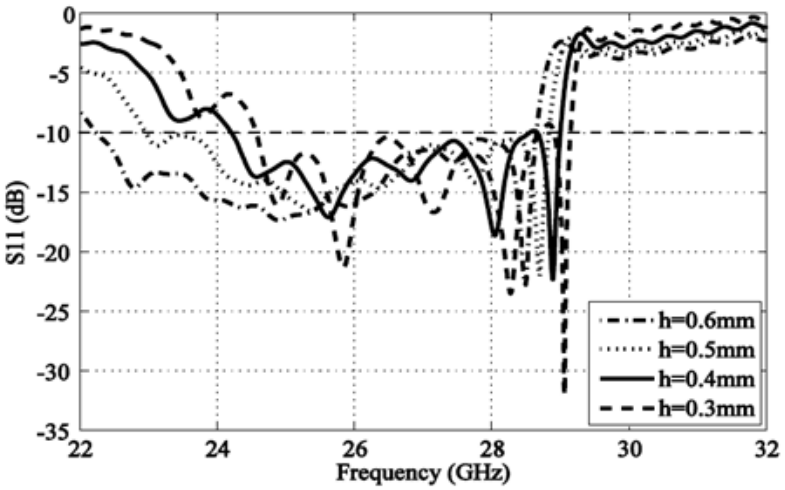

Figure 5.14: Parametric analysis with respect to height 'h' of MMW flexible enhanced Franklin antenna array.

B. Radiation Characteristics

The radiating beam of designed LWA offers suitable directionality, and covers a quadrant of sphere from broadside to end-fire direction by the beam scanning over the range of 24.6–30 GHz. At 24 GHz, the radiation pattern is almost broadside and it becomes end-fire at 29 GHz. The resulting directional beam is instrumental and the beam-steering modifications can be applied to array structure to perform pattern reconfiguration. Fig. 5.15 shows the simulated results of 3D far-field radiation pattern at different frequencies where beam steering can be observed with the frequency sweep.

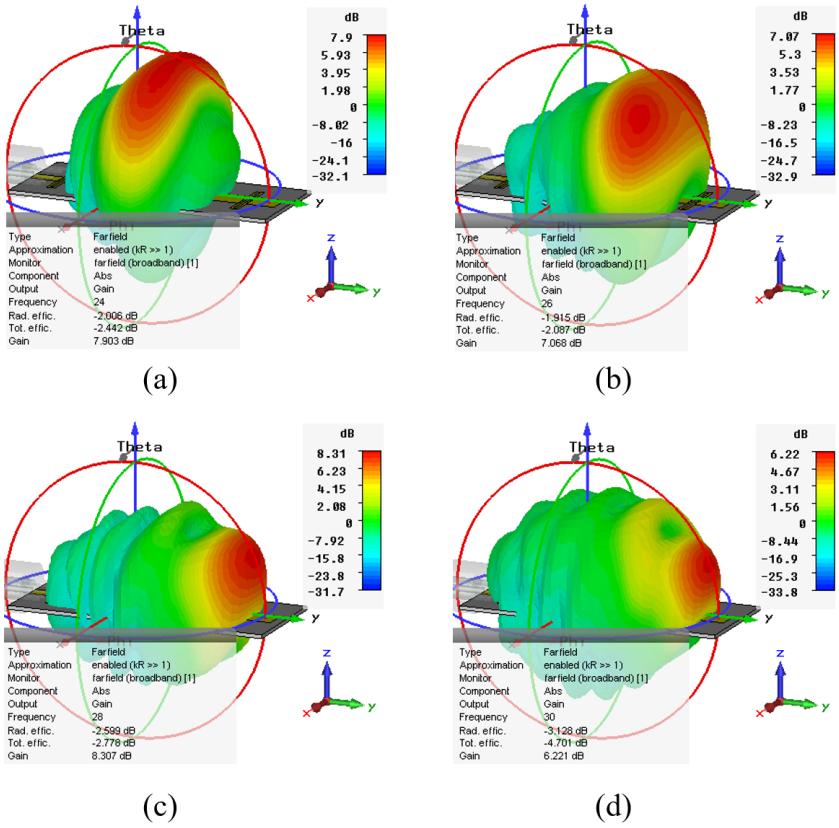

Figure 5.15: The flexible enhanced Franklin antenna array radiation patterns, along with the magnitude of the realised peak gain: (a) at 24-GHz; (b) at 26-GHz; (c) at 28-GHz; (d) at 30-GHz.

C. Realised Gain and Efficiency

The plot of Fig. 5.16 shows the simulated results of peak gain and efficiency against

frequency of the designed flexible antenna. The peak gain of 8.3 dBi has been observed at 28-GHz, as well as the magnitude is above 7 dBi in maximum part of bandwidth. The presented gain profile is computed by modelling the silver as a single conductive layer of 0.5 μm thickness in the CST software. Radiation efficiency is approximately 60% in maximum operating range of the proposed wideband operation. Due to lossy nature of most of the flexible substrates such as, paper, fabric etc. the efficiency of wearable antennas is usually low. Considering the loss of PET material and effect of insertion of tape layers for bonding, the proposed antenna is considered as reasonably efficient as compared to several other flexible materials.

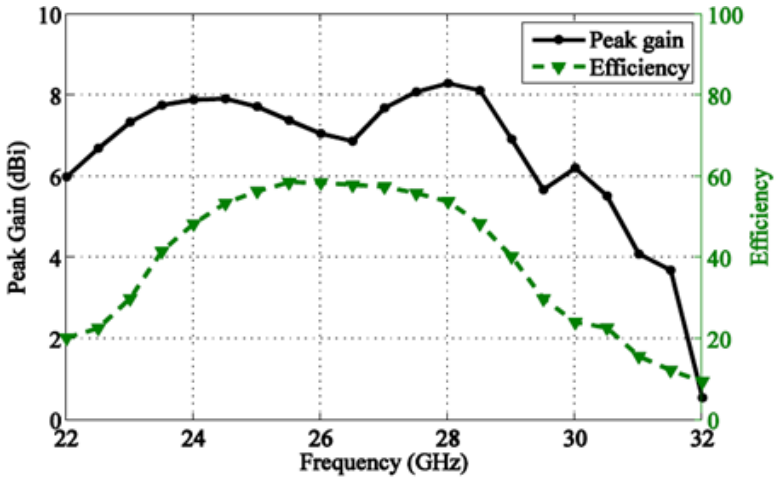

Figure 5.16: Simulated plot of peak gain and efficiency vs. frequency of the flexible enhanced Franklin antenna array.

5.7 Conclusion

In this chapter, enhanced Franklin array model has been developed as a novel approach to design a multiband MMW antenna array for the potential employment in the 5G cellular networks. In the first design, the conventional non-radiating phasing stub of $\lambda/2$ length was transformed into the radiating stub of $\lambda/3$ length. The proposed multiband antenna was developed to operate at the FCC-allocated 5G bands of 28-GHz, and 37–39 GHz. In second antenna configuration, the stub length was changed to $\lambda/4$ to attain

a triple-band response at 28-GHz, 33-GHz, and 37–39 GHz with the peak gain of 13.5 dB at 29-GHz. Also, the linear array was transformed into a well-matched 2D array configuration with the advantages of compactness, efficient design, and planar geometry. In the third antenna design, beam sweeping from broadside to end-fire direction like a LWA was achieved over a wide bandwidth of 24.6–30 GHz by changing the patch langth as $\lambda_L/4$ and stub length as $2 \times \lambda_U/4$. The proposed array was inkjet printing on a flexible PET substrate for the potential integration in wearable applications.

The proposed MMW arrays based on enhanced Franklin model are novel contributions in the development of 5G cellular antennas, with the advantages of high gain due to array topology and bandwidth from a multiband operation. However, the gain is not equally high in all the bands and these variations often restrict the utilisation of certain low gain bands in some particular applications. This suggests that there is a need of further improvement in antenna design to attain high and reasonably constant gain magnitudes over the entire bandwidth, which is demonstrated in the next chapter.

Chapter 6

Liquid Crystal Polymer based Conformal Antenna Array

6.1 Introduction

Flexible and conformal antennas, devices and other electronic circuitries are considered as fundamentally essential in the deployment of MMW based 5G systems in order to enhance the feasibility of integrating wireless networks in wearables and body-centric applications for a robust and reliable user-experience. The vision of 5G networks has been diversified beyond the boundaries of traditional hand-held mobile phones, and projected to deliver a versatile and ultra-dense communication system, which demands high bandwidth and high gain performance. Size reduction and device compactness, conformity of implements, as well as cost-effectiveness and light-weight are also significant 5G concerns. Recently, several advanced initiatives have been conducted in the implementation of high-speed, precise and low-cost manufacturing methods such as inkjet printing, screen printing and laser prototyping for antennas and RF devices on flexible substrates. These technologies have potentially increased the number of wireless devices incorporating flexible and conformal antennas and circuits.

However, most of the flexible antennas are reported for low frequencies and there is a need to focus on potential designs of high-frequency flexible antennas for 5G. Among the available MMW bandwidth, K_a–band is emphasised for 5G standards where FCC recommends 28- and 38-GHz bands, and Ofcom insists on the use of 26-GHz. These variants could be handled by designing an efficient antenna array for 5G front-ends which can offer an ultra-wide bandwidth to effectively cover multiple standards and provides a consistent gain in the intended operating range to ensure reliable performance. In addition to these, the design should be low-profile, less-complex, cost-effective, and flexible enough to be bend, fold or mount on an irregular or non-planar surface.

Several flexible materials such as polymers and textiles have been used for developing wearable antennas at MMW frequencies. LCP is among the attractive choices for flexible antenna design at high-frequency due to low-loss characteristics, negligible moisture absorption, high resistance to chemicals and temperature handling up to 300°C. Flexible and foldable films of LCP material are commercially available in the range of 25–180 μm thickness with a dielectric constant of $2.9 \approx 3.1$, and usually cladded with copper for prototyping by using an etching process [180]. In this chapter, LCP based MMW antenna is designed, modelled and fabricated by two precise and advanced techniques of laser prototyping and inkjet printing for the prospective utilisation in 5G flexible applications. A comparative analysis on the antenna performance in terms of gain and bandwidth is presented in this chapter based on two different fabrication methods.

The inkjet-printed prototype requires post-printing drying, curing/annealing and sintering processes to enhance the conductivity of the printed layer, where heat or laser exposure is usually employed. Laser sintering is fast and efficient but requires an effective control over the intensity of laser beam and the exposure duration, while mishandling of these factors can cause severe damage to the printed pattern or even the substrate. Heat sintering is a time-consuming process and required heat exposure ranging from several minutes to hours which can cause shrinking, decolorisation or bending of substrate. Heat sintering has been improved and a much faster way to perform heat sintering is

developed and presented here in this research. It has been observed that using a heat press with a properly controlled temperature and duration instead of the oven could efficiently reduce the sintering duration from several minutes to a few seconds. In addition to this, a novel design of two-element array is also developed on LCP substrate to elaborate the concept of potential deployment of antenna in an array assembly where the bandwidth remains conserved and an improved gain profile is attained. It is worth mentioning that improving the gain in the overall range of 14 GHz (i.e. 26–40 GHz) is highly challenging task as the antenna arrays with conventional feeding networks are usually narrowband. This limitation has been improved in the proposed antenna array which constitutes high gain stability over the wide bandwidth of operation.

6.2 High-Gain Millimetre-Wave Flexible Antenna

6.2.1 Antenna Design

The proposed antenna is designed with the objectives of flexibility, compactness, fast fabrication and a gain above 8 dBi in the complete 14 GHz bandwidth of K_a–band. Another aspect is to achieve consistently high gain magnitudes to efficiently utilise the complete bandwidth. This novel antenna geometry is designed as a single-sided prototype comprising of a tapered rectangular patch with a CPW feed, while a pair of L-shaped stubs is symmetrically added as a part of the ground plane. Flexible film of LCP substrate of dimensions 11 $\times$ 12 mm^2 is used for conformal antenna fabrication. CST software is used for the design, modelling and numerical evaluation. The tapered geometry is responsible of increasing the radiating length of the patch. This particular type of ground geometry is designed to suppress the radiation of the omnidirectional monopole antenna along the horizontal (azimuth) plane, which causes the radiation to converge orthogonal to antenna (elevation) plane. In order to obtain the desired performance while preserving the simplicity of design, the numerical optimisation of several parameters is carried out. For instance, parametric analysis of the patch dimensions, tapered length,

size and geometry of the stubs and distance between the stub and patch are particularly important. The antenna design parameters and the respective dimensions of the CST model of Fig. 6.1 (a) are tabulated in Table 6-A.

In order to demonstrate the suitability of the proposed antenna in conformal applications, it is required to examine the antenna response when mounted in bending position. The CST model of the antenna is bent along the curved surface of a cylinder with radius 10 mm as shown in Fig. 6.1 (b). The observations based on the numerical results validate the robust and steady performance in conformal implements which is similar to the planar integrations. The antenna is subjected to two completely different fabrication methods which implies to variation in metal-layer thicknesses and electrical conductivities of the prototype which are included in the simulation model.

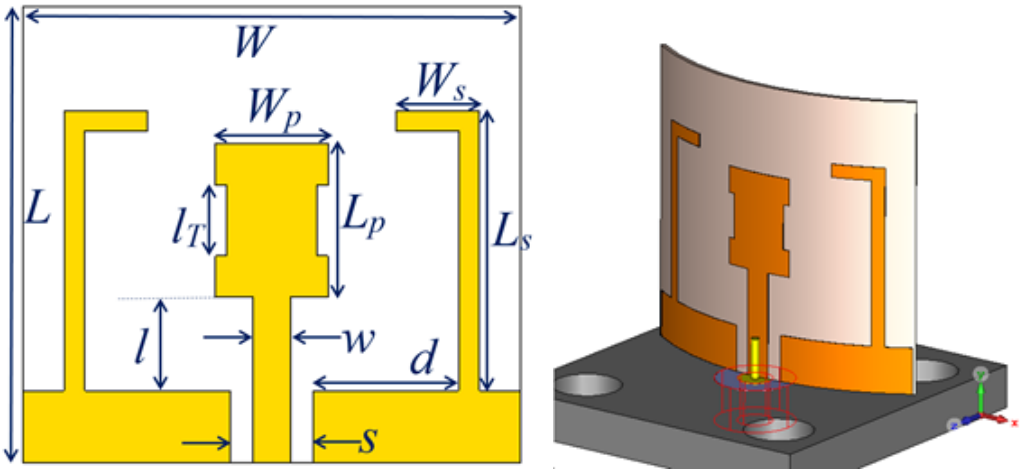

(a) (b)

Figure 6.1: MMW flexible LCP-based antenna: (a) Simulated model with design parameters, (b) Conformal antenna model.

6.2.2 Antenna Fabrication

Rogers ULTRALAM 3850 LCP (thickness = 100 μm, dielectric constant = 2.9, loss tangent = 0.0025) is deployed for antenna fabrication. Two fabrication methods, i.e. laser LPKF micromachining and inkjet printing with conductive ink are utilised for

Table 6-A: **Optimised Dimensions of MMW Flexible LCP-based Antenna**

Parameters	**Symbols**	**mm**
Patch width	W_p	2.7
Patch length	L_p	3.7
Ground stub width	W_s	2
Ground stub length	L_s	6.75
Feed width	w	0.9
Feed length from the ground edge	l	2.25
Tapered length	l_T	1.7
CPW feed gap	s	2.0
CPW-feed edge to stub distance	d	3.5

the performance evaluation. In the first process, LPKF Protolaser micromachining is utilised for antenna fabrication in University of Glasgow. LPKF Protolaser is capable of fabricating thin lines of 50 μm width with the precision of 20 μm on both rigid and flexible substrates. LCP sheet cladded with 17.5 μm thick copper is used, where the metallic plate from the bottom is fully removed and the top surface is patterned according to the design by means of a laser beam. However, in the second fabrication method, the copper metallisation on LCP is entirely etched off by the chemical treatment with ferric chloride ($FeCl_3$) solution (molar mass = 270.3 g/mol), and then rinsed with water to achieve a clean surface. The LCP is then subjected to flatbed inkjet printing with the silver nanoparticle ink (i.e., Colloidal Ag-J solid Ag) by using DMP-2831. The quality and conductivity of the printed pattern is dependent on ink composition. For instance, high ink viscosity due to greater proportion of metal nanoparticles yields better electrical conductivity, though results in a compromise on print quality as high viscosity disturbs the continuous jetting or flow of the ink from the printhead nozzles.

The ink composition determines the electrical properties of the printed pattern. The selected ink contains silver nanoparticles with a monolayer organic polymer encapsulation to prevent metal oxidation as well as to avoid coalescence, and suspended in an inert solvent. The solvent is developed compatible to the requirements of the printhead

nozzle to allow necessary wettability for seamless inkflow. The post-printing essential procedures are drying, curing/annealing, and sintering which decompose the monolayer polymer shells and combine the molten particles into a firm conductive layer. Silver metal particles demand a high melting temperature of 961.8 °C which could not be handles by most of the substrates, such as paper. Sintering is essential to improve the conductivity and usually requires a temperature in between 50–80% of the melting temperature of the corresponding metal. However, the advantage of using nanosized powders is, the sintering temperature can be easily reduced to even lower, i.e. 15–30% of the melting temperature [181]. The conductivity of the printed pattern varies in the range of $0.4 \approx 2.5 \times 10^7$ S/m, and primarily influenced by a number of successive iterations. A 0.5 μm thin silver pattern is printed on LCP by adjustment of settings such as, drop spacing of 15 μm (i.e., 1693.33 dpi), voltage of 15 V, and jetting frequency of 5 KHz.

After drying of the printed pattern, the particles are still partially captured in polymer and can be released by a sintering process. Sintering utilises high-energy exposure to break the polymer encapsulation, and conducted either by a laser source or an elevated temperature treatment, as a result of which the ink particles melts and combine together. Several methods have been developed in this regard involving high-energy laser beams or ovens. Usually a furnace/oven typically at 100–300 °C is utilised; for instance, one method suggests sintering of the LCP substrate for one hour at 270 °C [182]. Heat sintering is time-consuming and requires high-temperature curing for several minutes or even an hour which may cause damage to the substrate or printed ink pattern. Controlling percolation threshold is essential to prevent excessive substrate shrinkage which causes microcracking [183]. Other processes have also been suggested to replace oven such as, laser [184], microwave radiation [185], light flashing [186], and chemical sintering [187]. Much higher risk is involved while deploying laser sources and it is critical to control the intensity and exposure time to avoid any damage.

LCP substrate depicts an excellent temperature handling capability up to 300 °C but still prolong heating durations have been avoided in this antenna fabrication and a

novel, fast and efficient method of heat treatment is developed here. The inkjet printed prototype is dried in an oven at 150 °C for 5 minutes to evaporate the ink solvent and then a flatbed heat press with a preset temperature 160 °C is deployed for 30 seconds. The prototype is placed between Kapton films and protective Teflon sheets are also used for wrapping to avoid direct contact of the substrate with the flat iron-plates during the exposure time. The suggested method is anticipated as highly time-efficient among the reported heat sintering techniques and delivers a conductivity of 0.3 $\times$ 10^7 S/m with absolutely no damage to the substrate or inkjet printed pattern. The fabricated antenna prototypes by using two suggested methods are presented in Fig. 6.2. Both of the fabrication process offer high speed, high resolution and precise prototyping, and capable of cost-efficient bulk manufacturing.

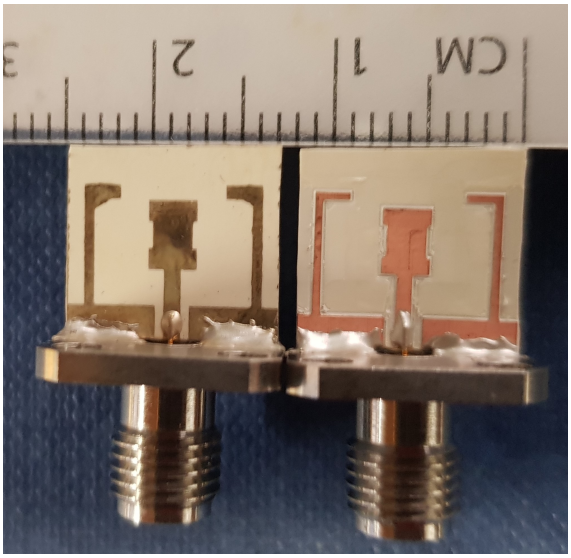

Figure 6.2: MMW LCP-based flexible antennas fabricated by inkjet printing (left side) and laser etched (right side).

The idea is to analyse the designed antenna response and performance when constructed with a subtractive method of laser micromachining which involves partial removal of metal cladding, and by using additive technique of inkjet printing for metal deposition on the surface. Both methods have different metal concentrations on the radiating area that can change the conductivity and eventually the radiation of the antenna. The motivation behind this study is to investigate the comparison of antenna performance

based on the extent of variation in the fabrication. Surface profile is observed by using profilometer measurements which shows fairly consistent and smooth surface of the order of micrometres. Fig. 6.3 shows the printed surface under the probes of profilometer and the measured surface roughness with respect to the distance covered by the probe on the sample surface. It is observed that the LCP substrate is fairly flat with very small surface gradients, mainly due to the LCP manufacturing process limitations.

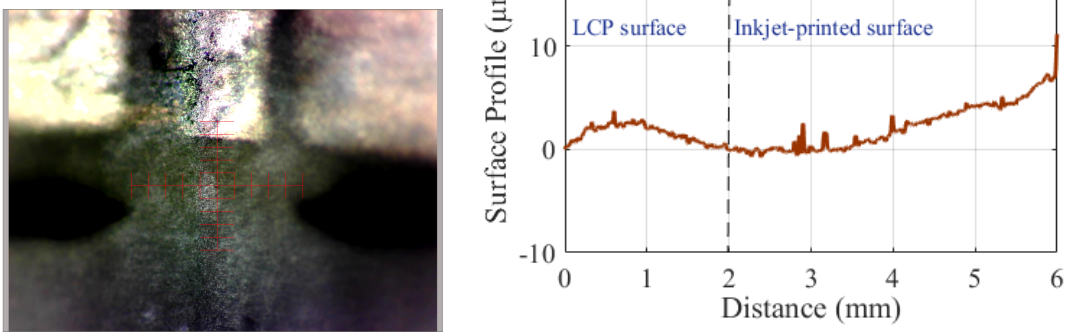

(a) (b)

Figure 6.3: Surface profile of inkjet printed and sintered LCP: (a) Surface under test, (b) Surface profile plot.

The inkjet-printed antenna pattern is subjected to further material characterisation steps to get a closer look under the macroscopic imaging. Scanning Electron Microscope (SEM) is utilised for this purpose. Initially, the inkjet-printed layer is examined before the sintering process, in which a granular nature of nanoparticles with irregular bulges or lumps is observed in the profile. These lumps are usually formed due to uneven consistency of the ink which may effect the seamless jetting of the ink by temporarily blocking the nozzle. Cleaning cycles are deployed during the printing process to purge the ink from the printhead which eliminates these large-sized particles blocking the nozzles. However, the particle coalescence is not completely unavoidable and can be seen on the printed pattern under a microscope. It is observed that after sintering, the surface becomes more flat as the heat treatments melt down the lumps, and molten neighbouring particles combine with each other and settle down, as shown in Fig. 6.4.

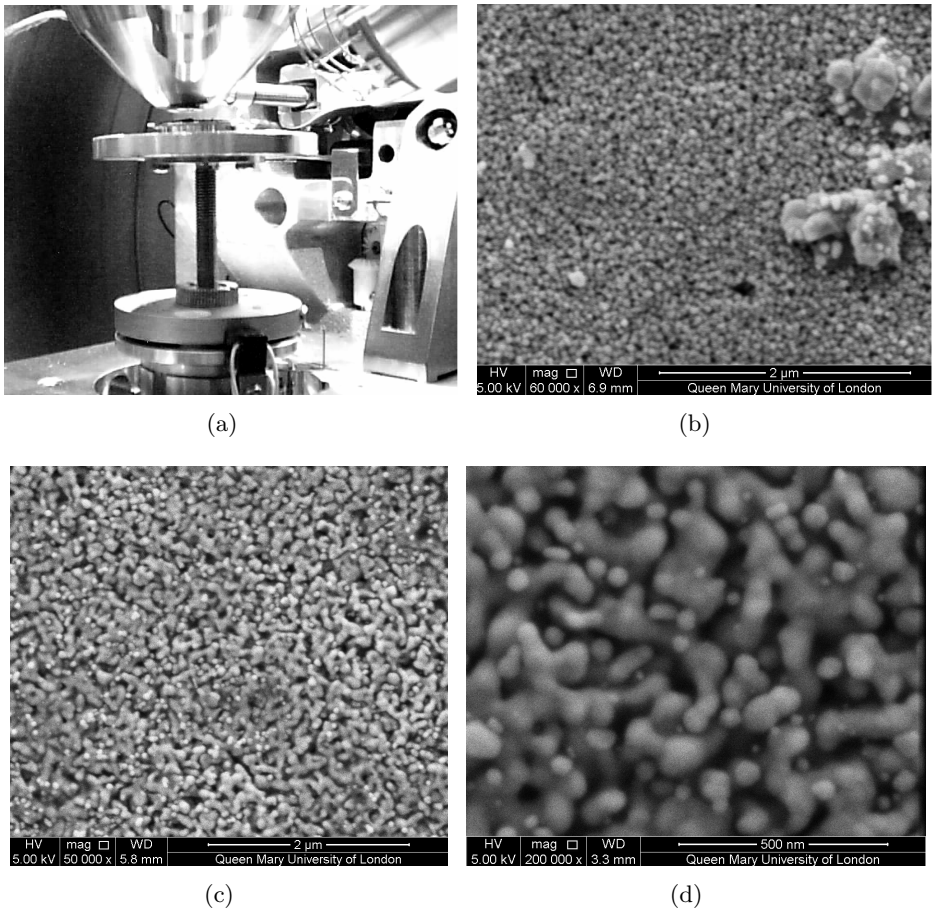

(a) (b)

(c) (d)

Figure 6.4: Imaging of printed and sintered layer: (a) SEM Microscope, (b) Before sintering: 2 μm resolution,(c) After sintering: 2 μm resolution,(d) Sintered layer: 500 nm resolution.

6.2.3 Proposed Antenna Performance Analysis

The proposed MMW flexible antenna is optimised by means of parametric analysis carried out on several design parameters, and eventually the estimated performance response is validated by experimental measurements and testing of the fabricated prototypes constructed by two methods. The S–parameters, radiation pattern, and peak realised gain depict that the measurements are similar to the simulations.

A. Impedance Bandwidth

The reflection coefficients of the two antenna prototypes with varying fabrication

techniques are measured and compared in Fig. 6.5. Both plots show that the bandwidth is approximately conserved in both cases, though the inkjet-printed prototype shows a shift towards lower frequencies. The resulted shift is mainly due to variation in conductivities and layer thickness of metal in both cases. As the proposed antenna is expected to be suitable for wearable integrations, it is essential to examine the possible deviations in antenna response when positioned in close proximity of the human body. Fig. 6.6 depicts the S_{11} plots obtained in the simulation and measurements of the antenna fabricated by laser milling. The micromachined antenna is subjected to testing under different scenarios of in-air, on fabric and on-body. The overall bandwidth profile remains consistent in these three configurations which refers to robustness of antenna performance towards the surrounding conditions.

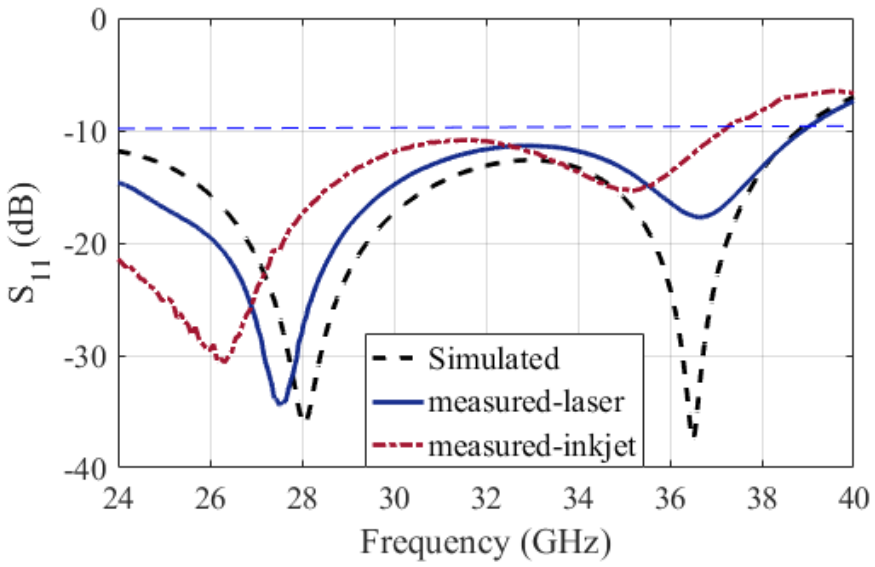

Figure 6.5: S_{11} plots of MMW LCP-based flexible antennas fabricated by both inkjet printing and laser etching.

B. Radiation Pattern

The radiation characteristics of the flexible MMW LCP based antenna exhibits an even distribution of radiation on the top and bottom surface where the maximum directivity is almost orthogonal to the antenna plane. The standard omnidirectional radiation

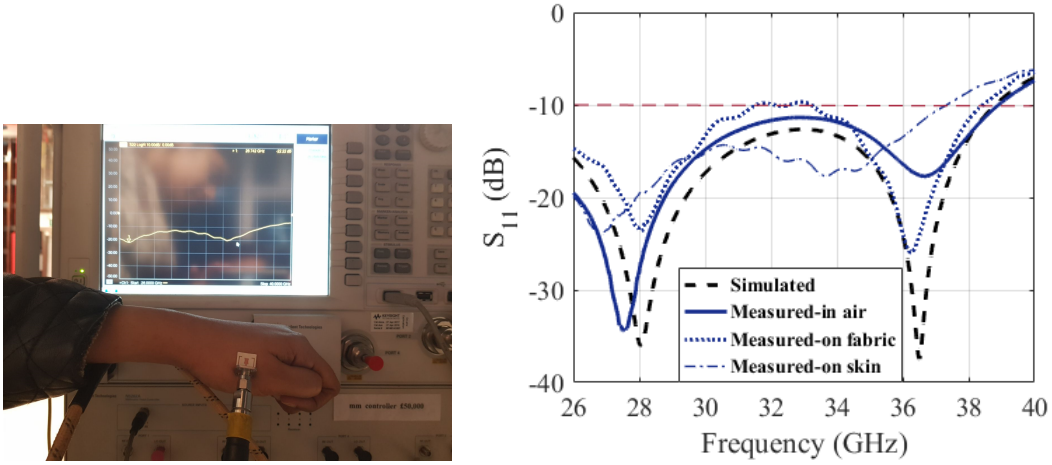

(a) (b)

Figure 6.6: Impedance bandwidth of laser etched MMW LCP-based flexible antenna: (a) On-body measurements, (b) S_{11} plots of antenna measurements.

is suppressed alone the horizontal axis due to designed stub geometry which is responsible of improving the radiation directivity. Fig. 6.7 presents the simulated results and measurements taken from experimental testing by dashed and bold lines respectively, at $\phi = 0°$ and $\phi = 90°$ on distinct frequencies of the K_a–band. Similar patterns are obtained from both of the antennas with varying fabrication methods, thus the results from only one antenna which is fabricated by laser micromachining, are presented here.

C. Realised Gain

The consistent gain profile is essential in the complete bandwidth to deliver a reliable antenna performance. Usually, the gain doesn't always remains same and may vary in the wide bandwidth of monopole patch antennas. This discrepancy often restricts the use of certain frequencies of high impedance bandwidth due to inadequate gain magnitude. The distinctive feature of the proposed antenna is its consistent realised gain profile and direction of maximum radiation, which suggests its equally reliable performance at any frequency of the bandwidth. The experimental testing of two antennas depicts similar gain profile and the gain remains fairly stable in the bandwidth. The measured gain of the laser-prototyped antenna is above 8 dBi, while inkjet-printed antenna shows a gain

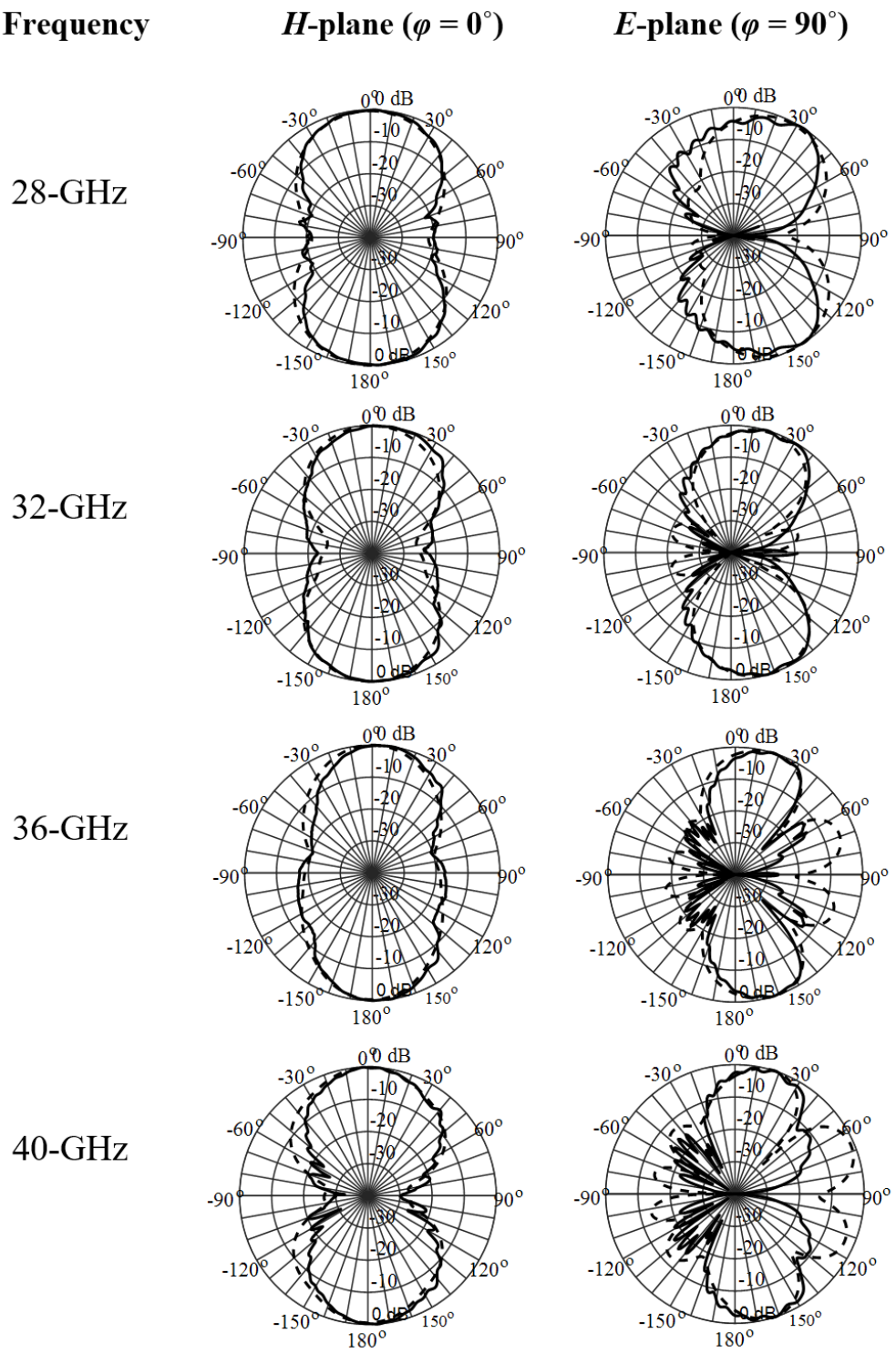

Figure 6.7: Simulated and measured radiation patterns of MMW LCP-based flexible antennas fabricated by laser etching.

above 7 dBi in the operating range. The simulated and measured results of the realised gain against frequency are presented in Fig. 6.8. Two antenna gain method is utilised for measurements and shows similar findings as obtained by the computational evaluations. Moreover, the simulated efficiency of the antenna is above 80% in the operating range.

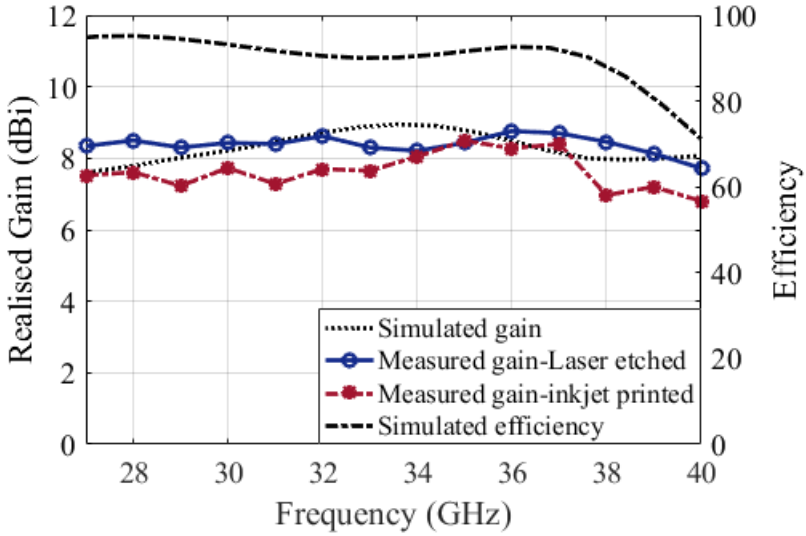

Figure 6.8: Realised gain and efficiency of MMW LCP-based flexible antennas.

6.3 Two-Element Antenna Array

6.3.1 Antenna Array Design and Fabrication

With the objective of retaining the bandwidth of the previous antenna and improving the gain further above 9 dBi, the array configuration of the proposed antenna is developed. In this section, the single MMW antenna design is extended to a conformal antenna array on a LCP substrate of $12.5 \times 19 \times 0.1$ mm^3. A two-element array of the tapered radiating patches is developed with a CPW-fed corporate feeding network and two additional small stubs are placed in close proximity of the feed. The distance between the patch centres is set as $\lambda/2$ of the lower resonant band (i.e. 28 GHz) to avoid coupling. The length of stubs is parametrically increased to effectively converge the radiation of the patch array.

Parametric analysis is carried out for the positioning of stubs. The additional smaller stubs are designed to couple with the feeding network to provide desired impedance matching. Fig. 6.9 (a) provides the CST model of the MMW antenna array with the designed parameters. The dimensions of the corresponding parameters are provided in Table 6-B. Fig. 6.9 (b) shows the prototypes of 2-element antenna array and the designed antenna fabricated by laser milling.

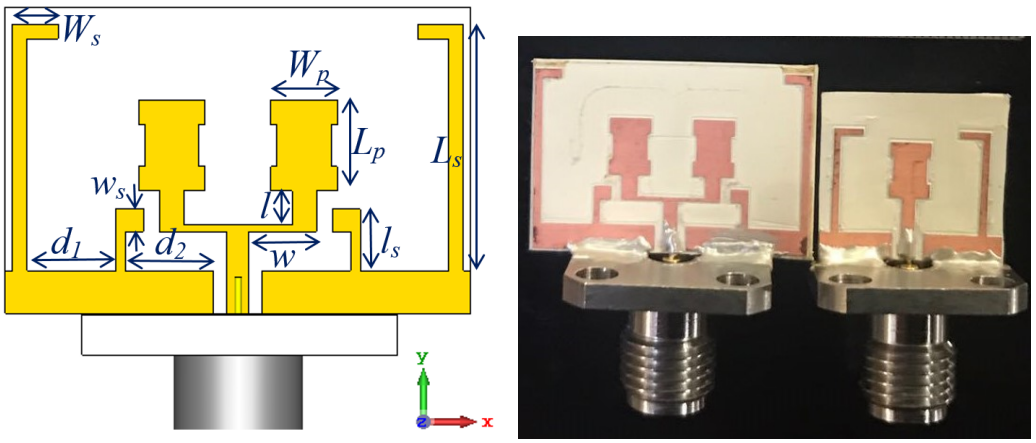

(a) (b)

Figure 6.9: MMW LCP-based two-element antenna array: (a) Simulated model with design parameters, (b) Fabricated antenna and array.

Table 6-B: **Dimensions of LCP-based 2-Element Antenna Array**

Parameters	**Symbols**	**mm**
Patch width	W_p	2.7
Patch length	L_p	3.7
Ground stub 1 width	W_s	1.85
Ground stub 1 length	L_s	10.05
Feed width	w	2.75
Feed length	l	1.4
distance between two stubs	d_1	3.6
Stub 2 width	w_s	0.9
Stub 2 length	l_s	2.5
Stub 2 distance from ground edge	d_2	3.6
Width of array prototype	W	19
Length of array prototype	L	12.5

6.3.2 Performance Evaluation

A. Impedance Bandwidth

The performance of antenna array is evaluated based on comparison with the results of single antenna design. The S_{11} plots of both single antenna and two-element antenna array are compared in Fig. 6.10, and it is observed that the bandwidth of single antenna prototype remains conserved in the array configuration. The simulated plots of antenna and array in planar configurations are represented by dotted lines while bold lines depict the measured results. In addition to this, bending effect of antenna is analysed numerically and presented in Fig. 6.11, when the antenna and array models are bent along the cylindrical curvature of 6 mm, 8 mm and 10 mm radii. It is observed that the intended bandwidth of the conformal antenna remains conserved which depicts a reliable performance in flexible and wearable applications.

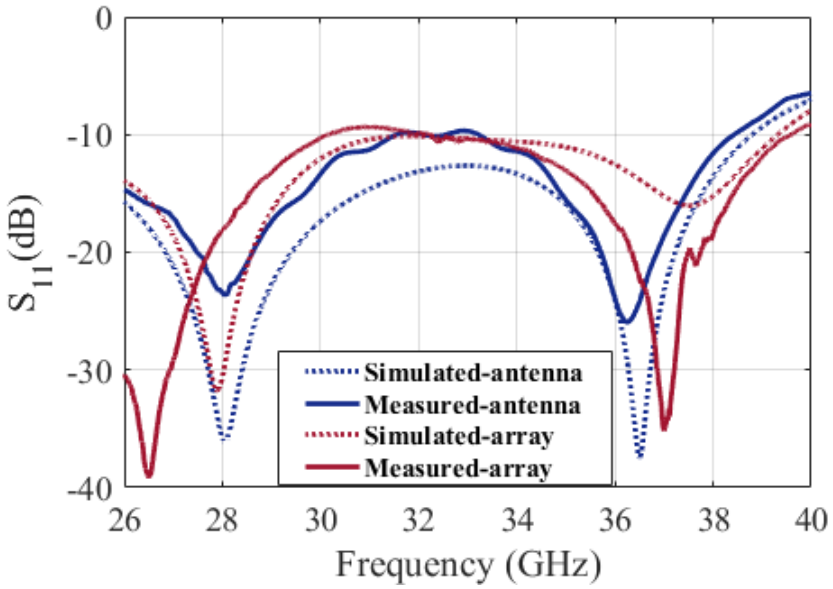

Figure 6.10: Comparison of S_{11} plots of designed MMW LCP-based flexible antenna and two-element array in planar configuration.

B. Radiation Pattern

The radiation pattern plots of designed antenna and array are compared and pre-

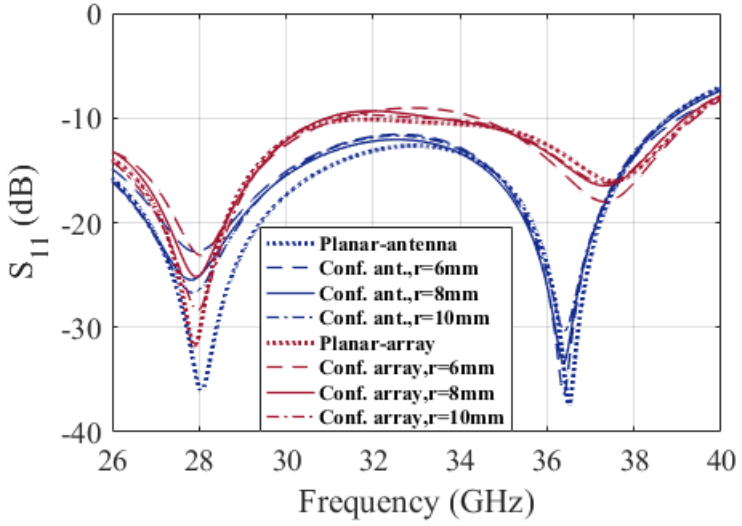

Figure 6.11: Parametric analysis of the conformity of the antenna and array along the surface of a cylinder of radii of 6mm, 8mm and 10mm.

sented in Fig. 6.12. The two-element antenna array also shows similar profile as of single antenna, though the main beam is further shifted from the $\theta = 0°$. Fig. 6.12 shows the simulated and measured results with dashed and bold lines respectively, of the designed antenna and two-element array, at $\phi = 0°$ and $\phi = 90°$ on distinct frequencies of the K_a–band. The $\phi = 0°$ plots show the expected radiation suppression alone the horizontal axis due to designed stub geometry. While $\phi = 90°$ plots depict that the main beam is tilted from the perpendicular axis where the big metal size of connector could be partially responsible for this tilt.

C. Realised Gain

Two antenna gain method is utilized for gain calculations and the results show similar findings as that of the computational evaluations. Numerically estimated efficiency profile of Fig. 6.13 also shows that the antenna is highly efficient in the operating range of the K_a–band. The realised gain of the antenna and array topology are also compared in Fig. 6.13 to validate the claim of high gain characteristics achieved over a wide operating range of K_a–band in the proposed array design. The array gain is higher than the single antenna at each distinct frequency, and the overall array gain is above 9 dBi in

the complete K_a–band with the peak gain of 11.35 dBi at 35 GHz. This distinguishing feature has made this antenna design highly efficient in terms of performance, and potentially suitable for 5G applications.

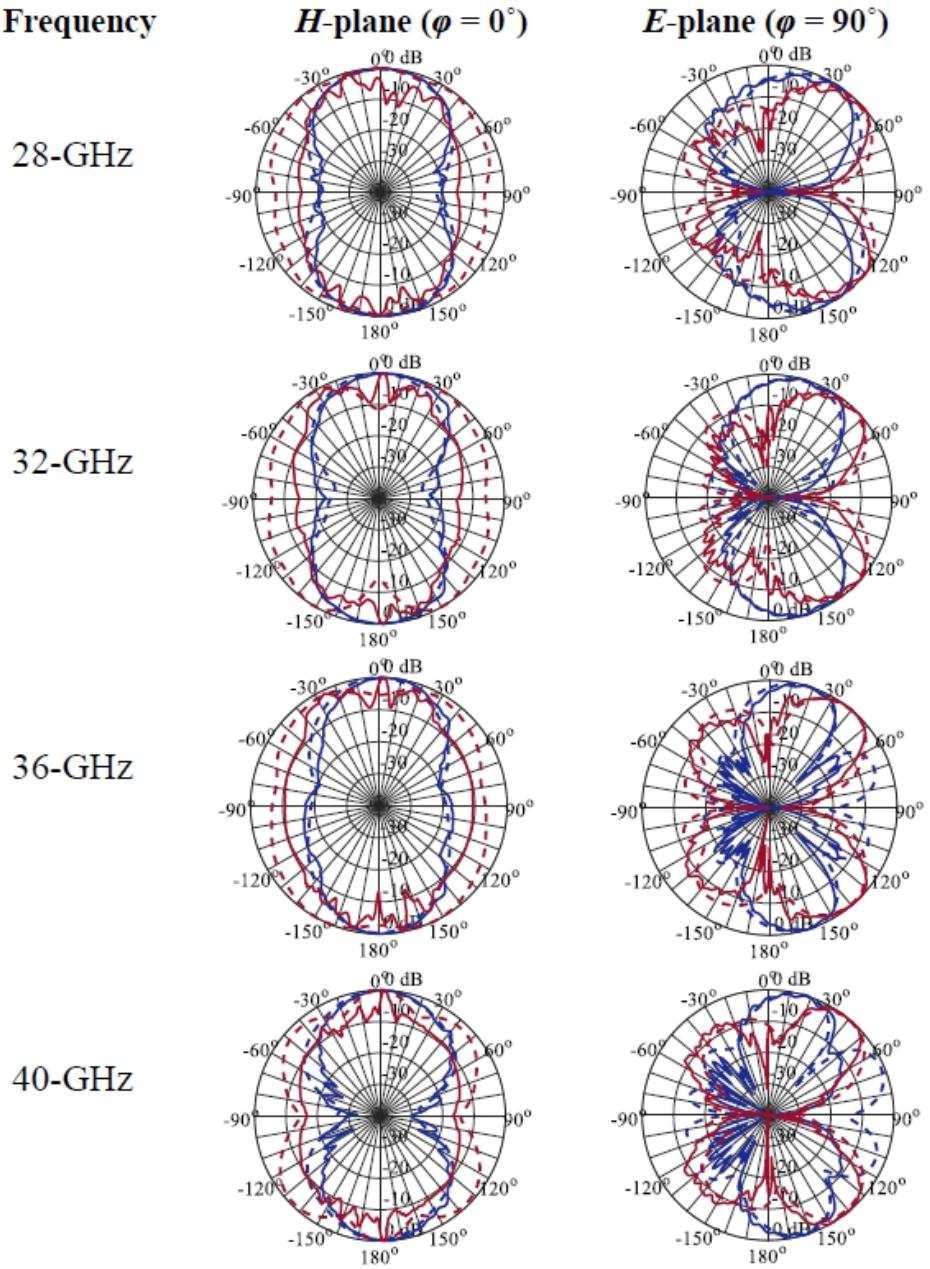

Figure 6.12: Comparison of radiation patterns of designed MMW LCP-based flexible antenna (in blue plots) and two-element array (in red plots) at: (a) $\phi = 0°$, (b) $\phi = 90°$.

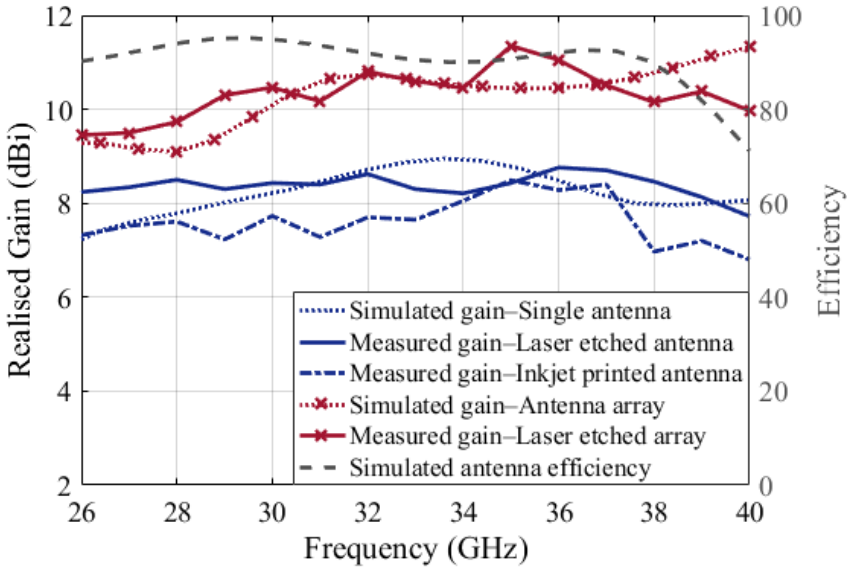

Figure 6.13: Comparison of realised gain plots of designed MMW LCP-based flexible antenna and two-element array configuration as well as the antenna efficiency plotted against frequency.

6.4 Conclusion

In this chapter, a novel geometry of K_a–band antenna has been proposed on a flexible LCP substrate for 5G conformal applications and wearable devices. The high gain profile has been achieved in the complete bandwidth with a measured peak gain of 8.34 dBi at 36 GHz. The antenna was fabricated on LCP substrate by using two advanced methods of laser milling and inkjet printing. Moreover, the conventional heat sintering method was improved with the development of a new time-efficient technique. The comparison of both fabrications was established based on the antenna performance. The design has been further enhanced in a two-element array with a corporate feeding network, where the array has effectively retained the bandwidth of K_a–band with the gain above 9 dBi in the complete operating range. Though, it is challenging to attain both high gain and bandwidth within one antenna, the proposed antenna array has delivered high bandwidth with consistent and high gain performance in a conformal, simple and light-weight geometry. The conformity analysis as well as the on-body effects on the antenna performance have also been discussed in this chapter.

Chapter 7

Conclusion and Future Work

7.1 Conclusion

High congestion issues in the limited bandwidth of sub-6 GHz wireless bands have initiated the need of utilising high frequency spectrum for communication purposes. MMWs are anticipated to be a future of wireless communication due to availability of unused spectrum to increase system capacity, higher data throughput and capability to accommodate exponential growth of users and devices. Realisation of a mobile network based on a MMW architecture is an unprecedented challenge as the signal attenuation associated with the propagation distance, atmospheric conditions, and dielectric losses become highly critical in comparison with the current wireless spectrum. These issues can be handled by the implementation of highly densified short-range radio infrastructures. Considering the demand of smartphones, wearable gadgets and other wireless devices, the antenna size, performance and cost are of crucial importance. MMWs offer the advantage of smaller antenna size which provides an ease of integration in hand-held wireless devices. However, there are a number of antenna performance attributes essential for 5G cellular networks and an efficient antenna design can be considered as one of the key milestones to complete the transition from lower frequencies towards 5G networks.

Flexibility of system architecture, especially antenna performance is of high importance in this regard. It is suggested that antenna should provide a high bandwidth to support high-speed communication, high gain to overcome attenuations, and preferably flexible enough to be incorporated in both planar and non-planar geometries. Additionally, the antenna should be simple, compact, cost-effective as well as feasible for bulk fabrication. Many techniques such as, photolithography, inkjet printing, laser milling etc. are available to achieve high resolution fabrication. An investigation of the features of inkjet printing and feasibility of using flexible polyester films is being made in order to explore more in conformal and flexible MMW antennas. Inkjet printing is suggested as a cost-effective way of precise and accurate bulk production as multiple antennas can be printed with silver nanoparticle ink by using reel-to-reel process. Several aspects need critical importance before moving towards antenna printing, for instance, choice of flexible films and their mechanical and electrical properties, type of ink, and most importantly, the accuracy and precision of inkjet printing. Characteristics of conductive ink and substrates, and printer's configurations are to be comprehended in order to define the optimum resolution of antenna fabrication. It is important to consider these requirements for the development of an antenna comprising the desired features.

Antenna designs with the attractive features of high bandwidth to fulfil high capacity demands, high gain to deal with signal attenuations, adaptable performance to fit in cognitive radio applications, and conformity to be mounted on any kind of surface, are key objectives of this research. A comprehensive literature review has been performed in Chapter 2 to investigate the scope of wideband and multiband antenna, MIMO antennas and linear arrays for the cellular applications. The primary focus of this chapter is to highlight the significance and need of adaptive antennas in current wireless devices as well as in future networks. Several antenna have been designed in this thesis on K_a-–band (26.5–40GHz) of MMW spectrum exclusively focusing on FCC and Ofcom suggested bands for 5G. The techniques of frequency reconfiguration, MIMO configuration and multiband antenna arrays are primarily investigated in the proposed antenna struc-

tures for different scenarios of 5G. For instance, in Chapter 3 the technique of DGS has been implemented to develop high bandwidth antennas for both rigid and flexible substrates. The MIMO configuration of DGS based antenna is also presented to examine the antenna's stand-alone performance in multichannel communication. This chapter accomplishes two DGS based antenna designs in which the first design combines the advantages of wide bandwidth and MIMO configuration while the second design accumulates high bandwidth with the flexibility of the antenna structure. In order to explore more in wearable and conformal antennas, the feasibility of using flexible polyester films is keenly focused. Inkjet printing process has been introduced for the fabrication of the flexible antenna. However, the precision and quality of printing is greatly improved in the later chapters by proper adjustment of printers settings.

In Chapter 4, novel designs of frequency reconfigurable antennas have been proposed for 5G. Starting with a rigid substrate reconfigurable antenna, the design methodology has been gradually matured to flexible reconfigurable antennas with PIN diode switches. The foremost emphasis of this chapter is to contribute in the development of conformal antennas for 5G by integrating the desirable features of frequency reconfiguration and MIMO technology. Most of the flexible antennas presented here are fabricated by inkjet printing, yet another process of laser prototyping is also introduced for antenna fabrication. Copper laminated sheets of LCP have been used and LPKF laser milling machine has been employed for fast, accurate and well-defined antenna patterning. The final antenna is implemented with high-frequency miniaturised PIN diode switches and an appropriate biasing circuit is developed to perform diode operation.

The concept of linear antenna arrays has gathered huge interest due to capability to collimate radiation patterns of individual antennas into one highly directive beam. MIMO arrays are extremely beneficial in multichannel signal transmission and increase overall system capacity, yet these arrays in general are gain-limited as each antenna element performs individually. However, in linear arrays, the combine effect of multiple antennas results in a high gain performance. Though this advantage of planar arrays

comes with a limitation of bandwidth as antenna arrays of conventional patch geometries are usually narrowband. Chapter 5 concentrated on the demand of multiband antenna arrays provided with high gain and bandwidth performance. For this purpose, the geometrical aspects of conventional Franklin array have been modified to achieved multiband response on MMWs by developing an Enhanced Franklin array model. Moreover, 2D arrangement of enhanced Franklin array is also presented for the first time. The concept is also executed in suggesting a flexible wideband antenna array to justify the competence of the proposed model in wearable antennas.

A number of antennas have been reported in this research work so far, still it is observed that achieving a consistent high gain performance over the wide bandwidth is quite challenging, and developing such antennas on flexible substrates is not an easy task as the gain and efficiency of antenna degrades to significant extend due to high dielectric loss of flexible substrates. In Chapter 6, this limitation has been rectified considerably by proposing an efficient flexible antenna array with high bandwidth, and the gain remains consistently high over the operating bandwidth. LCP material has been used as a substrate, and the single antenna design itself has a high potential to be integrated in planar arrays as well as in MIMO assemblies.

7.2 Future Work

The emerging 5G technology is expected to reside on high frequency spectrum yet most of the current reported antennas have been designed for lower frequencies. Although massive research trends have been moved to MMWs for the realisation of 5G still the antenna requirements for upcoming system are unclear to some extent and there is a need to explore further the systematic antenna design process and the expected performance attributes on MMW spectrum. This research has focused entirely on antenna design to explore several prospects for MMW cellular antennas. A number of applications where rigid and planar antennas could not be placed, conformal antennas are required. Such

scenarios become more critical when high resolution and precise fabrication are in high demand at MMW frequencies due to small size of devices. In this research a considerable effort has been made in linking the cellular antennas with wearable electronics by presenting flexible antennas for MMW 5G applications. However, it is observed that there is a lot more to explore further in this domain. Some of the prospective suggestions for future have been made in this section.

- This work can be enhanced further with the implementation of MEMS and varactor switches on flexible reconfigurable antenna designs. MEMS switches introduce relatively lower loss and lesser power consumption than PIN diodes and offer good linearity. Varactors provide a continuous frequency tuning range over a bandwidth instead of discrete shifts of resonant bands.

- Passive reconfiguration techniques could also be implemented instead of traditional switching schemes for the design of adaptable MMW antennas. Passive reconfiguration includes capacitive and inductive loading for frequency tuning and thus reduces the structural complexity of antenna by eliminating active components.

- In this research, only frequency reconfiguration has been investigated though pattern and polarisation reconfiguration could also be examined on flexible reconfigurable antennas in future. Pattern reconfiguration is capable of achieving beamforming at the antenna's end without using extra circuitries of phase shifters. Moreover, polarisation reconfigurability is highly desired to avoid propagation losses due to polarisation mismatch especially in portable devices.

- There is a need of a number of efficient and low-cost fabrication choices to achieve good quality of prototyping of MMW antennas. Several other fabrication methods such as screen printing and photolithography can also be implemented in future for the realisation of presented antennas and an analysis can be made for the optimal choice of fabrication method based on the performance differences.

- In order to estimate the effect of antenna on body due to absorption of radiations,

SAR measurements should be performed in the future using HUGO model in CST, as it is essential to consider the handset effect on the antenna functionality.

- Multilayer structures, vias, and other complex structures have been avoided in this research to attain fabrication simplicity. There is a need of more research efforts for the design and realisation of complex antennas at MMWs, so that state-of-the-art technologies of electronic band-gap (EBG) structures, corrugated structures, electroplated vias, etc. could be easily implemented on the flexible substrates at MMW frequencies.

- Graphene based inks have been found promising for antenna design at low frequencies. This trend can be explored further for the implementation of MMW flexible inkjet-printed graphene based antennas.

References

[1] M. Shafi *et al.*, "5G: A tutorial overview of standards, trials, challenges, deployment, and practice," *IEEE J. Sel. Area. Commun.*, vol. 35, no. 6, pp. 1201–1221, 2017.

[2] J. G. Andrews *et al.*, "What will 5G be?," *IEEE J. Sel. Area. Commun.*, vol. 32, no. 6, pp. 1065–1082, 2014.

[3] S. Rangan, T. Rappaport, and E. Erkip, "Millimeter wave cellular wireless networks: potentials and challenges," *Proc. IEEE*, vol. 102, no. 3, 2014, pp. 366–385.

[4] L. Zhang *et al.*, "Distributed adaptive range extension setting for small cells in heterogeneous cellular network," *IEEE 85th Veh. Technol. Conf.*, 2017, pp. 1–7.

[5] Z. Ying, "Antennas in cellular phones for mobile communications," *Proc. IEEE*, vol. 100, no. 7, pp. 2286–2296, July 2012.

[6] E. G. Larsson *et al.*, "Massive MIMO for next generation wireless systems," *IEEE Commun. Mag.*, vol. 52, no. 2, pp. 186–195, 2014.

[7] `https://cdn.rohde-schwarz.com/it/seminario/Massive_MIMO_antenna_OTA_170420_Italy.pdf`

[8] L. Guan, P. Rulikowski and R. Kearney, "Flexible practical multi-band large scale antenna system architecture for 5G wireless networks," *Electron. Lett.*, vol. 52, no. 11, pp. 970–972, 2016.

[9] O. Boric-Lubecke *et al.*, "Microwave and wearable technologies for 5G," *12th Int. Conf. Telecommun. Modern Satellite, Cable Broadcast. Services*, 2015, pp. 183–188.

[10] N. F. M. Aun, *et al.*, "Revolutionizing wearables for 5G: 5G technologies: recent developments and future perspectives for wearable devices and antennas," *IEEE Microw. Mag.*, vol. 18, no. 3, pp. 108–124, 2017.

[11] A. Gupta and R. K. Jha, "A survey of 5G network: architecture and emerging technologies," *IEEE Access*, vol. 3, pp. 1206–1232, 2015.

[12] M. K. Samimi and T. S. Rappaport, "3-D millimeter-wave statistical channel model for 5G wireless system design," *IEEE Trans. Microw. Theory Techn.*, vol. 64, no. 7, pp. 2207–2225, 2016.

[13] D. Nandi and A. Maitra, "Study of rain attenuation effects for 5G Mm-wave cellular communication in tropical location," *IET Microw., Antennas Propag.*, vol. 12, no. 9, pp. 1504–1507, 2018.

[14] Use of Spectrum Bands Above 24 GHz for Mobile Radio Services; Proposed Rule, *Federal Register*, vol. 81, no. 164 , pp. 58269–58308, 2016.

[15] `https://www.ofcom.org.uk/__data/assets/pdf_file/0021/97023/5G-update-08022017.pdf`

[16] `https://www.rohde-schwarz.com/en/solutions/wireless-communications/5g/5g-fundamentals/5g-fundamentals_229439.html`

[17] E. Dahlman *et al.*, "5G wireless access: requirements and realization," *IEEE Commun. Mag.*, vol. 52, no. 12, pp. 42–47, 2014.

[18] P. Bhartia and I. J. Bahl, Millimeter Wave Engineering and Applications, Canada: John Wiley Sons Inc., 1984.

[19] T. S. Rappaport, J. N. Murdock, and F. Gutierrez, "State of the art in 60 GHz integrated circuits systems for wireless communications," *Proc. IEEE*, vol. 99, no. 8, pp. 1390–1436, 2011.

[20] T. Baykas *et al.*, "IEEE 802.15.3c: the first IEEE wireless standard for data rates over 1 Gb/s," *IEEE Commun. Mag.*, vol. 49, no. 7, pp. 114–121, 2011.

[21] `https://www.ofcom.org.uk/__data/assets/pdf_file/0014/104702/5G-spectrum-access-at-26-GHz.pdf`

[22] T. S. Rappaport *et al.*, "Millimeter wave mobile communications for 5G cellular: It will work!," *IEEE Access*, vol. 1, pp. 335–349, 2013.

[23] Q. Zhao and J. Li, "Rain attenuation in millimeter wave ranges," *IEEE Int. Symp. Antennas, Propag. EM Theory*, Oct. 2006, pp. 1–4.

[24] J. Wells, "Faster than fiber: The future of multi-G/s wireless," *IEEE Microw. Mag.*, vol. 10, no. 3, pp. 104–112, 2009.

[25] F. Mehran and A. Rahimian, "Physical layer performance enhancement for femtocell SISO/MISO soft real-time wireless communication systems employing serial concatenation of quadratic interleaved codes," *20^{th} Iranian Conf. Electrical Eng. (ICEE)*, 2012, pp. 1188–1193.

[26] A. Rahimian and F. Mehran, "RF link budget analysis in urban propagation microcell environment for mobile radio communication systems link planning," *Int. Conf. Wireless Commun. Signal Processing (WCSP)*, 2011, pp. 1–5.

[27] C. Bouras and G. Diles, "Energy efficiency in sleep mode for 5G femtocells," *2017 Wireless Days*, 2017, pp. 143–145

[28] S. Hur *et al.*, "Millimeter wave beamforming for wireless backhaul and access in small cell networks," *IEEE Trans. Commun.*, vol. 61, no. 10, pp. 4391–4403, 2013.

[29] T. Bai, R. Vaze, and R. W. Heath, "Analysis of blockage effects on urban cellular networks," *IEEE Trans. Wireless Commun.*, vol. 13, no. 9, pp. 5070–83, 2014.

[30] J. Zhang *et al.*, "5G millimeter-wave antenna array: design and challenges," *IEEE Wireless Commun.*, vol. 24, no. 2, pp. 106–112, 2017.

[31] W. Hong, K. h. Baek and S. Ko, "Millimeter-wave 5G antennas for smartphones: overview and experimental demonstration," *IEEE Trans. Antennas Propag.*, 2017.

[32] A. Dadgarpour, M. S. Sorkherizi and A. A. Kishk, "Wideband low-loss magneto-electric dipole antenna for 5G wireless network with gain enhancement using Meta lens and gap waveguide technology feeding," *IEEE Trans. Antennas Propag.*, vol. 64, no. 12, pp. 5094–5101, 2016.

[33] P. Agarwal, S. N. Ali and D. Heo, "Reconfigurable phased-array design techniques for 5G and beyond communications, *IEEE Int. Symp. Radio-Frequency Integration Tech. (RFIT)*, 2017, pp. 53–55.

[34] G. M. Rebeiz *et al.*, "Millimeter-wave large-scale phased-arrays for 5G systems," *IEEE MTT-S Int. Microwave Symp.* , 2015, pp. 1–3.

[35] L. Zhang *et al.*, "Integration of dual-band monopole and microstrip grid array for single-chip tri-band application," *IEEE Trans. Antennas Propag.*, vol. 61, no. 1, pp. 439–443, Jan. 2013.

[36] T. Y. Yang, W. Hong and Y. Zhang, "Wideband millimeter-wave substrate integrated waveguide cavity-backed rectangular patch antenna," *IEEE Antennas Wireless Propag. Lett.*, vol. 13, pp. 205–208, 2014.

[37] H. S. Lin and Y. C. Lin, "Millimeter-wave MIMO antennas with polarization and pattern diversity for 5G mobile communications: The corner design," *IEEE Int. Symp. Antennas Propag. Soc.*, 2017, pp. 2577–2578.

[38] M. S. Sharawi, Printed MIMO Antenna Engineering. Norwood, MA, USA: Artech

House, 2014.

[39] S. S. Jehangir and M. S. Sharawi, "A single layer semi-ring slot yagi-like MIMO antenna system with high front-to-back ratio," *IEEE Trans. Antennas Propag.*, vol. 65, no. 2, pp. 937–942, 2017.

[40] M. A. Abdalla and A. A. Ibrahim, "Compact and closely spaced metamaterial MIMO antenna with high isolation for wireless applications," *IEEE Antennas Wireless Propag. Lett.*, vol. 12, pp. 1452–1455, 2013.

[41] R. Hussain, *et al.*, "Compact 4G MIMO antenna integrated with a 5G array for current and future mobile handsets," *IET Microw., Antennas Propag.*, vol. 11, no. 2, pp. 271–279, 2017.

[42] M. M. M. Ali and A. R. Sebak, "Design of compact millimeter wave massive MIMO dual-band (28/38 GHz) antenna array for future 5G communication systems," *17th Int. Symp. Antenna Tech. Applied Electromag. (ANTEM)*, 2016, pp. 1–2.

[43] Y. W. Hsu, *et al.*, "Dual-polarized quasi Yagi-Uda antennas with end-fire radiation for millimeter-wave MIMO terminals," *IEEE Trans. Antennas Propag.*, 2017

[44] F. Wang *et al.*, "Compact wideband MIMO antenna for 5G communication," *IEEE Int. Symp. Antennas Propag. Soc.*, 2017, pp. 939–940

[45] D. Peroulis, K. Sarabandi, and L. P. B. Katehi, "Design of reconfigurable slot antennas," *IEEE Trans. Antennas Propag.*, vol. 53, no. 2, pp. 645–654, 2005.

[46] Balanis, C.A., Modern Antenna Handbook, John Wiley Sons, Inc., 2008.

[47] Z. Yuan and W. Chang-Ying, "An approach for optimizing the reconfigurable antenna and improving its reconfigurability," *IEEE Int. Conf. Signal Processing, Commun. Comput. (ICSPCC)*, 2016, pp. 1–5.

[48] L. Ke and Z. Wang, "Degrees of freedom regions of two-user MIMO Z and full

interference channels: the benefit of reconfigurable antennas," *IEEE Trans. Inf. Theory*, 2012, vol. 58, no. 6, pp. 3766–3779.

[49] J. M. Hannula, J. Holopainen, and V. Viikari, "Concept for frequency reconfigurable antenna based on distributed transceivers," *IEEE Antennas Wireless Propag. Lett.*, vol. 16, pp. 764–767, 2017.

[50] M. K. A. Rahim *et al.*, "Frequency reconfigurable antenna for future wireless communication system," *46^{th} European Microw. Conf. (EuMC)*, 2016, pp. 965–970.

[51] M. T. Ali *et al.*, "A design of reconfigurable rectangular microstrip slot patch antennas," *IEEE Int. Conf. System Eng. Tech. (ICSET)*, 2011, pp. 111–115.

[52] T.-Y. Han and C.-T. Huang, "Reconfigurable monopolar patch antenna," *Electron. Lett.*, vol. 46, no. 3, pp. 199–200, 2010.

[53] H. Boudaghi, M. Azarmanesh, and M. Mehranpour, "A frequency reconfigurable monopole antenna using switchable Slotted Ground Structure," *IEEE Antennas Wireless Propag. Lett.*, vol. 11, pp. 655–658, 2012.

[54] M. R. Hamid *et al.*, "Vivaldi antenna with integrated switchable band pass resonator," vol. 59, no. 11, pp. 4008–4015, 2011.

[55] D. Anagnostou *et al.*, "Reconfigurable multifrequency antenna with RF-MEMS switches," U.S. Patent 7589674 B2, Sep. 15, 2009.

[56] H. Kang and S. Lim, "Electrically small dual-band reconfigurable complementary split-ring resonator (CSRR)-loaded eighth-mode substrate integrated waveguide (EMSIW) antenna," *IEEE Trans. Antennas Propag.*, vol. 62, no. 5, pp. 2368-–2373, 2014.

[57] P. K. Li *et al.*, "Frequency- and pattern-reconfigurable antenna for multistandard wireless applications," *IEEE Antennas Wireless Propag. Lett.*, vol. 14, pp. 333–336, 2015.

[58] F. Farzami *et al.*, "Pattern-reconfigurable printed dipole antenna using loaded parasitic elements," *IEEE Antennas Wireless Propag. Lett.*, vol. 16, pp. 1151–1154, 2017.

[59] W. Lin and H. Wong, "Wideband circular-polarization reconfigurable antenna with L-shaped feeding probes," *IEEE Antennas Wireless Propag. Lett.*, vol. 16, pp. 2114–2117, 2017.

[60] Y. Yashchyshyn, "Reconfigurable antennas by RF switches technology," *5^{th} Int. Conf. Perspective Technologies and Methods in MEMS Design*, 2009, pp. 155–157.

[61] H. AbuTarboush *et al.*, "A reconfigurable wideband and multiband antenna using dual-patch elements for compact wireless devices," *IEEE Trans. Antennas Propag.*, vol. 60, no. 1, pp. 36–43, 2012.

[62] T. Aboufoul *et al.*, "Multiple-parameter reconfiguration in a single planar ultra-wideband antenna for advanced wireless communication systems," *IET Microw., Antennas Propag.*, vol. 8, no. 11, pp. 849–857, 2014.

[63] X. l. Yang *et al.*, "Frequency reconfigurable antenna for wireless communications using GaAs FET switch," *IEEE Antennas Wireless Propag. Lett.*, vol. 14, pp. 807–810, 2015.

[64] A. G. Besoli and F. De Flaviis, "A multifunctional reconfigurable pixeled antenna using MEMS technology on printed circuit board," *IEEE Trans. Antennas Propag.*, vol. 59, no. 12, pp. 4413–4424, 2011.

[65] N. Behdad and K. Sarabandi, "A varactor-tuned dual-band slot antenna," *IEEE Trans. Antennas Propag.*, vol. 54, no. 2, pp. 401–408, 2006.

[66] S. Pendharker, R. K. Shevgaonkar, and A. N. Chandorkar, "Optically controlled frequency-reconfigurable microstrip antenna with low photoconductivity," *IEEE Antennas Wireless Propag. Lett.*, vol. 13, pp. 99–102, 2014.

[67] L. Liu and R. Langley, "Liquid crystal tunable microstrip patch antenna," *Electron. Letters*, vol. 44, no. 20, pp. 1179–1180, 2008.

[68] D. Pozar and V. Sanchez, "Magnetic tuning of a microstrip antenna on a ferrite substrate," *Electron. Lett.*, vol. 24, no. 12, pp. 729–731, 1988

[69] I. Yeom *et al.*, "Analysis of RF front-end performance of reconfigurable antennas with RF switches in the far field," *Int. J. Antennas Propag.*, 2014. pp. 14.

[70] K. Buisman *et al.*, "Distortion-free varactor diode topologies for RF adaptivity," *IEEE MTT-S Int. Microw. Symp. Digest*, 2005, pp. 157–160.

[71] M. Shirazi *et al.*, "A Switchable-frequency slot-ring antenna element for designing a reconfigurable array," *IEEE Antennas Wireless Propag. Lett.*, vol. 17, no. 2, pp. 229–233, 2018.

[72] J. H. Lim *et al.*, "Simultaneous frequency and isolation reconfigurable MIMO PIFA using PIN diodes," *IEEE Trans. Antennas Propag.*, vol. 60, no. 12, pp. 5939–5946, 2012.

[73] Y. I. Abdulraheem *et al.*, "Design of frequency reconfigurable multiband compact antenna using two PIN diodes for WLAN/WiMAX applications," *IET Microw., Antennas Propag.*, vol. 11, no. 8, pp. 1098–1105, 2017.

[74] N. Nguyen-Trong *et al.*, "A frequency- and polarization-reconfigurable circular cavity antenna," *IEEE Antennas Wireless Propag. Lett.*, vol. 16, pp. 999–1002, 2017.

[75] M. C. L. Purisima *et al.*, "Frequency and pattern reconfigurable antennas for community cellular applications," *IEEE Region 10 Conference (TENCON)*, 2016, pp. 3767–3770.

[76] E. Erdil *et al.*, "Frequency tunable microstrip patch antenna using RF MEMS technology," *IEEE Trans. Antennas Propag.*, vol. 55, no. 4, pp. 1193–1196, 2007.

[77] H. F. AbuTarboush *et al.*, "Reconfigurable tri-band H-shaped antenna with frequency selectivity feature for compact wireless communication systems," *IET Microw., Antennas Propag.*, vol. 5, no. 14, pp. 1675–1682, 2011.

[78] P. Y. Qin *et al.*, "A reconfigurable antenna with frequency and polarization agility," *IEEE Antennas Wireless Propag. Lett.*, vol. 10, pp. 1373–1376, 2011.

[79] N. Nguyen-Trong, L. Hall, and C. Fumeaux, "A frequency- and polarization-reconfigurable stub-loaded microstrip patch antenna," *IEEE Trans. Antennas Propag.*, vol. 63, no. 11, pp. 5235–5240, Nov. 2015.

[80] K. M.-J. Ho and G. M. Rebeiz, "A 0.9–1.5 GHz microstrip antenna with full polarization diversity and frequency agility," *IEEE Trans. Antennas Propag.*, vol. 62, no. 5, pp. 2398–2406, 2014.

[81] N. Nguyen-Trong, L. Hall and C. Fumeaux, "A frequency- and pattern-reconfigurable center-shorted microstrip antenna," *IEEE Antennas Wireless Propag. Lett.*, vol. 15, pp. 1955–1958, 2016.

[82] N. Nguyen-Trong, A. Piotrowski and C. Fumeaux, "A frequency-reconfigurable dual-band low-profile monopolar antenna," *IEEE Trans. Antennas Propag.*, vol. 65, no. 7, pp. 3336–3343, 2017.

[83] L. J. Chu, "Physical limitations of omni-directional antennas," *J. Appl. Phys.*, vol. 19, no. 12, pp. 1163–1175, 1948.

[84] R. F. Harrington, "Effect of antenna size on gain, bandwidth, and efficiency," *J. Res. Nat. Bureau Standards*, vol. 64, no. 1, pp. 1–12, 1960.

[85] M. A. C. Namien *et al.*, "An electrical small frequency reconfigurable antenna for DVB-H," *IEEE Int. Workshop Antenna Technology (iWAT)*, 2012, pp. 245–248.

[86] F. Canneva *et al.*, "Reconfigurable miniature antenna for DVB-H standard," *IEEE Int. Symp. Antennas Propag. Soc.*, 2010, pp. 1–4.

[87] B. Mun *et al.*, "A compact frequency-reconfigurable multiband LTE MIMO antenna for laptop applications," *IEEE Antennas Wireless Propag. Lett.*, vol. 13, pp. 1389-–1392, 2014.

[88] S. C. Del Barrio, A. Morris, and G. F. Pedersen, "Antenna miniaturization with MEMS tunable capacitors: Techniques and trade-offs," *Int. J. Antennas Propag.*, vol. 2014, Article ID 709580, 2014.

[89] J. M. Hannula *et al.*, "Frequency reconfigurable multiband handset antenna based on a multichannel transceiver," *IEEE Trans. Antennas Propag.*, vol. 65, no. 9, pp. 4452–4460, 2017.

[90] L. H. Trinh *et al.*, "Reconfigurable antenna for future spectrum reallocations in 5G communications," *IEEE Antennas Wireless Propag. Lett.*, vol. 15, pp. 1297–1300, 2016.

[91] C. Nez lvarez, R. Cheung and J. S. Thompson, "Performance analysis of hybrid metalgraphene frequency reconfigurable antennas in the microwave regime," *IEEE Trans. Antennas Propag.*, vol. 65, no. 4, pp. 1558–1569, 2017.

[92] Wei-Shiuan Chang, *et al.*, "Pattern reconfigurable millimeter-wave antenna design for 5G handset applications," *10^{th} European Conf. Antennas Propag. (EuCAP)*, 2016, pp. 1–3.

[93] K. X. Wang *et al.*, "Polarization reconfigurable millimeter wave antenna with wideband and high gain performance," *IEEE Conf. Antenna Meas. Applications (CAMA)*, 2016, pp. 1–3.

[94] Y. Yang, K. Y. Chan, and R. Ramer, "60GHz pattern reconfigurable quasi-Yagi antenna proof through computational design," *Int. Workshop Antenna Technology (iWAT)*, 2014, pp. 53–56.

[95] M. A. Hossain, I. Bahceci and B. A. Cetiner, "Parasitic layer based radiation pattern

reconfigurable antenna for 5G communications," *IEEE Trans. Antennas Propag.*, vol. PP, no. 99, pp. 1-1, 2017.

[96] Hanyue Xia *et al.*, "Design and analysis of a compact reconfigurable phased antenna array with 3D coverage for 5G applications in portable devices," *Progress in Electromag. Research Symp. (PIERS)*, 2016, pp. 2459–2463.

[97] L. Ge *et al.*, "Polarization-reconfigurable magnetoelectric dipole antenna for 5G Wi-Fi," *IEEE Antennas Wireless Propag. Lett.*, vol. 16, pp. 1504–1507, 2017.

[98] K. H. Lu and T. N. Chang, "Circularly polarized array antenna with corporate-feed network and series-feed elements," *IEEE Trans. Antennas Propag.*, vol. 53, no. 10, pp. 3288–3292, 2005.

[99] B. Lee, G. C. Kang, and S. H. Yang, "Broadband high efficiency microstrip antenna array with corporate-series feed," *Microw. Optical Tech. Lett.*, vol. 43, no. 3, pp. 181–183, 2004.

[100] R. K. Gupta and G. Kumar, "High-gain multilayer 2 × 2 antenna array for wireless applications," *Microw. Optical Tech. Lett.*, vol. 50, no. 11, pp. 2911–2917, 2008.

[101] J. S. Row and S. W. Wu, "Circularly-polarized wide slot antenna loaded with a parasitic patch," *IEEE Trans. Antennas Propag.*, vol. 56, no. 9, pp. 2826–2832, 2008.

[102] K. F. Lee *et al.*, "On the use of U-slot in the design of dual-and triple-band patch antennas," *IEEE Antennas Propag. Mag.*, vol. 53, no. 3, 2011, pp. 60–74.

[103] L. W. Li, *et al.*, "A broadband and high-gain metamaterial microstrip antenna," *Applied Physics Lett.*, 96, April 2010, pp. 164101/1–3.

[104] T. Seki, *et al.*, "Millimeter-wave high-efficiency multilayer parasitic microstrip antenna array on Teflon substrate," *IEEE Trans. Microw. Theory and Tech.*, vol. 53, no. 6, 2005, pp. 2101–2106.

[105] S. Ye *et al.*, "High-gain planar antenna arrays for mobile satellite communications [Antenna Applications Corner]," *IEEE Antennas Propag. Mag.*, vol. 54, no. 6, pp. 256–268, 2012.

[106] O. M. Haraz, "Broadband and 28/38-GHz dual-band printed monopole/ elliptical slot ring antennas for the future 5G cellular communications," *J. Infrared Millim. Terahertz Waves*, vol. 37, no. 4, pp. 308–317, 2016.

[107] A. D. Philip *et al.*, "Stacked microstrip linear array with highly suppressed side-lobe levels and wide bandwidth," *IET Microw. Antennas Propag.*, vol. 11, no. 1, pp. 17–22, 2017.

[108] A. Nadeem, *et al.*, "28/38-GHz dual-band millimeter wave SIW array antenna with EBG structures for 5G applications," *Int. Conf. Inf. Commun. Tech. Research (ICTRC)*, 2015, pp. 1–4.

[109] M. H. Osama, *et al.*, "Four-element dualband printed slot antenna array for the future 5G mobile communication networks," *IEEE Int. Symp. Antennas Propag. USNC/URSI National Radio Science Meeting*, 2015, pp. 1–2.

[110] Z. Chen and Y. P. Zhang, "FR4 PCB grid array antenna for millimeter-wave 5G mobile communications," *IEEE MTT-S Int. Microw. Workshop Series on RF and Wireless Tech. for Biomedical and Healthcare Applications (IMWS-BIO)*, 2013, pp. 1–3.

[111] A. Elboushi, Z. Briqech, and A. Sebak, "4-elements MMW array with EBG feeding network," *IEEE Int. Symp. Antennas Propag. (APS/URSI)*, 2013, pp. 162–163.

[112] O. M. Haraz *et al.*, "Dense dielectric patch array antenna with improved radiation characteristics using EBG ground structure and dielectric superstrate for future 5G cellular networks," *IEEE Access*, 2014, vol. 2, pp. 909–913.

[113] F. -G. Zhu, J. -D. Xu, and Q. Xu, "Reduction of mutual coupling between closely

packed antenna elements using defected ground structure," *Electron. Lett.*, 2009, vol. 45, no. 12, pp. 601–602.

[114] A. I. Hammoodi, H. M. Al-Rizzo, and A. A. Isaac, "Mutual coupling reduction between two monopole antennas using fractal based DGS," *IEEE Int. Symp. Antennas Propag. Soc.*, 2015, pp. 416–417.

[115] S. Biswas, D. Guha, and C. Kumar, "Control of higher harmonics and their radiation in microstrip antennas using compact defected ground structures," *IEEE Trans. Antennas Propag.*, 2013, vol. 61, no. 6, pp. 3349–3354.

[116] F. Y. Zulkifli, E. T. Rahardjo, and D. Hartanto, "Radiation properties enhancement of triangular patch microstrip antenna array using hexagonal defected ground structure," *Prog. Electromagn. Res. Mag.*, vol. 5, pp. 101–109, 2008.

[117] H. Alias, *et al.*, "Aperture coupled microstrip antenna array integrated with DGS and parasitic elements," *IEEE Symp. Wireless Tech. Applications (ISWTA)*, 2013, pp. 259–263.

[118] K. R. Mahmoud and A. M. Montaser, "Optimised 4×4 millimetre-wave antenna array with DGS using hybrid ECFO-NM algorithm for 5G mobile networks," *IET Microw., Antennas Propag.*, vol. 11, no. 11, pp. 1516–1523, 2017.

[119] W. Hong *et al.*, "Study and prototyping of practically large-scale MMWave antenna systems for 5G cellular devices," *IEEE Commun. Mag.*, vol. 52, no. 9, pp. 63–69, 2014.

[120] D. Betancourt and J. Castan, "Printed antenna on flexible low-cost PET substrate for UHF applications," *Progress Electromag. Research C*, vol. 38, pp. 129–140, 2013.

[121] H. R. Khaleel, H. M. Al-Rizzo, and A. I. Abbosh, "Design, fabrication, and testing of flexible antennas," *Advancement In Microstrip Antennas With Recent Applications*,

A. Kishk, Ed., InTech, 2013.

[122] A. Chauraya *et al.*, "Inkjet printed dipole antennas on textiles for wearable communications," *IET Microw., Antennas Propag.*, vol. 7, no. 9, pp. 760–767, 2013.

[123] L. Wang, *et al.*, "A flexible modified dipole antenna printed on PET film," *IEEE Asia-Pacific Conf. Antennas Propag. (APCAP)*, 2012, pp. 239–240.

[124] N. J. Kirsch, N. A. Vacirca, and E.E. Plowman, "Optically transparent conductive polymer RFID meandering dipole antenna," *IEEE Int. Conf. on RFID*, 2009, pp. 278–282.

[125] H. K. Yoon, *et al.*, "A CPW-fed polarization diversity antenna for UWB systems," *IEEE Int. Symp. Antennas Propag. Soc. (APS)*, 2008, pp. 1–4.

[126] S. R. Forrest, "The path to ubiquitous and low-cost organic electronic appliances on plastic," *Science*, vol. 428, no. 6986, pp. 911–918, 2004.

[127] S. Cook and A. Shamim, "Inkjet printing of novel wideband and high gain antennas on low-cost paper substrate," *IEEE Trans. Antennas Propag.*, vol. 60, no. 9, pp. 4148–4156, 2012.

[128] B. Tehrani, *et al.*, "Inkjet printing of a wideband, high gain mm-wave Vivaldi antenna on a flexible organic substrate," *IEEE Int. Symp. Antennas Propag. Society (APSURSI)*, 2014, pp. 320–321.

[129] `http://phys.org/news/2015-05-inkjet-kesterite-solar-cells.html`

[130] `http://www.sigmaaldrich.com/technical-documents/articles/material-matters/inkjet-printing-as.html`

[131] Richard C. Jaeger, "Lithography". *Introduction to Microelectronic Fabrication*, 2nd Ed. Upper Saddle River: Prentice Hall, 2002.

[132] `http://www.lpkf.com/products/rapid-pcb-prototyping/`

laser-circuit-structuring/micromaterial-processing-protolaser-u4.htm

[133] C. -X., Wang *et al.*, "Cellular architecture and key technologies for 5G wireless communication networks," *Commun. Mag.*, vol. 52, no. 2, pp. 122–130. 2014.

[134] Y. Li *et al.*, "A 5G MIMO antenna manufactured by 3-D printing method," *IEEE Antennas Wireless Propag. Lett.*, vol. 16, pp. 657–660, 2017.

[135] W. Di *et al.*, "A planar MIMO antenna for mobile phones," in *Proc. PIERS*, 2013, pp. 1150–1152.

[136] J. O. Yang, F. Yang, and Z. M. Wang, "Reducing mutual coupling of closely spaced microstrip MIMO antennas for WLAN application," *IEEE Antennas Wireless Propag. Lett.*, vol. 10, pp. 310–313, 2011.

[137] C.-Y. Chiu *et al.*, "Reduction of mutual coupling between closely-packed antenna elements," *IEEE Trans. Antennas Propag.*, vol. 55, no. 6, pp. 1732–1738, 2007.

[138] L. Minz, and R. Garg, "Reduction of mutual coupling between closely spaced PIFAs," *Electron. Lett.*, vol. 46, no. 6, pp. 392–394, 2010.

[139] A. Diallo *et al.*, "Study and reduction of the mutual coupling between two mobile phone PIFAs operating in the DCS1800 and UMTS bands," *IEEE Trans. Antennas Propag.*, vol. 54, no. 11, pp. 3063–3074, 2006.

[140] B. Shao *et al.*, "Process-dependence of inkjet printed folded dipole antenna for 2.45 GHz RFID tags," *3rd European Conf. Antennas and Propag. (EuCAP)*, 2009, pp. 2336–2339.

[141] K. Hettak *et al.*, "Flexible polyethylene terephthalate-based inkjet printed CPW-fed monopole antenna for 60 GHz ISM applications," *European Microwave Integrated Circuits Conf. (EuMIC)*, 2013, pp. 476–479.

[142] G. Breed, "An introduction to defected ground structures in microstrip circuits,"

High Frequency Electronics, 2008.

[143] L. H., Weng *et al.*, "An overview on defected ground structure," *Progress In Electromag. Research B*, vol. 7, pp. 173–189, 2008.

[144] A. K. Verma, and A. Kumar, "Synthesis of microstrip lowpass filter using defected ground structures," *IET Microw. Antennas Propag.*, vol. 5, no. 12, pp. 1431–1439, 2011.

[145] J. Pei *et al.*, "Miniaturized triple-band antenna with a defected ground plane for WLAN/WiMAX applications," *IEEE Antennas Wireless Propag. Lett.*, vol. 10, pp. 298–301, 2011.

[146] M. M. Fakharian, P. Rezaei, and A. A. Orouji, "Microstip antenna with a reconfigurable dumbbell-shaped defected ground plane for DCS-1800 and PCS-1900," *IEEE Int. Symp. Antennas Propag. Soc. (APS)*, 2013, pp. 576–577.

[147] A. A. R. Saad, E. E. M. Khaled, and D. A. Salem, "Wideband slotted planar antenna with defected ground structure," in *Proc. PIERS*, 2011, pp. 1092–1097.

[148] X. J. Liao, H. C. Yang, and N. Han, "An improved dual band-notched UWB antenna with a parasitic strip and a defected ground plane," in *Proc. Int. Symp. Intelligent Signal Process. Commun. Sys.*, 2010, pp. 1–4.

[149] M. A. Antoniades, and G. V. Eleftheriades, "A compact monopole antenna with a defected ground plane for multi-band applications," *IEEE Int. Symp. Antennas Propag. Soc. (APS)*, 2008, pp. 1–4.

[150] S. Jun, and K. Chang, "A 60 GHz monopole antenna with slot defected ground structure for wigig applications," *IEEE Int. Symp. Antennas Propag. Soc. (APS)*, 2013, pp. 2139–2140.

[151] A. Mansoul *et al.*, "A selective frequency-reconfigurable antenna for cognitive radio applications," *IEEE Antennas Wireless Propag. Lett.*, vol. 13, pp. 515–518, 2014.

[152] A. Romputtal and C. Phongcharoenpanich, "Frequency reconfigurable multiband antenna with embedded biasing network," *IET Microw., Antennas Propag.*, vol. 11, no. 10, pp. 1369–1378, 2017.

[153] L. N. Pringle *et al.*, "A reconfigurable aperture antenna based on switched links between electrically small metallic patches," *IEEE Trans. Antennas Propag.*, vol. 52, no. 6, pp. 1434–1445, Jun 2004.

[154] H. Rajagopalan, J. M. Kovitz and Y. Rahmat-Samii, "MEMS reconfigurable optimized E-shaped patch antenna design for cognitive radio," *IEEE Trans. Antennas Propag.*, vol. 62, no. 3, pp. 1056–1064, 2014.

[155] A. K. Horestani *et al.*, "Reconfigurable and tunable S-shaped split-ring resonators and application in band-notched UWB antennas," *IEEE Trans. Antennas Propag.*, vol. 64, no. 9, pp. 3766–3776, 2016.

[156] P. Hindle, "2010 GaAs foundry services outlook," *Microwave Journal*, vol. 53, no. 6, pp. 20–28, 112, Jun. 2010.

[157] T. Boles and A. Freeston, New nanosecond switch technology," *Microwave Journal*, vol. 53, no. 6, pp. 56–60, Jun 2010.

[158] D. W. Prather *et al.*, "Optically upconverted, spatially coherent phased-array-antenna feed networks for beam-space MIMO in 5G cellular communications," *IEEE Trans. Antennas Propag.*, vol. 65, no. 12, pp. 6432–6443, 2017.

[159] R. Hussain and M. S. Sharawi, "Planar meandered-F-shaped 4-element reconfigurable multiple-inputmultiple-output antenna system with isolation enhancement for cognitive radio platforms," *IET Microw., Antennas Propag.*, vol. 10, no. 1, pp. 45–52, 2016.

[160] M. Ur-Rehman *et al.*, "A low profile antenna for millimeter-wave body-centric applications," *IEEE Trans. Antennas Propag.*, 2017.

[161] Q. Pei-Yuan *et al.*, "Millimeter wave frequency reconfigurable quasi Yagi antenna," *in Asia-Pacific Microw. Conf. Proc.*, 2010, pp. 642–645.

[162] M. Nandel and R. Goel Sagar, "Optimal and new design of T-shaped tri-band fractal microstrip patch antenna for wireless networks," *Int. Conf. on Computational Intelligence and Commun. Networks (CICN)*, vol., no., pp.92–96, Nov. 2014.

[163] O. El Maleky *et al.*, "Reconfigurable T-shaped antenna for S-band applications," *5th Int. Conf. on Multimedia Computing and Systems (ICMCS)*, 2016, pp. 451–455.

[164] J. Singh, E. S. Rani, and E. M. Singh, "Design of microstrip patch antenna array for traffic speed detector application," *5th International Conf. on Advanced Computing Commun. Technologies (ACCT)*, Feb. 2015, pp. 4–7.

[165] F. Xu, K. Wu, and X. Zhang, "Periodic leaky-wave antenna for millimeter wave applications based on substrate integrated waveguide," *IEEE Trans. Antennas and Propag.*, vol. 58, no. 2, pp. 340–347, Feb. 2010.

[166] S. X. Ta, H. Choo, and I. Park, "Broadband printed-dipole antenna and its arrays for 5G applications," *IEEE Antennas Wireless Propag. Lett.*, vol. 16, pp. 2183–2186, 2017.

[167] S. Ershadi *et al.*, "Wideband subarray design for 5G an antenna arrays," *in Proc. URSI Asia-Pacific Radio Science Conf. (URSI AP-RASC)*, 2016, pp. 185–187.

[168] A. Holub and M. Polivka, "Collinear microstrip patch antenna," *InTech Passive Microwave Components and Antennas*, pp. 513–530, Apr. 2010.

[169] M. Polivka, A. Holub, and M. Mazanek, "Collinear microstrip patch antenna," *Radioengineering*, vol. 14, no. 4, pp. 40–42, 2005.

[170] C. H. Kuo, C. C. Lin and J. S. Sun, "Modified microstrip Franklin array antenna for automotive short-range radar application in blind spot information system," *IEEE Antennas Wireless Propag. Lett.*, 2017.

[171] K. Solbach, "Microstrip-Franklin antenna," *IEEE Trans. Antennas Propag.*, vol. 30, no. 4, pp. 773–775, Jul. 1982.

[172] P. P. Wang, M. A. Antoniades, and G. V. Eleftheriades, "An investigation of printed Franklin antennas at X-band using artificial (metamaterial) phase-shifting lines," *IEEE Trans. Antennas Propag.*, vol. 56, no. 10, pp. 3118–3128, Oct. 2008.

[173] M. Polivka and A. Holub, "Planar version of collinear microstrip patch antenna," *Proc. Int. Conf. Microwaves, Radar Wireless Commun. (MIKON)*, May 2006, pp. 959–962.

[174] S. H. Chang *et al.*, "A Franklin array antenna for wireless charging applications," *PIERS*, vol. 6, no. 4, 2010.

[175] P. Cabrol and P. Pietraski, "60 GHz patch antenna array on low cost Liquid-Crystal Polymer (LCP) substrate," *IEEE Long Island Systems, Applications and Technology Conference (LISAT)*, 2014, pp. 1–6.

[176] V. Lakafosis *et al.*, "Progress towards the first wireless sensor networks consisting of inkjet-printed, paper-based RFID-enabled sensor tags," *Proc. of the IEEE*, vol. 98, no. 9, pp. 1601–1609, 2010.

[177] L. Yang *et al.*, "RFID tag and RF structures on a paper substrate using inkjet-printing technology," *IEEE Trans. Microwave Theory Tech.*, vol. 55, no. 12, pp. 2894–2901, Dec. 2007.

[178] G. Shaker, M. Tentzeris, and S. Safavi-Naeini, "Low-cost antennas for mm-Wave sensing applications using inkjet printing of silver nano-particles on liquid crystal polymers," *IEEE Int. Symp. Antennas and Propagation Society (APSURSI)*, pp. 1–4, Jul. 2010.

[179] S. Lim *et al.*, "Inkjet printing and sintering of nano-copper ink," *J. Imaging Sci. Technol.*, vol. 57, no. 5, Sep. 2013. 50507.

[180] Q. H. Abbasi *et al.*, "Ultrawideband band-notched flexible antenna for wearable applications," *IEEE Antennas Wireless Propag. Lett.*, vol. 12, pp. 1606–1609, 2013.

[181] M. Hummelgard *et al.*, "Electrical sintering of silver nanoparticle ink studied by in-situ TEM probing, *PLoS One*, vol. 6, no. 2, e17209, 2011.

[182] H. ling Kao *et al.*, Inkjet printed series-fed two-dipole antenna comprising a balun filter on liquid crystal polymer substrate, *IEEE Trans. Compon., Packag., Manuf. Technol.*, vol. 4, no. 7, pp. 1228–1236, Jul. 2014.

[183] S. Sivaramakrishnan *et al.*, "Controlled insulator-to-metal transformation in printable polymer composites with nanometal clusters," *Nature Materials* vol. 6, pp. 149–155, 2007.

[184] N. R. Bieri *et al.*, "Microstructuring by printing and laser curing of nanoparticle solutions," *Applied Physics Letters* vol. 82, no. 20, pp. 3529–3531, 2003.

[185] J. Perelaer, B. de Gans, and U. Schubert, "Ink-jet printing and microwave sintering of conductive silver tracks" *Advanced Materials* vol. 18, pp. 2101–2104, 2006.

[186] K. C. Yung *et al.*, "Ink-jet printing and camera flash sintering of silver tracks on different substrates," *J. Materials Processing Technology*, vol. 210, no. 15, pp. 2268–2272, 2010.

[187] S. Magdassi *et al.*, "Triggering the sintering of silver nanoparticles at room temperature," *ACS Nano* vol. 4, pp.1943–1948, 2010.